CR-86396

RESEARCH AND DEVELOPMENT STUDY ON WIDE BAND-GAP SEMICONDUCTOR FILMS

By A. J. Noreika, M. H. Francombe and S. A. Zeitman

December 1969

Prepared under Contract No. NAS 12-568 by
WESTINGHOUSE ELECTRIC CORPORATION
Pittsburgh, Pa.

Electronics Research Center

NATIONAL AERONAUTICS AND SPACE ADMINISTRATION

Dr. Robert F. Adamsky
Technical Monitor
NAS 12-568
Electronics Research Center
575 Technology Square
Cambridge, Massachusetts 02139

Requests for copies of this report should be referred to:

NASA Scientific and Technical Information Facility
P.O. Box 33
College Park, Maryland 20740

CR-86396

RESEARCH AND DEVELOPMENT STUDY ON WIDE BAND-GAP SEMICONDUCTOR FILMS

By A. J. Noreika, M. H. Francombe and S. A. Zeitman

December 1969

Final Report

December 1968 - December 1969

Prepared under Contract No. NAS 12-568 by
WESTINGHOUSE ELECTRIC CORPORATION
Pittsburgh, Pa.

Electronics Research Center

NATIONAL AERONAUTICS AND SPACE ADMINISTRATION

TABLE OF CONTENTS

TABLE OF CONTENTS (Cont'd.)

LIST OF ILLUSTRATIONS

LIST OF TABLES

SUMMARY

Thin films of AlSb, AlAs and AlP have been prepared by a three-temperature reactive evaporation technique, while films of AlN, BN and of two mixed nitrides, viz., (Al,Si) N and (Al,B) N, were deposited using a reactive sputtering method. Reactive sputtering was also used to produce films of AlSb. The structural, optical and electrical properties of these films were examined and related to conditions of deposition. The properties were compared with published data for these materials in (where available) thin film, or alternatively bulk, single-crystal form. Since AlN is known to exhibit piezoelectric behavior, thin film transducer structures of this nitride were also prepared and evaluated.

The freshly deposited films of AlSb were found to be structurally and optically similar to bulk crystals. It was observed, however, that in times varying from a few hours to several weeks, both structural and optical properties altered. The changes were caused by hydrolysis of the compound when exposed to the laboratory environment and were observed also in films of AlAs and AlP. The structural alteration took the form of a change from a well-crystallized deposit to an amorphous-like one, the change taking place initially at the exposed surface. Granular deposits prepared at elevated temperatures were observed to degrade most rapidly. Optical change was evident in the form of marked increase of absorption in the visible and ultraviolet. Electrical measurements on some films contacted with tantalum showed the presence of a strong photovoltaic effect. Measurements of the spectral

variation of this effect indicated that it arose from a barrier-like phenomenon. Analyses of the data led to reasonable values both for the band gap of AlSb and the work function of tantalum.

Sputtered films of AlSb acquired a highly oriented structure at temperatures near 650°C, while evaporated films were only partly oriented. An investigation of relative growth rates at these temperatures showed the following: AlSb (evaporated) $\sim$ 300 Å/min; AlSb (sputtered) $\sim$ 50 Å/min. The effect of exposure to the atmosphere was identical to that reported for the evaporated films.

AlAs films were prepared by the reactive evaporation method and are believed to be the first produced by this method. X-ray examination showed the films to consist mainly of the bulk cubic phase although electron diffraction studies on some Al-rich films revealed that surface layers comprised a highly oriented wurtzite modification. Optical data were consistent with indirect band gap of 2.1 eV (in agreement with the bulk form). Electrical measurements suggested that the measured conductivity of the films was dominated by a spread of shallow impurity levels which could not be characterized by a single activation energy. The change in properties when exposed to air was less drastic than that experienced by the AlSb films, the optical absorption decreasing after a prolonged exposure.

AlP was also prepared in thin film form by the reactive evaporation method. Experience with the chemical instability of both the AlSb and AlAs films led to use of alcohol-filled containers to protect the AlP film during optical and electrical studies. The optical

absorption data are consistent with a compound with an absorption edge near 2.5 eV, again in good agreement with the bulk compound. Structurally the film was found to adopt the cubic bulk form possessing a weak (110) fibre texture. The electrical resistivity studies suggested that conductivity was influenced (as in the AlAs films) by a spread of shallow impurity levels.

Study of the properties of reactively sputtered AlN films comprised a considerable part of the overall program. The emphasis on this compound was motivated by excellent chemical stability characteristics and by the observations of good dielectric behavior. Structurally, films of AlN assumed the bulk, wurtzite (hexagonal) arrangement. Epitaxial deposits were prepared on single-crystal Si and SiC substrates and strongly textured films on vitreous silica. Optically, the films as-deposited in a high-pressure glow-discharge system showed absorption characteristics with an anomalously low edge, which suggested the presence of nitrogen vacancies or argon occlusion (a similar effect had been observed in experiments dealing with argon annealed single crystals). Annealing in nitrogen at temperatures near the depositing temperature was required before the bulk absorption characteristics (with an absorption edge near 5.9 eV) were observed. Later experimentation with a low pressure triode sputtering arrangement yielded films with the bulk properties in the as-deposited state.

Refined optical measurements performed on both AlN and BN films provided reliable values for the absorption edge in films of these materials. In AlN, $E_G = 5.9 \pm 0.08$ eV; in BN, $E_G = 5.7 \pm .05$ eV. The

value obtained for BN is consistent with an isotropic form of the compound. Absolute determinations of absorption coefficient were not forthcoming from these measurements. The mosaic-like structure of the AlN and the microcrystalline form of BN facilitate light scattering processes within the films which produce an added "effective" absorption.

Although AlN films seemed unsuitable as semiconductors, dielectric measurements indicated possible use as a refractory dielectric. The room temperature value of dielectric constant, ε, was that of the bulk, 8.5. Both ε and the dissipation factor, $D = \tan \delta$, showed less variation with temperature (25° to 350°C) than for the bulk ceramic material, indicating fewer conductive impurities. Observations of electrical breakdown and conduction behavior showed that films, less than 1500 A thick, demonstrated erratic behavior under applied voltage. This effect was attributed to leakage at grain boundaries. Films of greater thickness showed no instability until fields greater than 9×10^6 V/cm were applied. The main features of the I-V characteristic at low fields were reversible and consistent with a space-charge limited mechanism. However, at higher fields the characteristics became unstable and changed irreversibly.

Thin film AlN transducers were prepared by reactively sputtering from a high-purity Al target onto faces of heated, single-crystal rods of Al_2O_3. The rod was chosen so that the crystallographic c-axis was along its long axis, thus, acoustic microwave pulses when applied set up longitudinal waves in the rod. The measure of transducer efficiency was the ability of the AlN films to attenuate the acoustic

wave train (a measure of electromechanical coupling). This ability depends strongly on film orientation, the more nearly film-substrate orientations are similar, the better the coupling. When deposited at 820°C, a strong (0001) fibre orientation is normally observed in the films. Piezoelectric evaluation indicates performance of such films is similar to that of well-oriented CdS films.

Si_3N_4 and BN were introduced, separately, into AlN films in an effort to suppress the crystalline habit of AlN (pyrolytically deposited BN films are virtually amorphous). The motivation was the stabilization of films thin enough to yield reasonable values of capacitance without having to resort to large area electrodes (the AlN values for capacitance per unit area are 0.04 $\mu F/cm^2$ for a 2000 Å layer).

Mixed films of the AlN-BN mixture were reactively co-sputtered from aluminum and boron targets. The experiments on these films must be regarded as only partly successful. Some reduction of crystallinity could be achieved in all deposits, the structure becoming more amorphous-like as the BN content increased (films containing about 40% BN, however, were not yet truly amorphous). Furthermore, deposits prepared at temperatures between 600° and 900°C showed limited solubility of BN in AlN, ∿6-7%, resulting in a crystalline AlN-like phase. The solubility was estimated from the shrinkage of the original AlN cell. The overall boron content of the films was determined by electron microprobe measurements. Thus, unless the films contained a very high proportion of BN (>50%) completely amorphous structures were not forthcoming; the very high-proportion BN films, it is assumed, would reflect the BN properties

rather than those of AlN. When measurements of dielectric constant and loss were made at room temperature on mixed deposits (25% atomic weight boron), the results were $\varepsilon_{av} \sim 6.9 \pm 0.3$, a value as might be expected for a mixed film. Dissipation factor D, had increased over that for pure AlN, the value (100 kHz) being 0.035. Breakdown fields are found to exceed 5×10^6 V/cm.

Several experiments utilizing a MIS configuration were performed to observe conduction behavior differences of the mixed (Al,B)N films from those of pure AlN when subjected to an electric field. In the latter, application of a field resulted in what appears to be the motion of both positive and negative ions. An alternate explanation is that the AlN film is polarizable and that the degree and direction of the polarization are determined by the magnitude of the sweep voltage. Since the AlN structure is piezoelectric, one suspects the polarization as being stress induced. In mixed (Al,B)N films, the polarization behavior is not apparent, interface charge instead being responsible for the sense in which the C-V loop is traversed.

Films of the AlN-Si_3N_4 mixture were reactively co-sputtered from cathodes with nominal Al:Si ratios of 6:1 and 1:1. The behavior of the former differed only slightly from the pure AlN films showing similar optical and electrical properties. Films prepared from the latter cathode, however, assumed an almost amorphous structure and completely reversible I-V characteristics which displayed a trap influenced space-charge limited behavior. Dielectric properties were more erratic and demonstrated an added dispersion with frequency.

Deposition of BN alone was next studied, both to ascertain the properties of the pure phase relative to that of mixed (Al,B)N and to compare such films to others reported in the literature. The reactive sputtering technique was again used. In these experiments, the cathode comprised plugs of boron imbedded in a BN matrix.

Structurally, the films were microcrystalline (crystal size < 50 Å). Initially, the dielectric properties deviated appreciably from those of the bulk. Much of this was later traced to interaction between film and substrate. When tantalum was used as the bottom electrode, films of BN retained good values of ε, i.e., $3.7 \leq \varepsilon \leq 5.1$. These values compare favorably with both pyrolytically deposited films ($\varepsilon = 5.1$) and hot pressed bulk BN ($\varepsilon = 3.9$). When platinum was used as the bottom electrode, values of ε varied from 0.8 to 1.5. The effect became progressively worse as the temperature during deposition was raised. When the temperature was sufficiently high, $\sim$ 800°C, a Pt-B phase was likely formed. (The formation of "Pt-B" is partly indicative of a reluctance of boron to convert fully to BN and suggests that even in the deposits prepared on Ta electrodes a non-stoichiometric, boron-rich, nitride may exist. An appreciable solid solution of boron in Ta is also known to exist in samples quenched above 1000°C.) The best films prepared by reactively sputtering boron in an argon-nitrogen mixture show very little change of ε with temperature between 20° and 500°C. The variation is less than that observed in the bulk. When the dissipation factor was measured, room temperature values ranged consistently between 0.02 and 0.07 (film thicknesses between 1000 and 5000 Å). These values are considerably greater than those reported

for thick pyrolytic deposits, e.g., in 75-100 μm deposits, $D \tilde{-} 1.4 \times 10^{-4}$, but compare more favorably with thin pyrolytic deposits (5000 Å) on Cu and Mo, viz., $.003 < D < .01$. When thicker sputtered deposits were prepared (1-3 μm) on Ta, values of D decreased, $D < .005$.

Deposits prepared on silicon in the MIS configuration indicate that ion motion is associated with the dielectric layer. Although the evidence is circumstantial, the presence of unreacted boron is again suspected.

1. INTRODUCTION

Comparative studies of the preparative aspects and of the structural, electrical and optical properties of films of member compounds of the Al-V group were the primary objectives of this program. Encouraging results from the most refractory member of the group, viz., AlN, later fostered increased interest in a boron analogue of this compound, i.e., BN, which appeared to possess similar optical and electrical properties.

The Al-V compounds represent a particularly interesting group because of the broad range of electrical and optical properties covered by its members. AlSb, for example, possesses an energy gap comparable to that of Si and a spectral response which is almost a theoretical match to the solar spectrum. Light emissive junctions with frequencies in the visible and ultraviolet appear feasible with AlP. AlN, with a band gap greater than SiC seems suitable as an insulating coating for integrated circuitry providing both mechanical and environmental protection. Use as a capacitive layer in active and passive thin film devices is also contemplated for this compound. Some collected bulk properties of the various compounds are given in Table I.

Of the Al-V group, only AlN and AlSb have been studied to any extent. The difficulty of preparation (all of the compounds melt only in an overpressure of the Group V element) making melt-growth and

Table I Aluminum-V Compounds and Boron Nitride -- Collected Properties

	E_g (300°K)	μ, w^2/v-sec	ρ (ohm-cm)	dE/dt	n	ε	Lattice Parameter	m.p.
AlN	5.9	μ_p=14 290°K	10^{13}	-3.5×10^{-4} at 0°K	∥2.18 ⊥2.00	8.5	a_o=3.104 c_o=4.965 a_o=3.111 c=4.980	2200°C at 2 atm
AlP	2.45 2.42	μ_n=3500		5.8×10^{-4}	3.4		5.43 5.4625	>2000
AlAs	2.16 (indirect) 2.9 (direct)	μ_n=100 for n=6×10^{17} μ_n=1200 μ_p=200					5.63	>1600°
AlSb	1.60	μ_p=400(300°K) =5000(50°K)	10^{-2} to 10^{-3}		3.4 3.18	10.3(static) 9.0(optic)	6.1355	1065°C
BN	7.53 (direct) 2.7 (indirect)		10^{13} (pressed) 10^{15} (CVD)		ω=2.20 E=1.66	5.12	a=2.51 c=6.69	Subl. 3000°C

zone refining techniques difficult to apply, and the chemical instability of several of the members (AlP reacts readily in moist air and is a known generator of phosphine (Ref. 1); AlAs (Ref. 2) and AlSb (Ref. 3) deteriorate rapidly on exposure to a normal atmospheric environment) have limited the scientific investigation.

In its bulk form, AlN has been used for many refractory purposes, e.g., for crucibles, furnace walls, etc. (Ref. 4). Fabrication of such components is by hot-pressing AlN powder with an organic binder and sintering. In this form it is similar to polycrystalline alumina (Ref. 5) regarding dielectric properties, e.g., $\varepsilon(\mathrm{AlN}) = 8.5$; $\varepsilon(\mathrm{Al_2O_3}) = 9.0$. The compound is chemically resistant to oxidation at high temperatures but can be attacked by concentrated solutions of NaOH.

More basic interest in the AlN has been generated in recent years as preparative techniques have improved. Small single crystal platelets, prepared mainly by the nitriding of Al vapor in N_2 at temperatures between 1800° and 2200°C, have been used for fundamental investigations of optical absorption behavior (Ref. 6), lattice vibration spectra (Ref. 7), and of defect structure (Ref. 8,9). Such crystals tend to be both small in area ($\sim$ 1 mm^2) and colored by impurity components, the most common being oxygen or carbon (Ref. 5). Efforts to increase size and improve purity and to adapt the material to a form suitable for use in modern microcircuit technology have resulted in the preparation of AlN by numerous vapor deposition schemes. These include: the pyrolysis of $AlCl_3$ and NH_3 (Ref. 10), the plasma assisted decomposition of $AlCl_3$ (Ref. 11), chemical transport of AlN via hydrogen and ammonia halides, (Ref. 12) and reactive evaporation

(Ref. 13,14) and reactive sputtering of Al (Ref. 15). In general, considerable success has been achieved by these techniques. Oriented deposits,often epitaxial, have been prepared on several substrates (Ref. 10,15). Dielectric properties of reactively sputtered and chemically deposited films exhibit limited dispersion over a wide temperature range, 20°-350°C (Ref. 15,16). These data imply film purity better than that obtainable in the hot-pressed bulk AlN. AlN films prepared by reactive evaporation (Ref. 13) have recently been used as microwave acoustic transducers (AlN is piezoelectric as a consequence of a wurtzite structure-space group C_{6v}^4). Great interest resides in this particular application where room temperature transducer performance may be extended to temperatures greater than 400°C.

AlSb has been prepared in both bulk and thin film form. The former is achieved by pulling techniques (Ref. 17,18) utilizing antimony seeds and aluminum melts or by float-zone methods (Ref. 19). P-type ingots are most common. Vacuum evaporation techniques (Ref. 20,21) have also been used to prepare thin films of AlSb. Co-evaporation of the separate elements is by far the favored method since direct evaporation of a powdered charge tends to decompose, the volatile Group V element evaporating or subliming more rapidly.

Some success in preparation of large area deposits of AlP has been achieved by the use of chemical methods similar to those used for AlN, i.e., the heterogeneous reaction of a volatile Al-halide with a group V vapor at the surface of a heated substrate. Reid, et al. (Ref. 22) found that the iodide of aluminum is to be preferred in the

epitaxial growth of AlP on silicon or GaAs since the transport of the aluminum can thus be effected at a lower temperature than by use of a chloride carrier. A lower source temperature is preferred to prevent contamination via reaction with the walls of the silica reaction chambers which are normally used. Other preparations have utilized the direct reaction between aluminum and phosphorus (Ref. 1) or phosphine (Ref. 23) or the heating of a stoichiometric mixture of aluminum and zinc phosphide (Ref. 24). In these reactions, however, the resulting products generally comprise small crystals in an aluminum matrix.

AlAs is perhaps the most difficult of the Al-V compounds to prepare in bulk form. The main difficulty appears to be a technological one involving the melt-container reaction. Limited success has been achieved by crystallization from solution at an arsenic pressure less than 1 atm. by slow cooling an aluminum rich melt (Ref. 25) (alumina crucibles are preferred). Small crystal platelets (p-type) in a matrix of solvent are the products of this reaction. Impurities include alumina from the crucible. Crystallization by a casting technique at an arsenic pressure of 2 atm has also produced the compound (Ref. 26) as has direct heating of aluminum and arsenic in sealed ampoules (Ref. 27,28). No reference to thin films of AlAs were uncovered during a literature survey of the compound.

BN, introduced at a later stage of the investigation, is another refractory material which in bulk form is used to fabricate crucibles. It possesses both high thermal conductivity and low thermal expansion (Ref. 29). It is less brittle than AlN and is inert to most reagents even at high temperatures. As with AlN, preparation of the bulk is

usually by hot-pressing a powder together with binding and fluxing agents. Purity of the compound is thus limited and physical and electrical properties are degraded. The pyrolytic reactions of ammonia with either the hydride (Ref. 30) or chloride (Ref. 31) of boron have also been used to prepare BN. Bulk pyrolytic BN so prepared is of reasonably high purity and exhibits dielectric properties (ε = 5.12, $D = 1.4 \times 10^{-4}$ (Ref. 32), which are more uniform and more representative of BN than those of the hot-pressed material. There is relatively little reported on thin films of BN. Data reported for pyrolytically prepared films indicate considerable variations of conductivity and stability with temperature of deposition. Doping of Si substrates with boron is also prevalent (Ref. 30) since temperatures between 600° and 1400°C are required to promote reaction. The very high temperatures sometimes required, in fact, place severe limitations on available substrates. The aim of the present experiments regarding BN deposition was to explore deposition by reactive sputtering using apparatus and technology developed for the study on reactively sputtered AlN (Ref. 15). Reaction at low temperatures was anticipated from the earlier AlN results which should be more compatible with temperature limitations of semiconductor device technology. Dielectric and optical properties have been studied and potential MIS devices using BN as the insulating dielectric were examined.

The authors wish to thank Drs. W. J. Choyke, J. DeKlerk, J. E. Johnson, and W. J. Takei for specialized technical assistance rendered during the course of the investigation.

During the course of the Contract several publications were issued with the permission of NASA-ERC. These included, "Dielectric Properties of Reactively Sputtered Films of Aluminum Nitride", J. Vac. Sci. Technol., 6, 1969, pp. 194-7 and "Structural, Optical and Dielectric Properties of Reactively Sputtered Films in the System AlN-BN", J. Vac. Sci. Technol., 6, 1969, pp. 722-6.

2. EVAPORATED FILMS

2.1 Aluminum Antimonide (AlSb)

2.1.1 Preparation - Essentially the same approach was used to prepare films of AlSb as that described by Johnson (Ref.20) and by David et.al. (Ref.21). However, the geometry of the deposition system was modified in order to obtain more film samples in a single pump-down. An aluminum metal charge (99.998%) was contained in a BN crucible which was mounted in a resistively heated tantalum holder (Fig. 1A). The antimony, in the form of small lumps, was distributed uniformly around a resistively heated circular V-shaped trough made from 5 mil tantalum sheet. Quartz shields were provided so that the antimony source was shielded from the aluminum and the vapor mixture could exit primarily through an aperture at the top of the reaction chamber. Substrates, contained in resistively heated tantalum envelopes were mounted on a sectored wheel (Fig. 1B) which could be rotated externally so as to bring them sequentially over the aperture. Excess vapor which bypassed the substrates was collected in a tantalum canopy clamped to a liquid nitrogen trap above the reaction chamber. Views of the complete system are shown in Figs. 2 and 3.

Calibration curves of substrate temperature (measured at the front face of quartz substrates) vs. heater current were plotted for substrates heated in the tantalum envelopes. The antimony and aluminum source temperatures were measured directly during each run with a thermocouple and optical pyrometer, respectively. The substrate temperatures

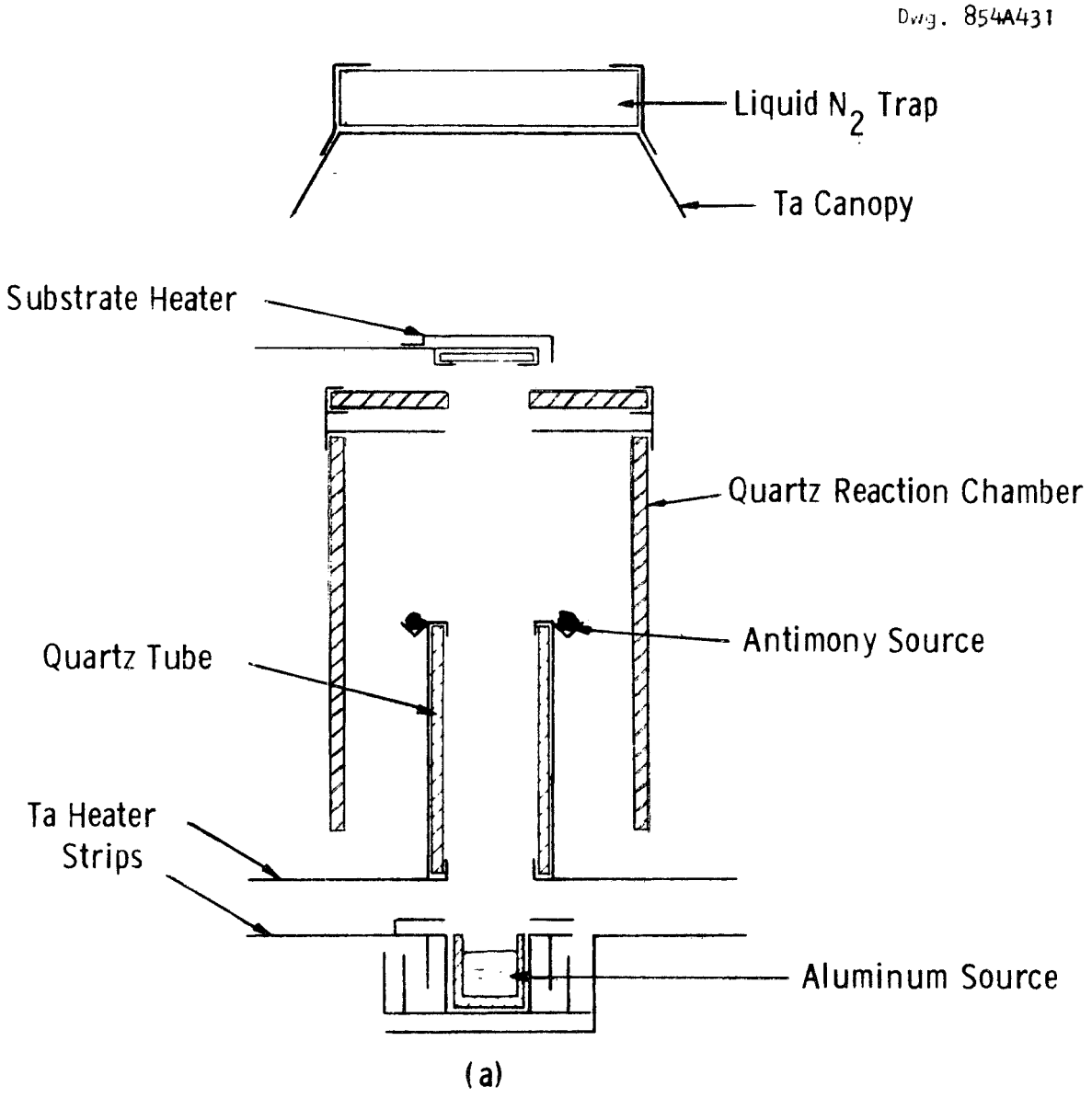

Fig. 1A Schematic of system for co-evaporation of AlSb films, (a) front elevation of reaction chamber.

Dwg. 854A430

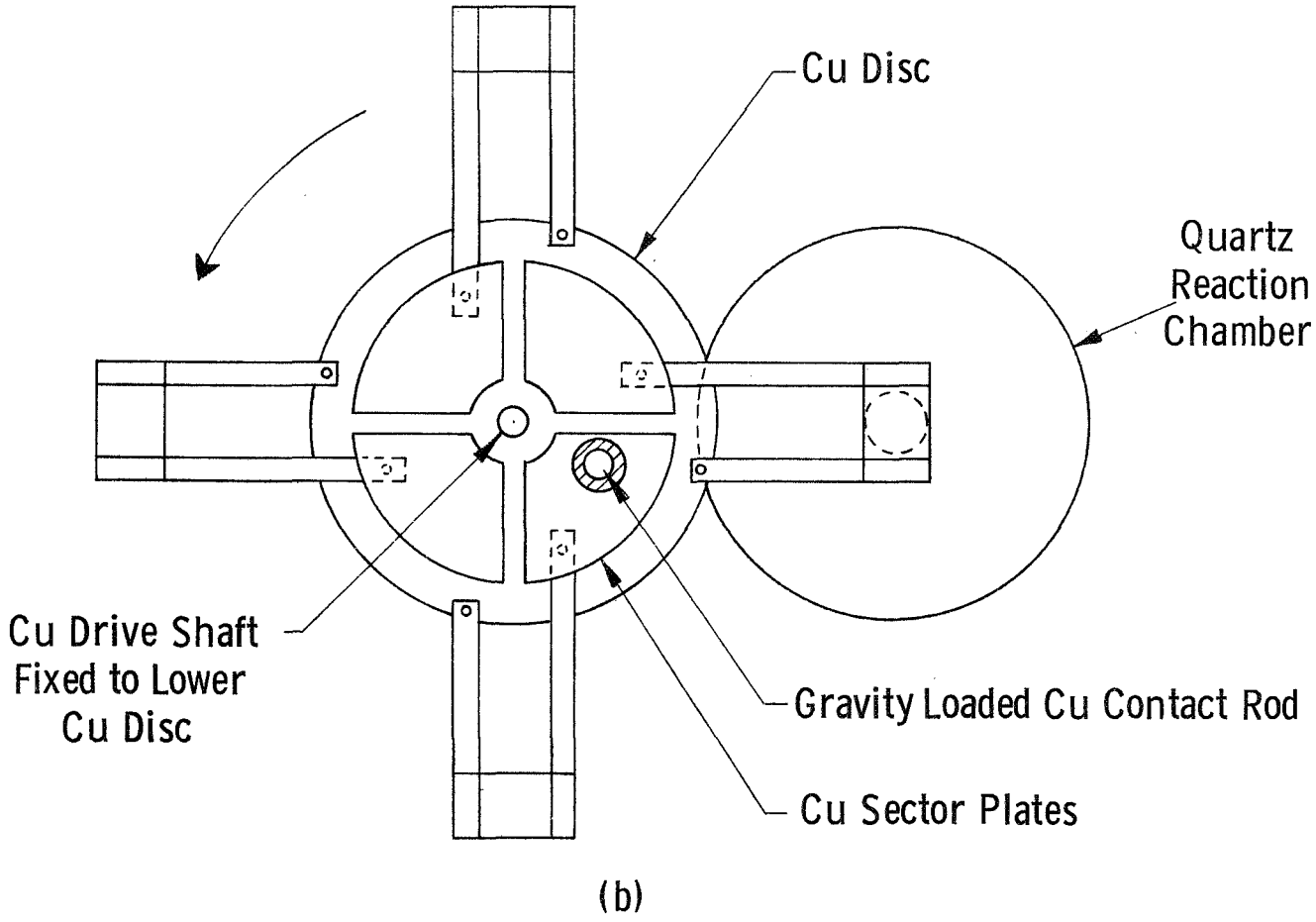

Fig. 1B (b) plan view of mounting system used for sequential exposure of four substrates.

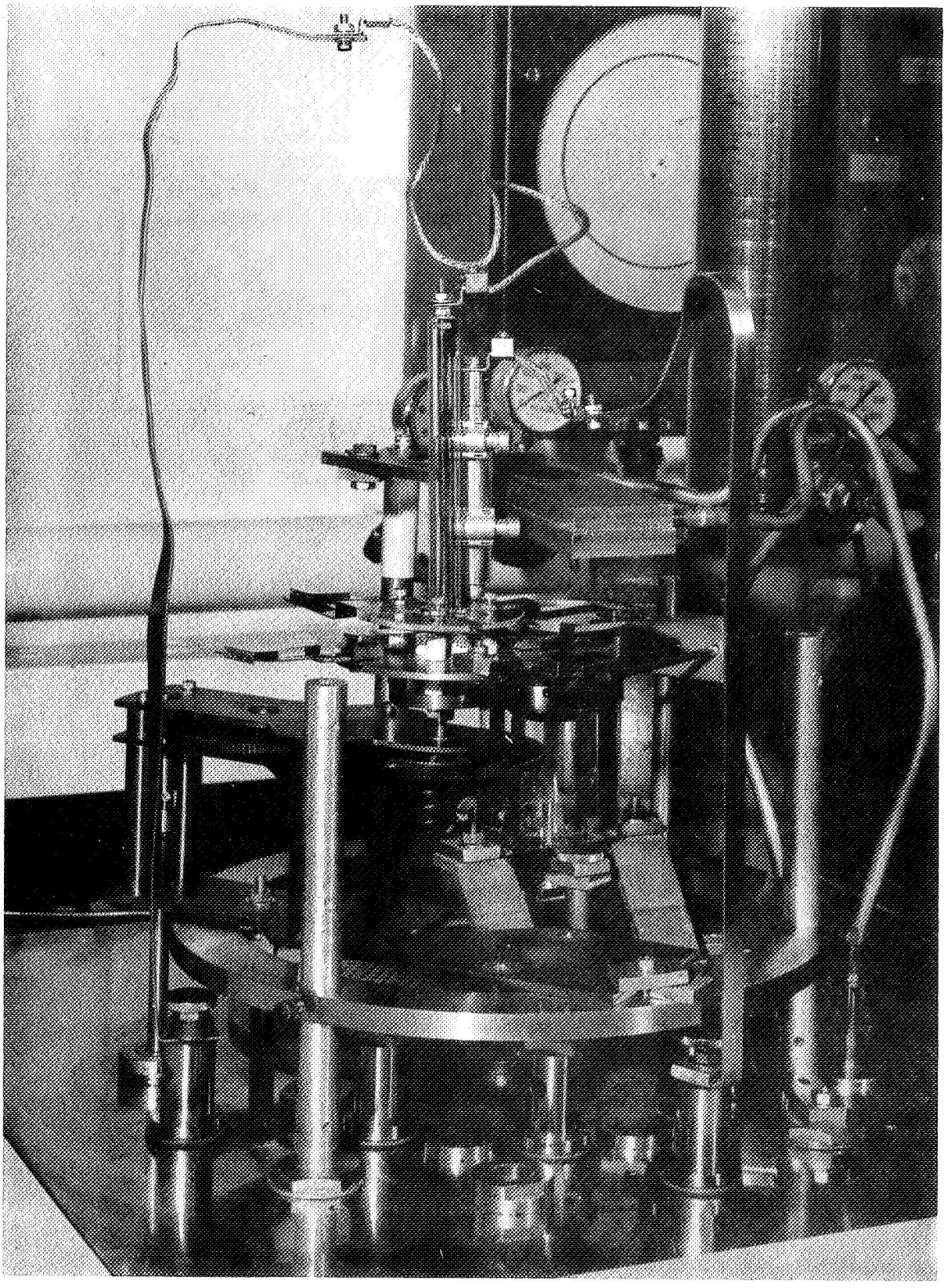

Fig. 2 System for growth of AlSb films by three temperature evaporation methods.

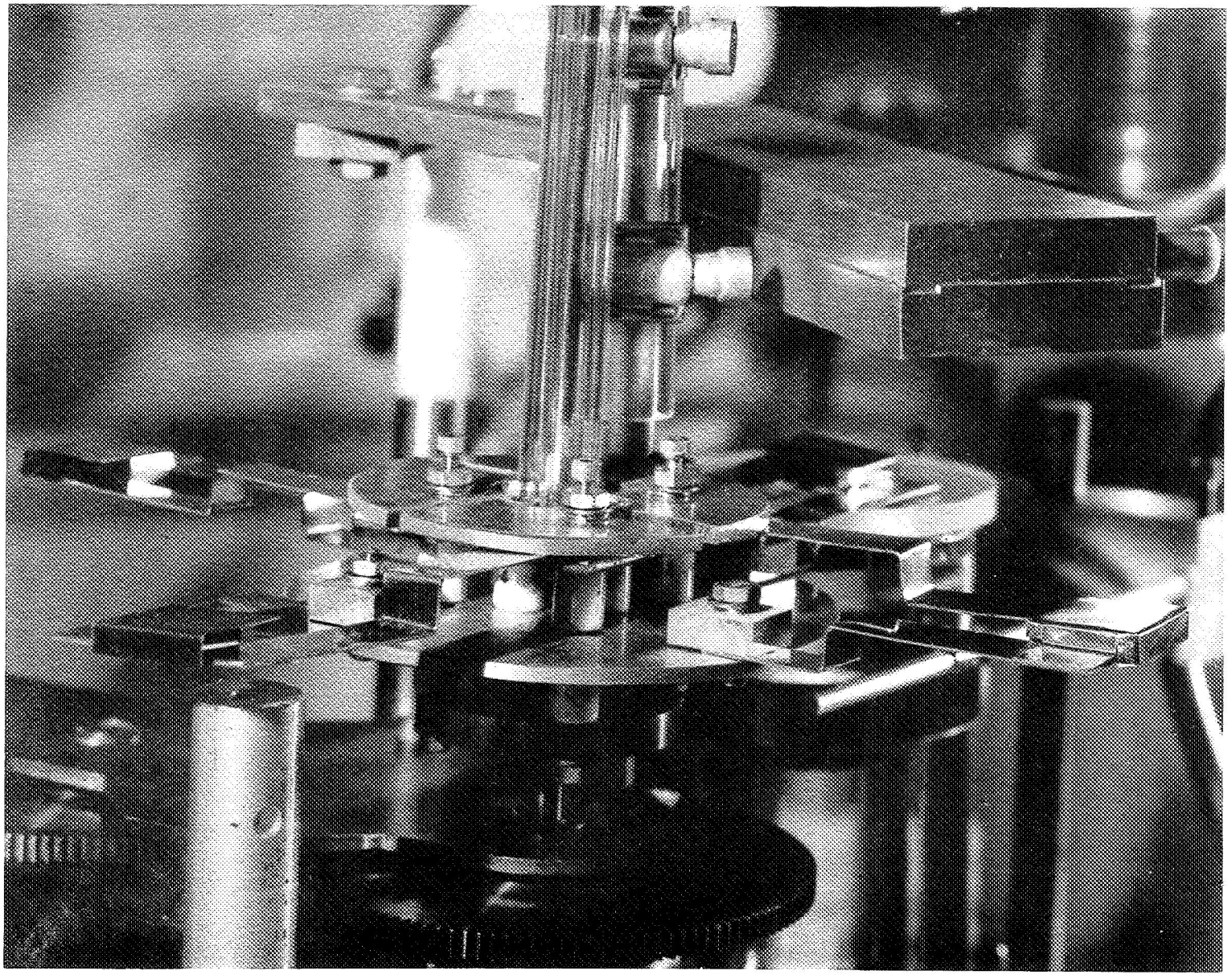

Fig. 3 System for three-temperature evaporation of AlSb films showing close-up of substrate assembly.

ranged from 500 to 750°C, antimony source temperature from 495°C (V.P. 2×10^{-3} torr) to 540°C (V.P. 10^{-2} torr), and the aluminum temperature was held constant at 1200°C. A simple calculation based on these vapor pressure values and on the geometry of the system indicates that this range of Sb source temperatures should correspond to an ideal range of Sb/Al vapor flux ratios of 4 to 1. Typically, with an Sb source temperature of 520°C and substrate temperature of 600°C, a growth rate of about 300 Å per minute was obtained. Substrates used included (111) crystals of CaF_2, (0001) oriented sapphire (Al_2O_3) crystals, (111) silicon wafers and vitreous silica (often coated with sputtered Ta to facilitate electrical measurement).

2.1.2 Structural Properties - When efforts were made to examine the crystallinity and orientation of the AlSb films using reflection electron diffraction, meaningful results were not obtained since the patterns yielded only diffuse diffraction features consistent with an amorphous surface structure. To obtain a more representative characterization of the entire film, the deposits were studied by glancing-angle X-ray diffraction using a Philips powder camera. The results showed that in each case, despite the amorphous surface layer, the films immediately after preparation possessed well-crystallized, and in many cases, strongly oriented structures.

Most of the samples examined were single-phase with the cubic zinc blende type structure of AlSb. In those cases where a second phase was present, this was identified as Al and its appearance could be accounted for by the fact that the Sb source was depleted or that its

temperature had fallen during the run. In contradiction to the claims of David et. al. (Ref.21) who reported free Sb in films deposited at temperatures below 650°C, no uncombined Sb was detected in the present study even at 550°C. This is consistent both with the earlier work of Johnson (Ref.20) in these laboratories and with the findings of Gunther (Ref.33) who reports 400°C as the lowest condensation temperature for Sb on InSb.

Structures varying from randomly oriented to almost completely epitaxial were obtained on the (111) face of CaF_2. Very strong (111) and (110) fiber orientations were produced on amorphous quartz substrates and, as shown in Table II, these appear to vary markedly in type with the temperature of deposition. Similar effects are found in both evaporated Ge films (Ref.34) and in sputtered (Ref.35) and co-evaporated (Ref.36) GaAs films deposited on vitreous silica.

2.1.3 Optical Studies - Absorption spectra for AlSb films deposited at from 600 to 700°C onto CaF_2 or sapphire were also studied. Measurements were made with a Cary spectrophotometer over a wavelength range 1900 Å to 20,000 Å. No significant difference in the spectra was noted for the various preparations, except for anticipated thickness dependences. Portions of the spectra from several films are plotted in Fig. 4. Data in this figure have been plotted only for those regions where the transmission is less than 10%, for which effects due to surface contamination and oxidation are least significant (Ref.37). Results from those samples exhibiting strong interference patterns near the 1.6 eV edge were not included.

Table II X-Ray Diffraction Data for Evaporated AlSb Films

Sample No.	Substrate	T_s (°C)	T_{Sb} (°C)	Thickness (Å)	Remarks
195-1	(111)CaF_2	550°	495	8,000	AlSb with weak Al phase
195-2	"	"	513	10,500	AlSb only, strong (110) texture
195-3	"	"	536	"	AlSb only, (110) texture
195-4	"	"	540	9,000	Epitaxial AlSb, weak Al phase
196-1	SiO_2	550°	520	∿10,000	AlSb only, strong (111) texture
196-2	"	600	520	∿10,000	AlSb only, strong (110) texture
196-3	"	700	520	∿10,000	AlSb only, weak (110) texture
196-4	"	750	520	∿10,000	AlSb only, weak (100) texture
197-1	(111)CaF_2	650	520	∿50,000	AlSb, weak Al phase
197-2	(0001)Al_2O_3	650	520	∿50,000	AlSb, strong (110) texture, very weak Al phase
199-2	(111)CaF_2	600	540	∿40,000	AlSb only, imperfectly epitaxed.

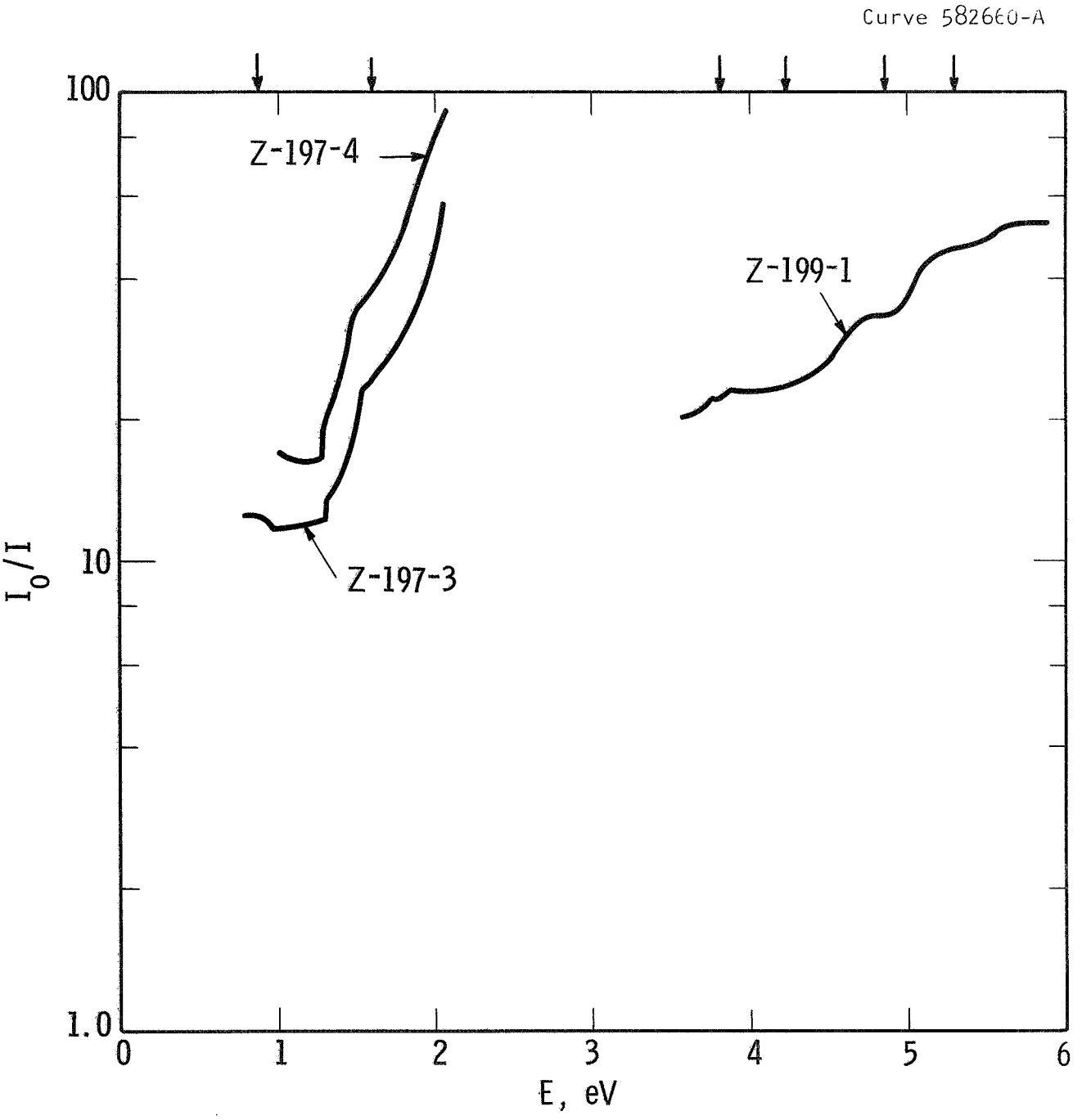

Fig. 4 Absorption spectra of AlSb films (significant features found by reflectance spectra are indicated by the arrows, including the band-gap value of 1.6 eV). Samples Z-197-3 and Z-199-1 are on CaF_2; Z-197-4 is on sapphire.

The single feature most prominent in the several regions of the spectra is that the several peaks observable at energies greater than the 1.6 eV absorption edge are all at energies less by about 0.1 eV than those tabulated from reflectance measurements on single crystals. This difference could be due in part to the difference in absorption versus reflection measurements and also, in part, due to the effects of impurities and structural disorder on the band structure of the material (Ref. 37). The absorption at energies just below the fundamental 1.6 eV edge also show added components which are due to states within the forbidden gap.

When AlSb films were allowed to age, they soon became visibly darker and more opaque. In this state, some were re-measured. A typical observation was that made on sample Z-197-4, the original absorption spectrum of which is given in Fig. 4. After several months storage in a nitrogen box, the spectrum was similar but a 1% transmission screen was required in the reference compartment of the spectrophotometer. Thus, a reduction in transmission to $\sim$1% of the earlier value had occurred.

2.1.4 Chemical Stability - As shown by the change in optical properties referred to above, the AlSb films, even when grown at thicknesses up to several microns, are highly unstable; Sorokin (Ref. 38) reports notable changes in resistivity and photoconductivity on removal from the vacuum chamber. Efforts were made to determine the character of the chemical and structural changes involved but these met with limited success.

Glancing angle X-ray diffraction patterns were obtained from films prepared on cleaved CaF_2 and on vitreous silica substrates at times varying from a few hours to several weeks after the samples had

been prepared. The results obtained differed widely and showed that complete structural degradation could occur in times varying from about three days to two weeks depending upon the substrate material and growth temperature used. The effect observed involved the transformation from a well-crystallized single AlSb phase to an amorphous product which could not be identified by X-ray diffraction. Low temperature annealing at 250°C of the amorphous films in an argon (1% H_2) ambient caused severe peeling and resulted in the development of a crystalline Sb phase, some amorphous material still remaining. It was concluded that this amorphous component was probably an anhydrous, or possibly hydrated, oxide of Al.

The wide differences found in the rate at which the film structures deteriorated may be attributed to differences in the morphology of the films. In general, those deposits prepared at higher temperatures were more granular and rougher and showed a tendency to degenerate more rapidly due presumably to their larger effective surface area.

2.1.5 Electrical Studies - AlSb film samples co-evaporated at a temperature of 600°C, a nominal Sb:Al flux ratio of 5:1, and a total deposition rate of 300 Å/min onto vitreous silica substrates carrying metal film electrodes were used to investigate some electrical properties. Initially, measurements were made under vacuum on a film, 4 microns thick, deposited on sputtered Ta stripes. Resistances measured between stripes were very high, $> 10^{10}$ ohms, and showed a small and unsystematic dependence on temperature. It appeared that the high resistance was probably due to a barrier layer at the Ta/AlSb contact.

This hypothesis was confirmed when it was found that a photovoltage of several millivolts (open circuit) could be developed by shining a microscope illuminator on the sample. The strongest photoresponse came when the light was shone onto the AlSb directly over one of the electrodes.

The light energy dependence of the photovoltaic effect was determined by placing the sample in the beam from a monochromator, and measuring the short-circuit photocurrent, of the order of 10 pico amperes, with a Keithley 153 millimicroammeter. The intensity of illumination of the sample varied with wavelength as a quartz-iodine tungsten light source operated at constant voltage was used to illuminate the monochromator entrance slit. The relative energy of the beam as a function of wavelength was determined with a thermopile detector.

In Fig. 5, the relative photoresponse per incident quantum is plotted against the wavelength of the light and a reasonably linear correlation is seen, similar to that found by Abraham (Ref.39).

Mead and Spitzer (Ref.40) have also obtained similar data using single crystals of AlSb and other semiconductors that were fitted with evaporated gold electrodes under conditions such that no impurity layer was present between the AlSb and the gold film. By plotting the square root of the photoresponse of the Au/AlSb photocell vs the light energy, Mead and Spitzer were able to determine both the indirect and the direct band-gap of AlSb. The procedure involved decomposing the $(\text{photoresponse})^{1/2}$ vs energy data into a series of straight lines by a graphical procedure.

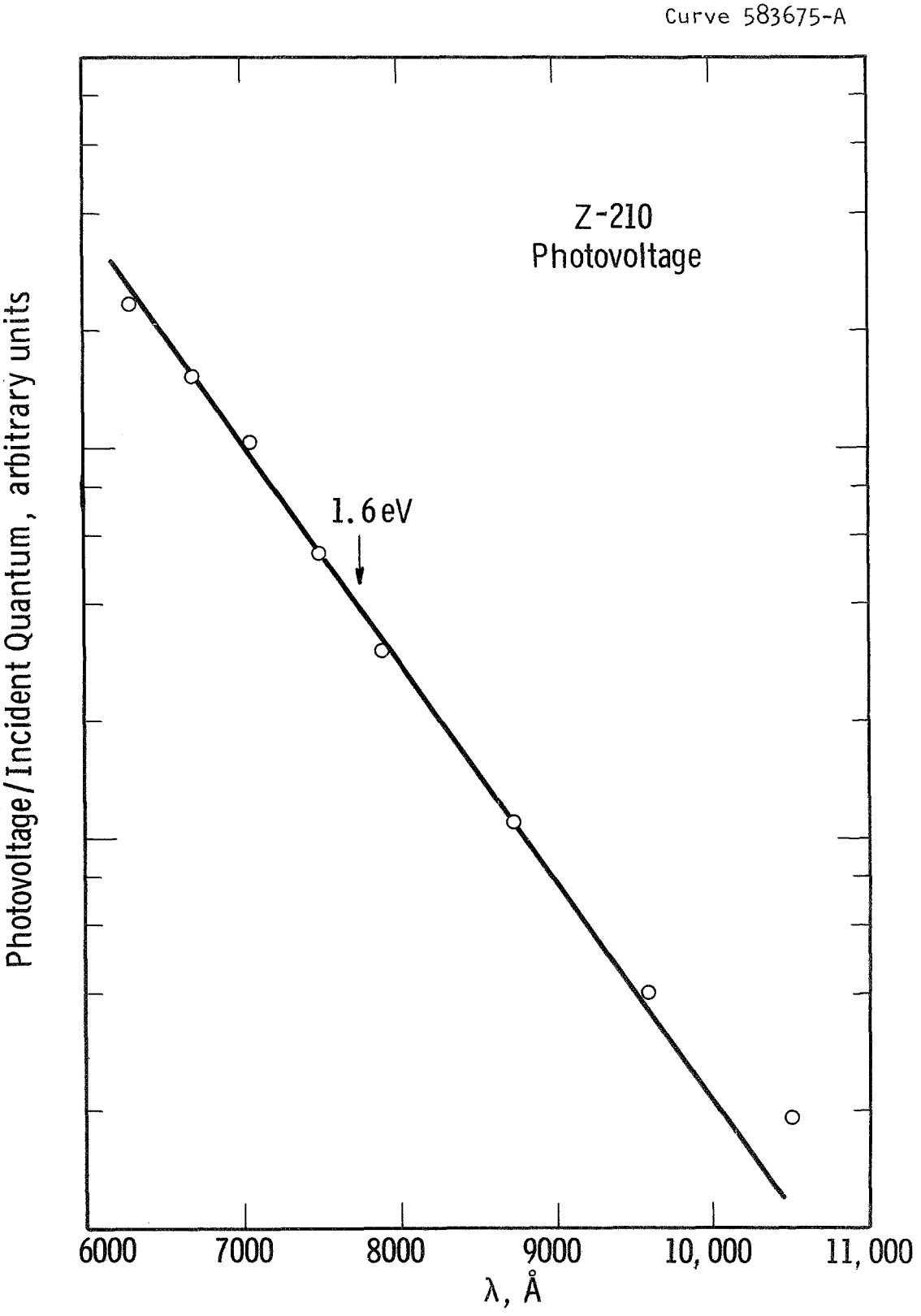

Fig. 5 Spectral variation of photovoltaic effect in AlSb film evaporated on Ta contacts.

In Fig. 6, we have similarly treated our photoresponse data. The square points are the raw data. A straight line was drawn through the points at lowest energy. Then, the $(\text{photoresponse})^{1/2}$ value of this extrapolated straight line was subtracted at each energy from the raw data points. The result is the sequence of circular points, which show another straight line behavior that extrapolate to zero at $h\nu \simeq 1.5$ eV, a value within experimental error of 1.6 eV, the indirect edge of AlSb.

It is interesting to note also that the present low energy data extrapolate to zero at 1.03 eV while the low energy data of Mead and Spitzer extrapolate to zero at 0.90 eV. The difference, 0.13 eV, is in excellent agreement with the difference between the "recommended values" for the work functions of Au, 4.3 eV, and Ta, 4.12 eV which is 0.18 eV (Ref. 41). The implication of this result is that a metal-semiconductor contact of high quality has been obtained comparable to those obtained by the sophisticated cleavage technique of Mead and Spitzer.

The measurements described above, however, do not provide information on the electrical resistivity of the AlSb film itself since the metal-semiconductor barrier dominates the measurements. When the Ta stripes were over-coated with Ni, reasonable ohmic contact to the AlSb film was obtained. During growth of the AlSb film (to a thickness of 1 micron), the resistance decreased in a manner suggesting that bulk-type behavior (i.e. an absence of size effects) was obtained after the first 1500 Å was deposited.

It was found that quite reproducible resistance-temperature behavior was obtained as a given film was cycled in vacuum over the range from the deposition temperature 600°C to ∿30°C, as shown in

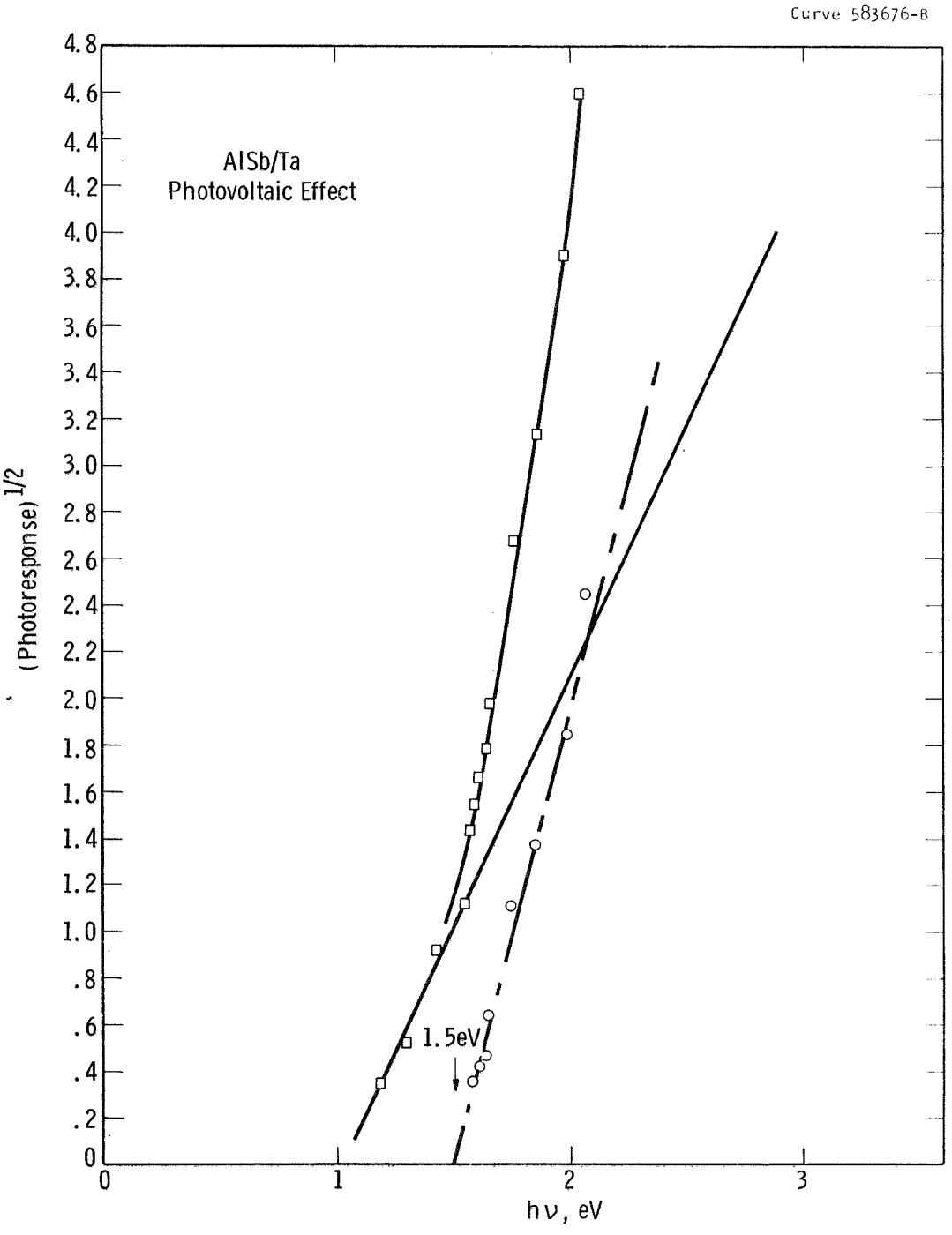

Fig. 6 Spectral variation of photoresponse from AlSb films.

Fig. 7. Over this temperature range, the film resistivity varied from about 2 x 10^5 ohm-cm at 30°C to 50 ohm-cm at 600°C.

Data from two runs are plotted in Fig. 7. It can be seen that for each film the data lie on two linear segments with a transition at about 300°C. The activation energies derivable from these data are not the same for the two films although the high temperature range is dominated for each film by a level at near mid-gap, 0.8 eV.

At lower temperatures, values of 0.23 and 0.32 eV were found. It is not clear why these low temperature values differ but it is conceivable that the difference is mainly a matter of the stoichiometry achieved in the film deposition, since Kover (Ref. 42) has attributed a donor level at 0.3 eV to Sb vacancies. It should be noted that Shaw and McKell (Ref. 43) have reported a level at 0.8 eV in high resistivity single crystals.

The resistivity of a semiconductor can be expressed as

$$\rho = \frac{1}{ne\mu_n + pe\mu_p} \tag{1}$$

where n and p are the electron and hole concentrations and μ_n and μ_p are their respective mobilities, while e is the electronic charge. The concentrations, n and p, can in turn be expressed as

$$n = N_c \exp(-E_{fn}/kT) \tag{2}$$

and

$$p = N_v \exp(-E_{fp}/kT) \tag{3}$$

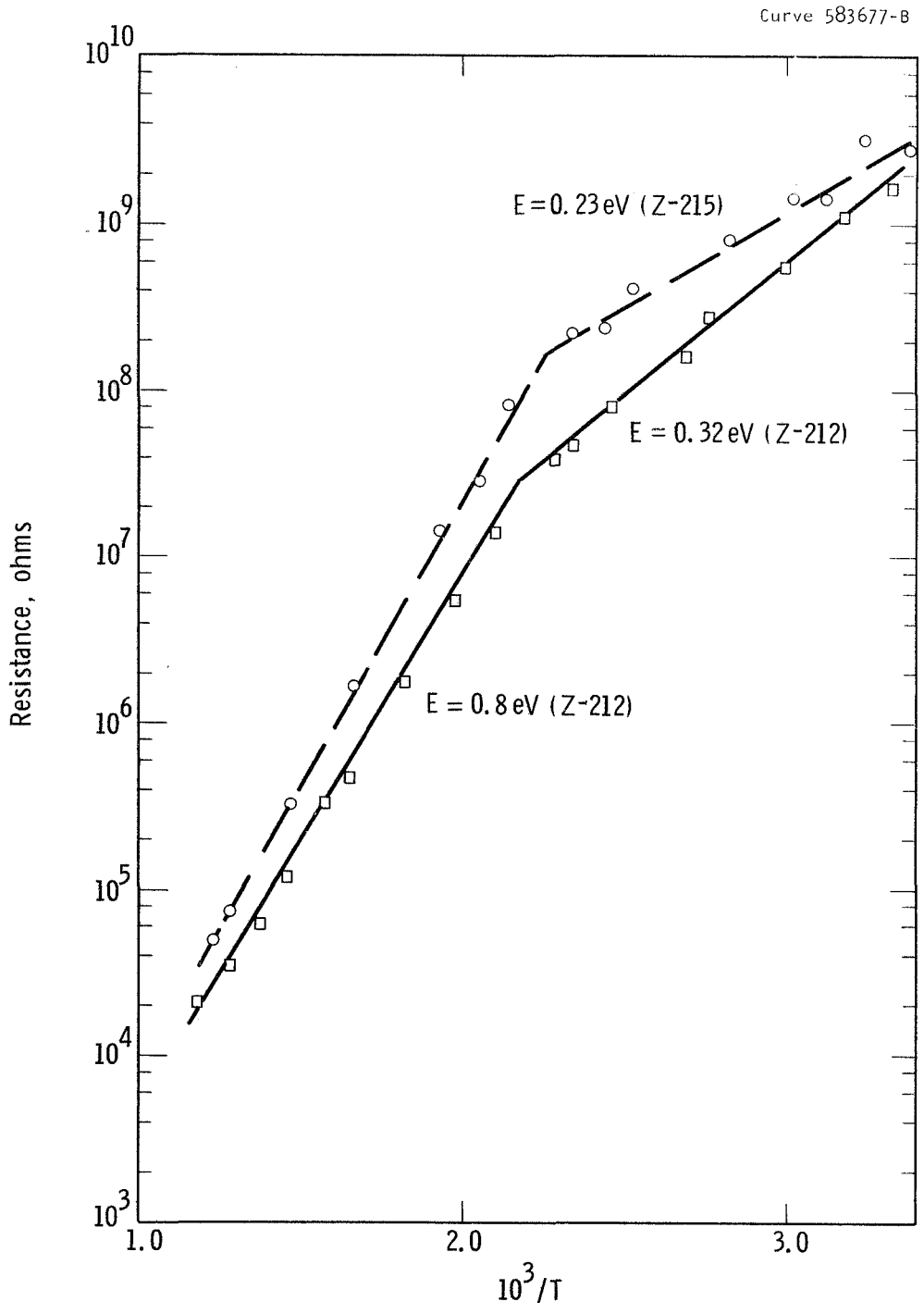

Fig. 7 Temperature dependence of resistance measured in situ on AlSb films deposited at 600°C; (Z-212) thickness 1μ, (Z-215) thickness 2μ.

where N_c and N_v are the conduction and valence band densities of states. The sum of the electron and hole Fermi energies, E_{fn} and E_{fp} are equal to the value of the energy gap, E_g (= 1.6 eV) when the sample is at thermal equilibrium.

From Eqs. (1), (2), and (3) it can be deduced that the resistivities at two temperatures should be in the ratio

$$\frac{\rho_{T_2}}{\rho_{T_1}} = \frac{n_{T_1} e\mu_{T_1}}{n_{T_2} e\mu_{T_2}} = \frac{\mu_{T_1}}{\mu_{T_2}} \left[\frac{\exp\ (-E_{fn}^{T_1}/kT_1)}{\exp\ (-E_{fn}^{T_2}/kT_2)} \right] \qquad (4)$$

if only one carrier dominates the conductivity at a given temperature.

If an attempt is made to compute the resistivity ratio from Eq. (4), the result is comparable to experiment only if the mobility ratio is given an impossibly large value, with the 0.8 eV portion of the curve having the larger μ. Small values of the ratio could be explained by a variety of phenomena but the ratio seems much too large if it is assumed, for example, that conduction occurs by both holes and electrons at higher temperatures and by electrons alone at lower temperatures.

It therefore appears that the data of Fig. 7 do not represent a "bulk" property of AlSb films. Explanation of the data probably lies in a "barrier" phenomenon, but it is not clear just what kind of barrier is involved. The governing phenomenon may be intergranular contacts, micro-cracks, or metal-semiconductor barriers.

2.2 Aluminum Antimonide - Reactively Sputtered

The preparation of AlSb by an alternate technique, viz., reactive sputtering was also achieved during the course of the present studies. Essentially, the method is similar to that described for AlN in Sec. 3.1.1, the Al substrate, substrate holders, experimental chamber and conditions for deposition being virtually identical. The scheme differs only in the means of injecting the group V element, in this case Sb, into the discharge in a gaseous or vapor form.

2.2.1 Preparation - An Al cathode designed to hold a number of solid Sb pieces was fabricated, as shown in Fig. 8. It was expected that the heat generated in the cathode by the discharge would provide a sufficient vapor pressure of Sb. A thermocouple was installed to monitor the temperature of the cathode during sputtering. With operating conditions approximating those of the AlN experiments, an equilibrium cathode temperature of 435°C was reached. The corresponding Sb vapor pressure was 10^{-4} torr, which should provide an arrival rate of Sb at the substrate surface of approximately 150 monolayers per minute.

Films were deposited on CaF_2 (111) substrates heated in the range 400 to 700°C; the temperature was confined to this range to prevent both condensation of excess Sb and thermal etching of substrates. Thicknesses of deposited films indicated growth rates of less than 50 Å/min. This relatively slow rate together with the blackened appearance of the cathode surface implied that an Al-Sb reaction had occurred at the cathode surface, and that subsequent sputtering of the compound was impeded by the high resistivity of the layer.

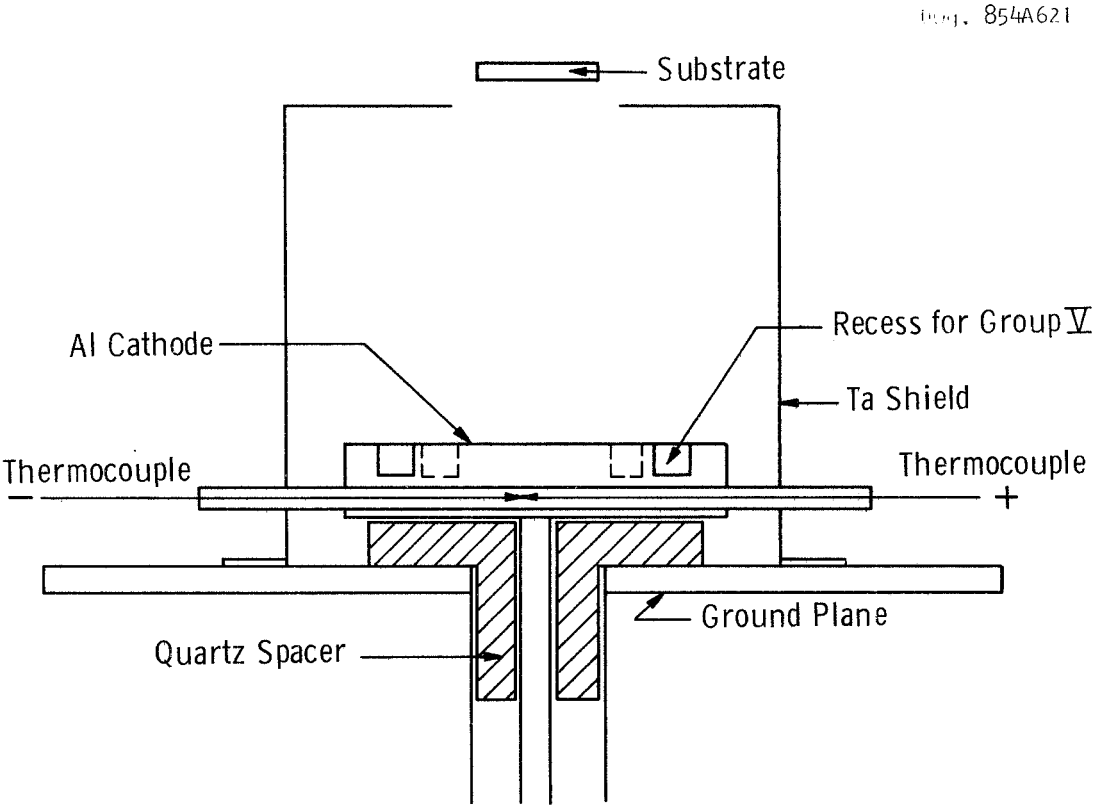

Fig. 8 Schematic of arrangement for diode reactive sputtering of AlSb films; recesses in cathode contain the Group V element (Sb).

In an effort to confine the reaction between the Sb vapor and Al to the substrate surface the arrangement was modified so that the Sb was supplied from a source external to the system (Fig. 9). During the bake-out cycle this source was kept cool by interposing a water-cooled flange between it and the main chamber. The films obtained by this method were Al-rich due apparently to insufficient transport of Sb from the external source.

2.2.2 Structural and Optical Properties

Transmission electron diffraction patterns obtained for films sputtered via the scheme illustrated in Fig. 8 are shown in Fig. 10. Deposits on (111) CaF_2 surfaces at 400°C show polycrystalline ring patterns. Films deposited on substrates at 650°C were highly oriented. The orientation relationship between the high temperature deposits and the substrate are as follows:

$$(111)_{AlSb} \;//\; (111)_{CaF_2},$$

$$[1\bar{1}0]_{AlSb} \;//\; [1\bar{1}0]_{CaF_2}.$$

Data from the absorption spectra of deposited films indicate band-gap values corresponding to measured values for bulk AlSb, viz. 1.55 to 1.6 eV. However, the very thin nature of the films made it difficult to obtain detail in the spectra.

2.3 Aluminum Arsenide (AlAs)

2.3.1 Preparation - In earlier temperature calibration experiments performed with the three-temperature evaporation system used for the

Dwg. 855A037

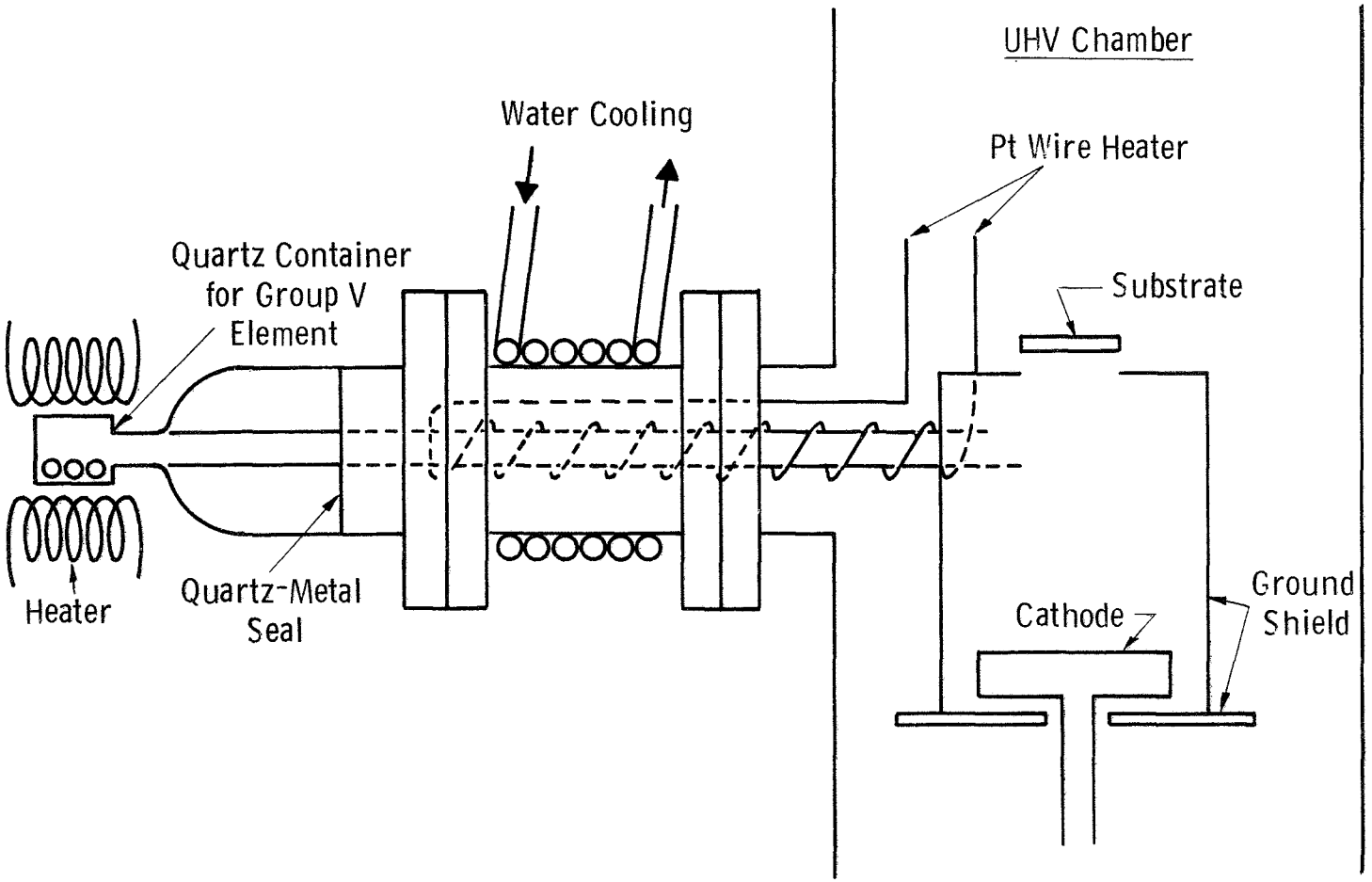

Fig. 9 Schematic of alternate sputtering system with external Sb source.

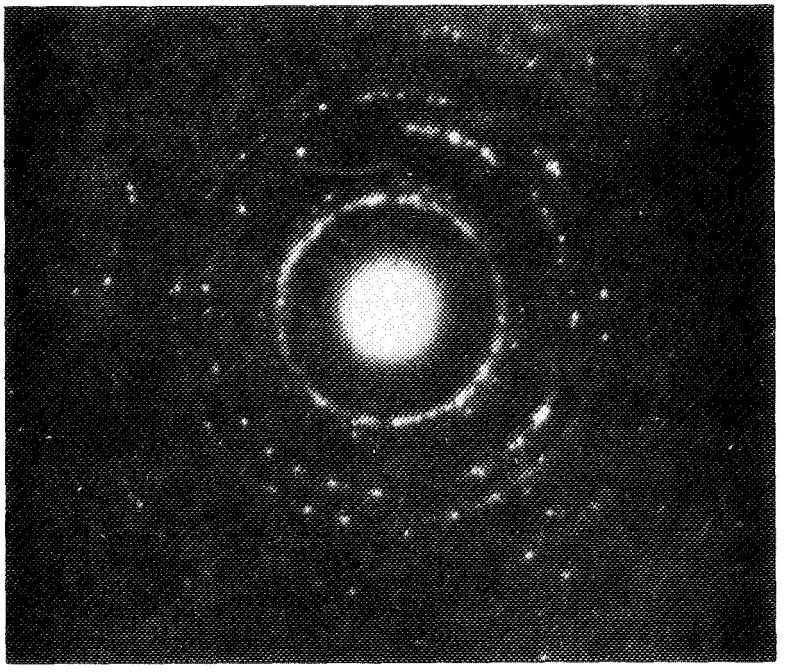

(a)

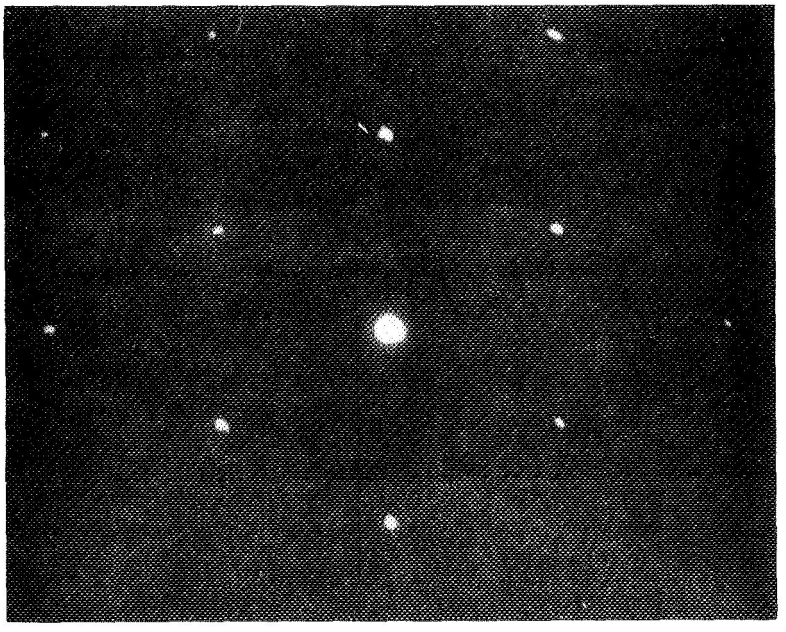

(b)

Fig. 10 Transmission electron diffraction patterns from sputtered AlSb films deposited on cleaved CaF_2 at (a) 400°C, approximate thickness 1500 A and (b) 650°C, approximate thickness 1000 A.

preparation of AlSb films, it was found that when both the Al source and the substrate were at temperature the Ta ring source containing the Sb could achieve temperatures, due to radiation, ranging from about 150°C to 280°C. The equilibrium vapor pressures for As at the higher temperature is 4×10^{-2} torr corresponding to an approximate arrival rate of 10^5 monolayers per minute. Since this value appeared to impose a rather large lower limit to the As flux, efforts were made to provide a greater degree of control by isolating the As source in a separately heated pyrex extension to the reaction chamber as shown in Fig. 11. The remaining features of the system were essentially the same as those used for the deposition of AlSb films, except that a large liquid-nitrogen cooled Meissner trap was also added to collect unreacted As.

Several experiments were carried out with the modified system using As source temperatures ranging from 200 to 380°C, substrate temperatures from 500 to 700°C, and with the Al source operating at 1150°C. At As source temperatures below about 320°C, the film products obtained were found, by X-ray analysis, to comprise a mixture of AlAs and free Al. At higher As temperatures, no deposit was obtained. Inspection of the Al source after these experiments showed it to be covered with a yellow layer of AlAs crystallites. It was concluded that this surface reaction product had prevented further evaporation of the Al despite the high operating temperature of the metal melt. This interpretation is consistent with the high temperatures reported for the decomposition of the compound (Ref. 44).

The results achieved with lower As source temperatures indicated that despite the large amount of As vaporized (the cold traps in

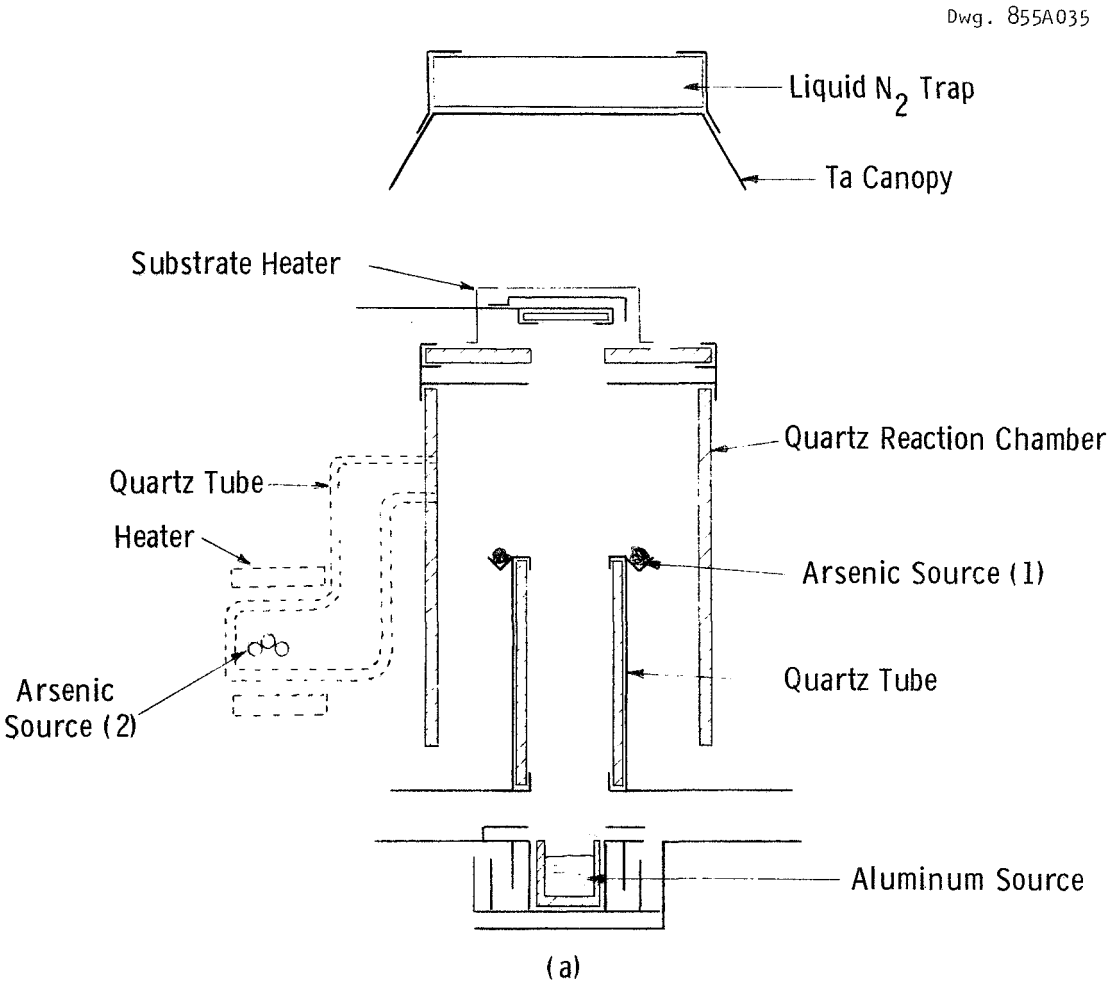

Fig. 11 Modified system for co-evaporation of AlSb films.

the chamber were found to be liberally coated with condensed As) transfer to the substrate surface with the arrangement shown in Fig. 11 was inefficient. It was reasoned that despite the poorer control in varying the As vaporization rate the non-equilibrium line-of-sight evaporation afforded by a Ta ring source arrangement might prove more effective. Thus, the modified system was abandoned.

With substrates held at temperatures below about 680°C, the following observations were made on varying the As (ring source) temperature. For As temperatures lower than 350°C, dark yellow opaque deposits were produced. When the As source temperature was increased above 360°C, the deposits obtained changed to a transparent yellow in appearance but were very thin. At higher As temperature (> 420°C), no visible deposit was obtained. In these runs the Al source was found to be again covered completely with a layer of yellow polycrystalline AlAs.

With substrates held at temperatures higher than 700°C, it was observed that if the Al source alone was operated, no condensation of Al occurred. Under these conditions, the deposit structure varied with the As source temperature in the following manner. When the As temperature was increased up to near 400°C, the deposition rate increased to a maximum of approximately 650 Å per minute -- the film products in each case possessing the pale yellow transparent appearance characteristic of pure AlAs. For higher As temperatures, reaction at the Al melt occurred, inhibiting evaporation of the metal. Some selected results for AlAs films grown under near-optimum conditions are presented in Table III.

It is interesting to compare the conditions described here for producing stoichiometric films with those normally used for other III-V

Table III Summary of Selected Results for Co-evaporated AlAs Films Deposited on Vitreous Silica

Sample No.	T_S (°C)	T_{As} (°C)	Thickness (Å)	Remarks*
Z-225	710	400	∿ 12,000	Clear yellow film.
Z-227-2	705	399	∿ 10,000	Film discolored, peeled after few hours' exposure to atmosphere.
Z-227-4	700	381	∿ 12,000	Clear yellow film.
Z-231-2	750	384	< 1,000	Nominal doping of 0.1% Te. Very low deposition rate.
Z-231-4	750	394	< 1,000	Films metallic yellow.
Z-234-4	740	364	∿ 20,000	Clear yellow film. Resistivity ∿ 70 ohm-cm.
Z-235-4	750	386	∿ 20,000	Clear yellow film. Resistivity ∿ 250 ohm-cm.

* Glancing-angle X-ray diffraction studies indicated that those films with a clear yellow color possessed the cubic zinc blende type structure of AlAs with a strong <111> fiber texture.

compounds such as InAs or GaAs. For these compounds, the melting point and critical condensation temperature of the Group III element is lower than the lowest temperature at which the Group V element alone condenses, and the upper end of the "stoichiometric temperature interval" is defined by the decomposition temperature of the compound (Ref. 45). For the Al class III-V films, the critical condensation temperature of the metal is much higher and lies between the condensation temperature for the Group V element and the decomposition temperature of the compound. Thus, by adjusting the ratio of the Al and Group V fluxes and depositing at temperatures above 700°C, it was possible to ensure stoichiometry for each of the Al compound films.

2.3.2 Structural Properties - The films which were grown using the As ring source were examined by electron (reflection) and glancing-angle X-ray diffraction. Films grown at lowest controllable As flux were found by X-ray diffraction to comprise mainly the cubic sphalerite form of AlAs (Ref. 46) together with a minor Al phase. However, the reflection electron diffraction patterns, although confirming the composition analysis indicated by the X-ray method, showed the AlAs phase to possess a highly oriented hexagonal wurtzite structure (Fig. 12). Subsequent re-examination of the X-ray data did in fact show a weak trace of reflections consistent with the hexagonal polymorph but suggested that the amount present was probably less than 1 or 2 percent of the cubic form. In summary, such a film consisted essentially of non-oriented cubic AlAs (together with some free Al), but possessed a thin surface region in which the AlAs phase had adopted a strongly fiber-textured wurtzite-type structure.

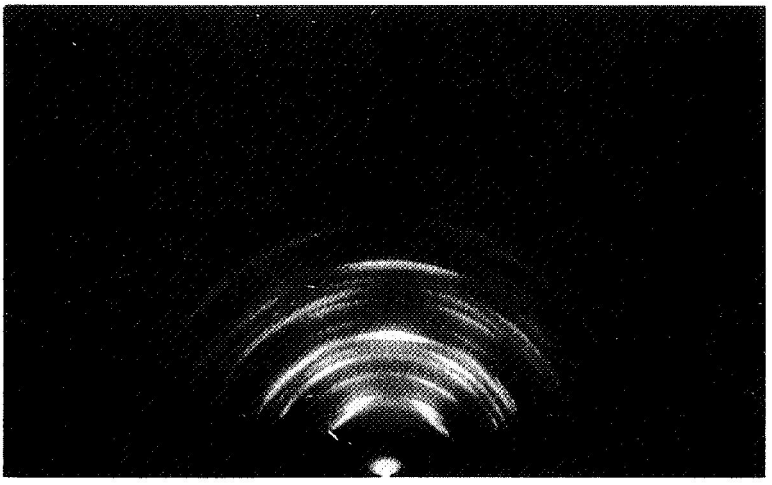

Fig. 12 Electron diffraction pattern from evaporated aluminum-rich AlAs film showing Wurtzite structure.

Films prepared at higher As flux densities and at higher substrate temperature, yielded no reflection electron diffraction patterns. X-ray diffraction, however, showed these to consist essentially of the cubic form of AlAs but with a strongly developed (111) fiber texture.

Towards the end of the structural investigations, a further AlAs film (KB59-1) grown by Dr. H. Kunig in these laboratories was submitted to us for structural and optical examination. This film has been deposited at 480°C by co-evaporation using the arrangement described previously by Johnson (Ref.20) for the preparation of AlSb films. In this system, the sources were arranged below and equi-distant from the substrate inside a thermally shielded enclosure in an effort to approach more closely equilibrium growth conditions at the substrate. The film comprised a poorly-crystallized, non-oriented, cubic AlAs phase but was appreciably thinner ($\sim$ 1500 Å) than the nominal thickness ($\sim$ 6000 Å) anticipated from the experimental conditions. In view of the fact that the Al source was observed to be covered extensively with a yellow layer of AlAs at the end of the run, it appears likely that the evaporation of Al was impeded or, more probably, stopped entirely before the experiment was completed.

2.3.3 Optical Studies and Chemical Stability - The optical absorption of several AlAs films was measured. Al-rich films were nearly opaque to visible light, and showed absorption thresholds at about one micron. The spectra of three later films, which were yellow to the eye, are shown in Fig. 13. Absorption features at the anticipated values of 2.1 eV (indirect edge) (Ref. 40) and 2.9 eV (direct edge)(Ref. 40) are present.

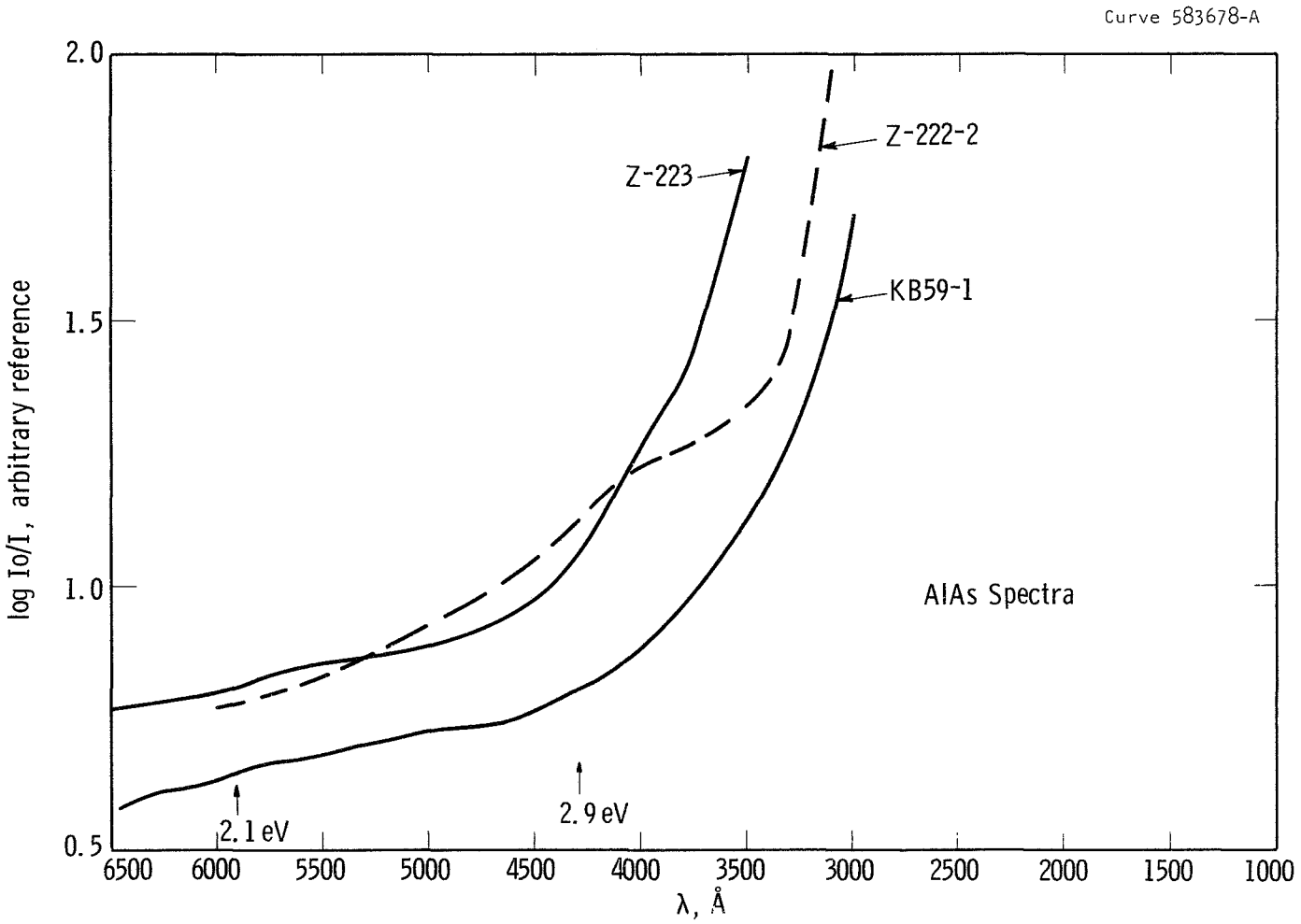

Fig. 13 Absorption spectra from evaporated AlAs films, (Z-222-2) 650°C, thickness 6000 A, (Z-223) 750°C, thickness 3000 A, (KB59-1) 480°C, thickness 1500 A.

The low temperature film KB59-1 seems to have a less developed set of absorption edges.

Measurements were made periodically to assess possible deterioration effects. One film stored in a dessicator between measurements, was measured each week for several weeks. An increase of the optical transmission of about 10% per week was observed. This is an opposite trend to that shown by the AlSb films.

A film of AlAs deposited onto a silica substrate previously coated with a set of Ta stripes and coated with MgF_2 in an attempt to protect the AlAs was examined electrically. The resistance from stripe to stripe was $\sim 10^9$ Ω just after deposition and $> 10^{10}$ Ω three days later, after storage in a N_2 flushed box. No photovoltaic or photoconductive effect could be observed in this film at this time, although a small photovoltaic effect had been observed three days earlier.

2.3.4 Electrical Studies - Resistivity measurements were made on film Z-234-4 referred to in Table III. To minimize chemical decomposition, this film was transferred rapidly from the evaporator to a vacuum system used for electrical measurements. A resistance vs $\frac{1}{T}$ plot (Fig. 14) was made for the range -190°C to 600°C and was found to be completely reversible. The log R vs. $\frac{1}{T}$ plot, however, was not linear suggesting that conductivity was dominated by a spread of shallow impurity levels which could not be characterized by a single activation energy. Similar results were later obtained on film Z-235-4 which was fitted with electrodes in a Hall bar configuration. This film was found to be p-type with a low mobility value in the range 0.5 cm^2/volt-sec. and an estimated carrier concentration of 10^{17} carriers/cm^3(measured at room temperature).

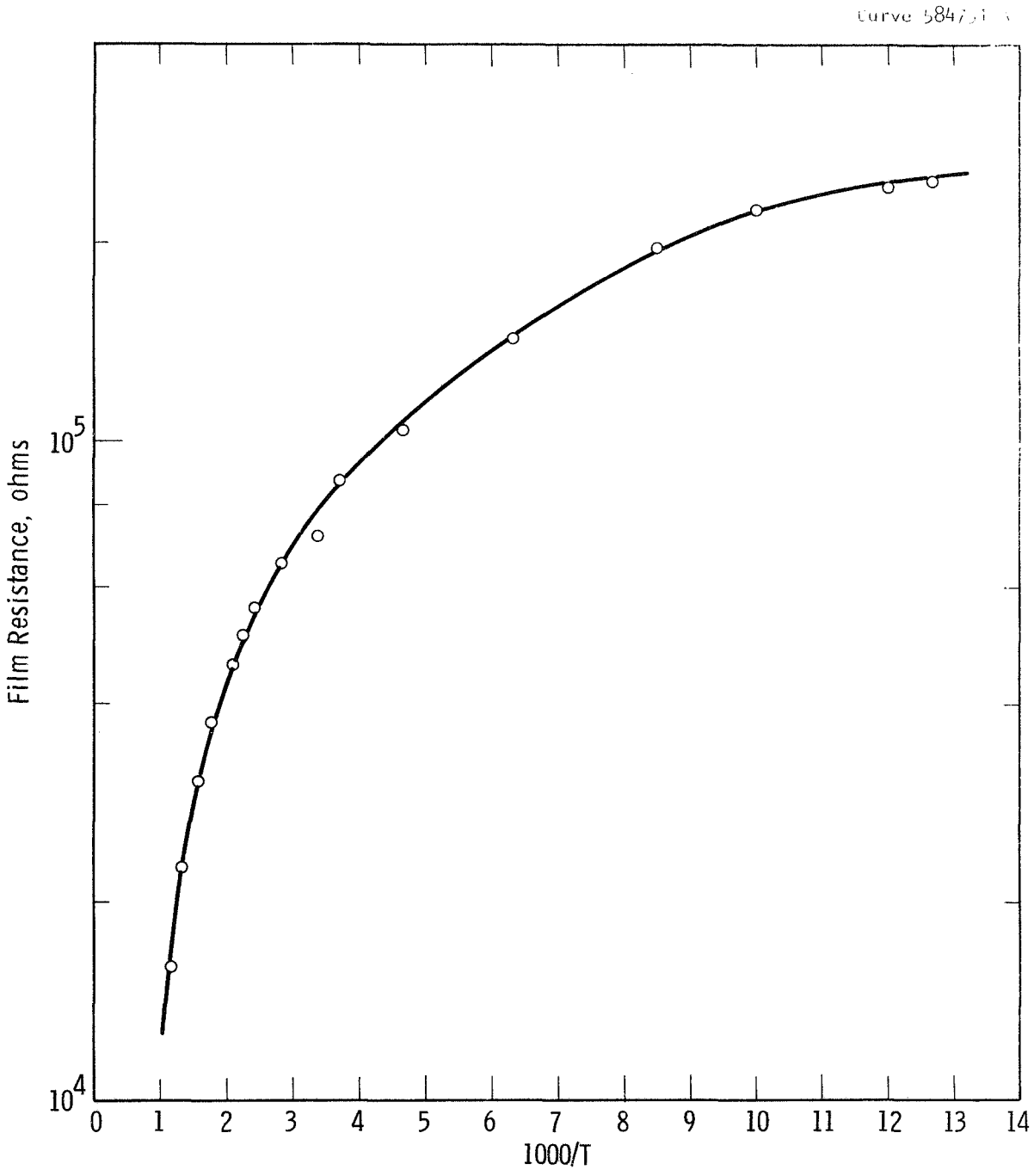

Fig. 14 Temperature dependence of resistance measured on AlAs film (Z-234) deposited at 720°C, thickness 2 microns.

An attempt was made to observe thermally stimulated current behavior in Z-234-4 by irradiating it when cold (at -190°C with a 100 watt mercury vapor lamp) and then monitoring its dark resistance as the temperature was raised at a constant rate of about 2°C per minute. No TSC effects were observed, which was perhaps not surprising in view of the relatively low resistivity and presumably high carrier concentration of the film material.

Two AlAs film samples were prepared with nominal Te doping levels (based on the vapor pressure data for As and Te) of 0.1%. Actual conditions realized during growth, however, caused Te enrichment above this normal concentration due to a rise in the temperature of the Group V element source. Also, rather low deposition rates were obtained in these experiments, so that the approximate thicknesses of the films were only of the order of 1000 A. A resistance vs $\frac{1}{T}$ plot was made for one of these films, Z-231-2, in the temperature range from 25 to 450°C. An anomalous and irreversible drop in resistance occurred in the range above 200°C, evidently caused by major structural changes in the film, or by chemical decomposition.

2.4 Aluminum Phosphide (AlP)

2.4.1 Preparation - In the time set aside for the evaporation phase of the experimental study, it was possible to undertake only one attempt at synthesizing AlP in thin film form. Source and substrate conditions were adjusted so as to match approximately those which had proved successful in the preparation of AlAs films, i.e. with a nominal P/Al flux ratio of about 5 to 1, and with a substrate temperature of about 720°C. The

silica substrate was coated with Ta-stripe electrodes in a Hall bar configuration leaving the central area of the substrate uncovered to permit optical absorption studies.

At the completion of the run, which lasted 30 minutes, a transparent yellow deposit was visible both on the silica substrate and on those areas of the bell jar wall which had been exposed directly to the aluminum source. On admitting air to the chamber and raising the jar, a strong smell of phosphine (Ref. 2) developed. The chamber was closed again and evacuated immediately to avoid further reaction.

To extract the film sample safely from the vacuum system and to preserve it for subsequent measurement, a special handling procedure was employed. The entire bell jar was encased with a polythene bag large enough to extend to the base plate with the jar in the raised position. A plastic ampoule and a pair of forceps were enclosed inside the bag. Pure argon was bled into the chamber until it reached atmospheric pressure, whereupon the jar was raised and the forceps used (through the flexible polythene wall) to transfer the film to the ampoule. After the ampoule had been removed via a slit in the polythene wall, moist air was flushed through the chamber and into an exhaust system for several hours, until no further odor of phosphine could be detected with the jar open.

2.4.2 Structural, Optical and Electrical Studies - A rapid transfer from bell jar to the electron microscope was effected to limit possible deterioration. Examination via reflection electron diffraction confirmed the presence of AlP in its bulk sphalerite form, Fig. 15. The diffraction pattern also showed the film to possess a weak (110) fiber texture.

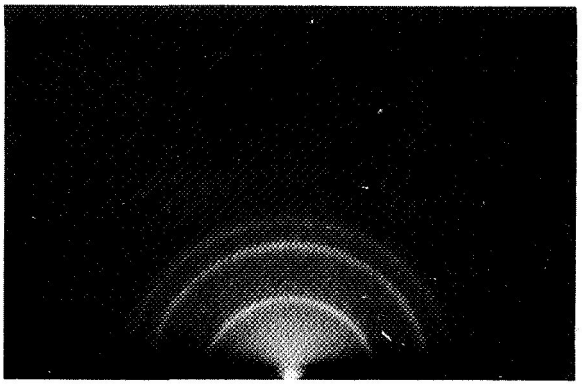

Fig. 15 Electron diffraction pattern of AlP film deposited on silica at 720°C.

To perform electrical resistivity studies the film was inserted into a second vacuum system and fitted with probes, precautions being taken to keep the film immersed completely in alcohol while the contacts were being adjusted. Similar precautions were observed while performing optical studies, the film being held in a large spectrophotometer cell filled with ethyl alcohol. Attempts were also made to measure the Hall effect with the film mounted in a tube containing flowing dry nitrogen.

The film resistivity, measured at room temperature by the four probe method via the Ta electrodes, was estimated to be 50 ohm-cm. Figure 16 shows the variation of film resistance with temperature between -180° and 600°C. The observed variation suggests that the conductivity is influenced by a spread of shallow impurity levels with activation energies ranging approximately between 0.04 and 0.15 eV. Attempts to determine the mobility for this film were unsuccessful, since the Hall voltage, for the small values of current which could be passed through the sample, was too low to be measured reliably.

Optical absorption was measured with the film immersed in ethyl alcohol. Figure 17 shows the spectrum obtained, together with a trace of the absorption of the spectrophotometer cell (containing alcohol) without the film. The absorption is seen to rise steadily at wavelengths less than 5000 Å, as would be expected for a material with a 2.45 eV band gap (Ref. 47). Also evident is a set of interference fringes which, using the value 3.4 for the refractive index of AlP (Ref. 46), show the film to be 9100 Å thick.

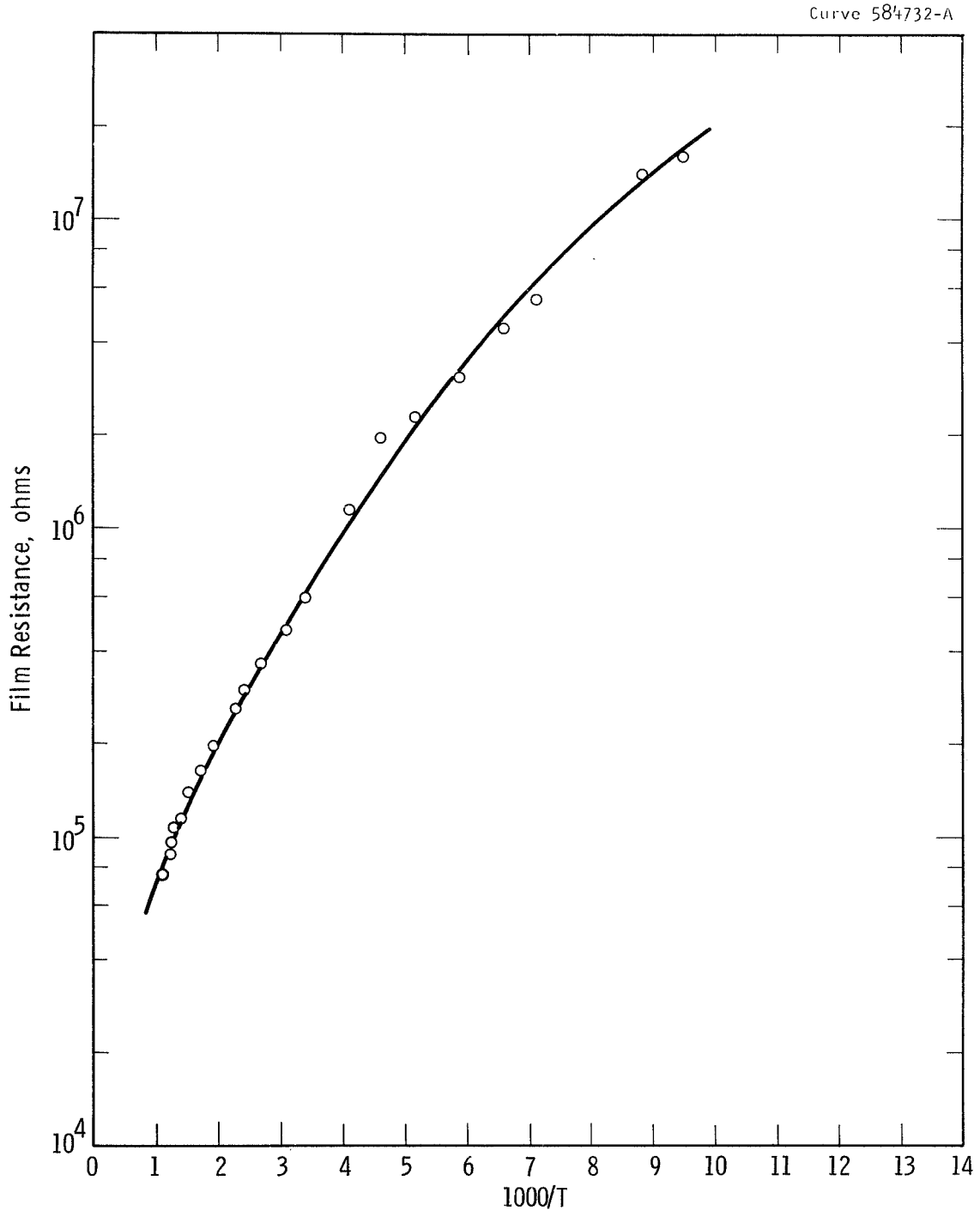

Fig. 16 Temperature dependence of resistance measured on AlP film (Z-237) deposited at 720°C, thickness 9100 A.

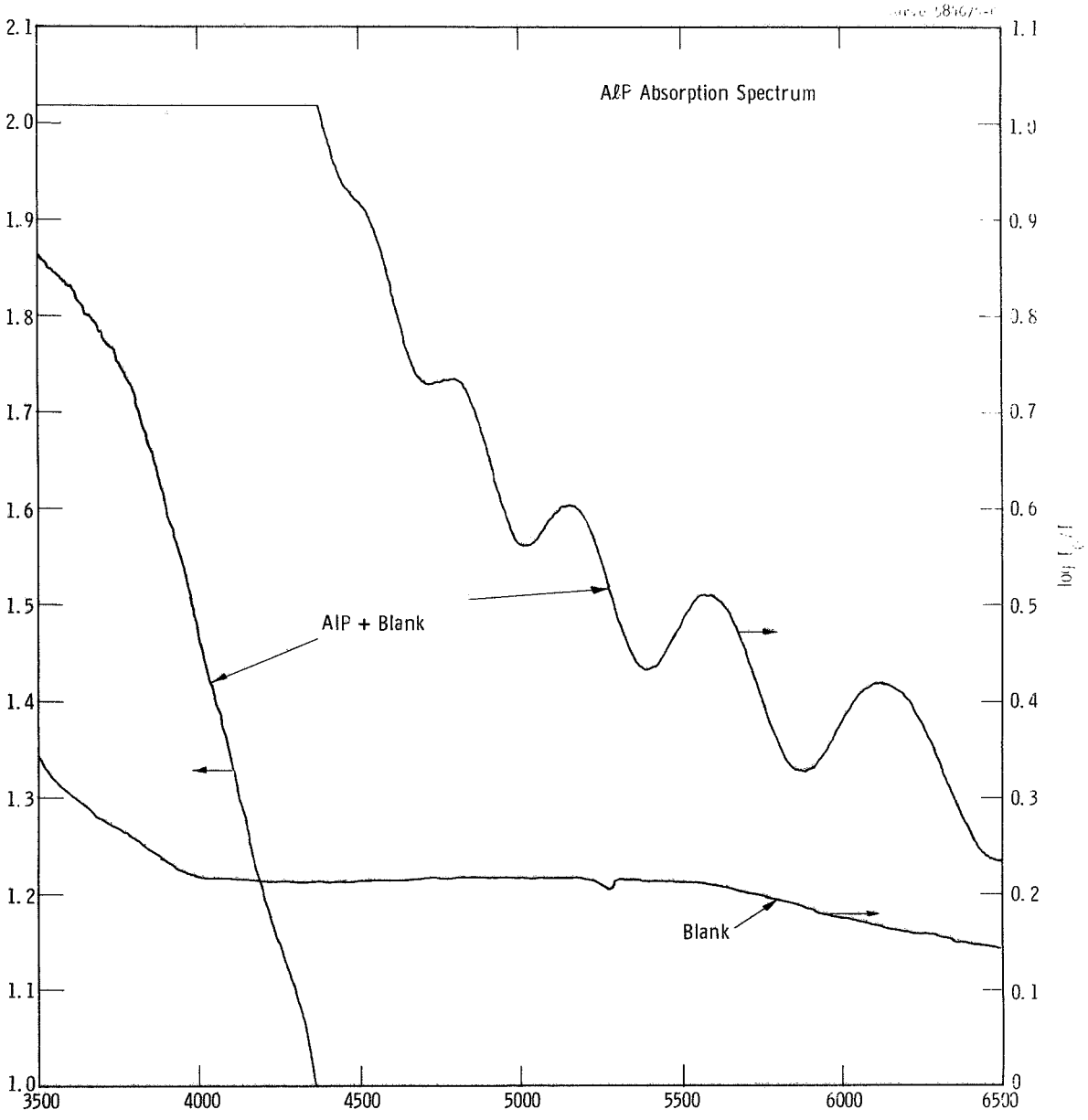

Fig. 17 Absorption spectrum of AlP film, obtained with sample immersed in ethyl alcohol. (Absorption of cell and alcohol shown as "blank".

2.5 Discussion

The results reported in the preceding sections indicate that the reactive evaporation technique is not only well suited to the preparation of films of AlSb, in confirmation of other published data, but may also be used for the growth of AlAs and AlP films. Successful preparation of stoichiometric films of the latter compounds, achieved for the first time by this method, appears favored by using conditions such that the substrate temperature exceeds the critical condensation temperatures both of the Group V elements and of aluminum, and by maintaining the vapor flux of the Group V element low enough to avoid compound formation at the Al source. This last condition is especially critical since it is difficult to achieve Al source temperatures high enough ($\sim$ 1600°C) to ensure thermal decomposition of the arsenide and phosphide compounds which might form on the surface of the molten metal. High rates of deposition, approximately 300 to 600 Å/min are attained with this method and there appears to be no difficulty in preparing films many microns in thickness.

The films, as a group, display bulk structural and optical properties. The main exception is the observation of a hexagonal wurtzite modification of AlAs in the surface layers of an Al rich deposit. Bulk type behavior is also shown in the relative chemical instabilities of AlSb, AlAs and AlP in moist air. These lead to changes in the structure and physical properties and to avoid this care must be taken immediately after preparation to protect the films prior to examination.

Ohmic contacts of good quality are achieved for the AlAs and AlP films using sputtered tantalum. The contacts to AlSb films, however, tend occasionally to be non-ohmic and electrical evaluation was complicated somewhat by the resulting barrier. The very rapid deterioration of these films makes it desirable that contacts be deposited "in situ" in order that the semiconducting properties can be observed.

Although relatively low resistivity film products were deposited, the carrier mobilities in the AlAs and AlP films were low, several orders of magnitude less than those recorded for bulk materials. The causes of low mobilities in the literature for films such as CdS, Si, Ge, GaAs, etc., are numerous; e.g., heavy compensation and attendant ionized impurity scattering (Ref. 48), grain boundary scattering (Ref. 48), dislocation scattering (Ref. 49), etc. In addition, the III-V compounds seem particularly prone to the formation of impurity bands at low impurity levels (Ref. 50). Both the observation of polycrystalline structures in the present films (with associated numerous boundaries) and the suggestion in the resistivity vs. temperature data of the presence of shallow impurity levels, seem consistent with this explanation.

3. SPUTTERED FILMS

3.1 Reactively Sputtered AlN - Diode System

3.1.1 Preparation - It is generally recognized that aluminum is one of the most difficult metals to sputter physically due to its highly resistive surface oxide which cannot easily be eliminated in the relatively high partial pressures of oxygen or water vapor encountered in conventional vacuo (10^{-5} - 10^{-6} torr). For this reason, although reference to the physical and reactive sputtering of other metals abound in the literature, virtually none is available for aluminum and its compounds.

In the present studies, it was felt that since AlN possesses the highest insulation resistance of the compounds under investigation, reactive sputtering of Al in N_2 would provide an excellent test of the feasibility of extending this method to the other Al-V compositions. To avoid the oxide retardation problem referred to above, a Varian, ion-pumped, bakeable stainless steel uhv table top system (of the VI312 type), capable of base pressures in the low 10^{-9} torr range, was used for the experiments.

The sputtering arrangement was of the simple diode type, Fig. 18, the relative cathode-anode spacing being 4 cm. A 5 cm diameter disk of aluminum (purity 99.999%) served as cathode. The anode was a larger disk, 8 cm diameter, of Ta with a rectangular cut-out measuring

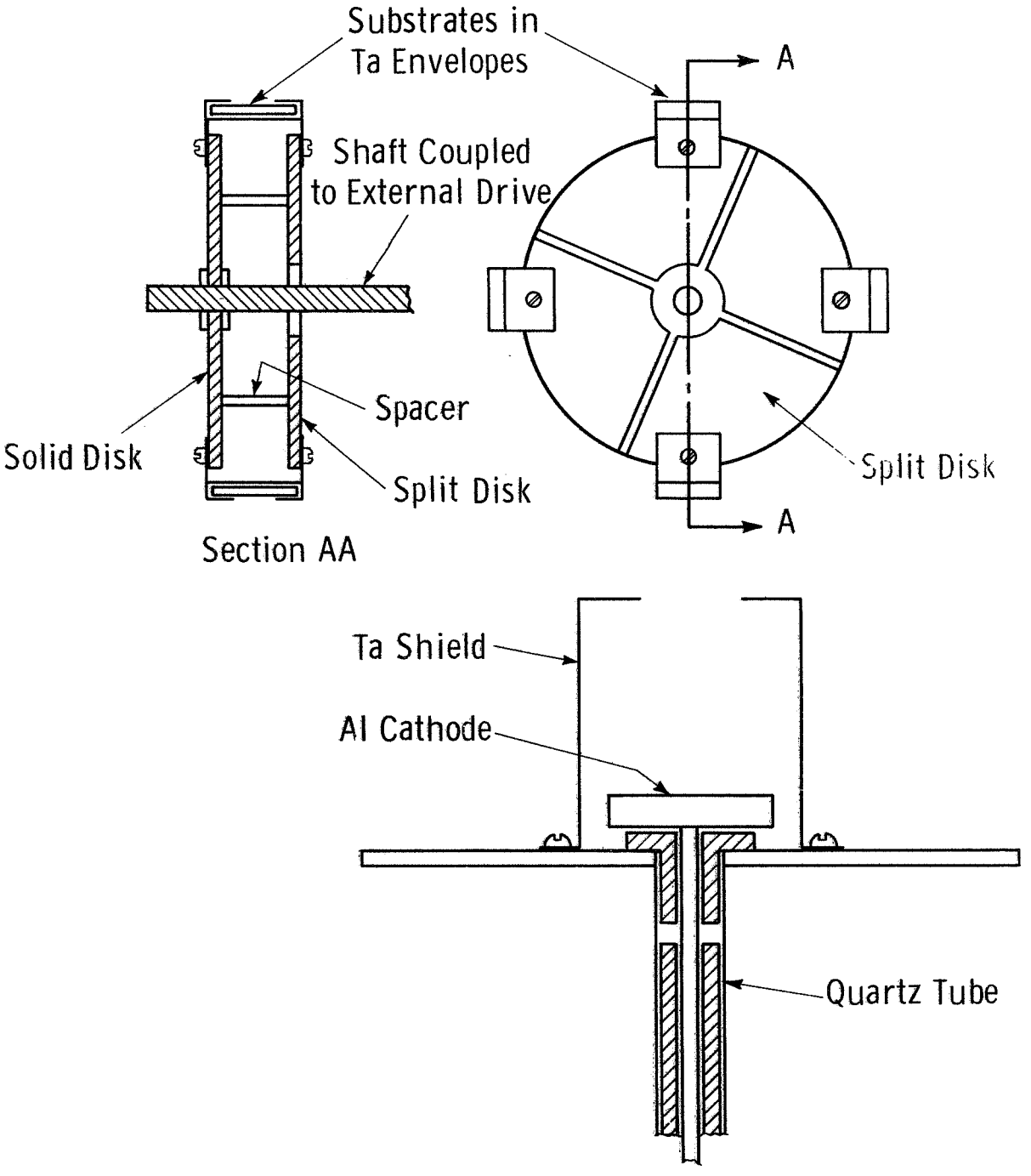

Fig. 18 Schematic of arrangement for diode reactive sputtering of AlN films. Resistive heating of substrates in Ta envelopes via the solid and split disks of the substrate holder.

2 x 1 cm at its center. Four substrates were mounted in resistively heated Ta envelopes (Si substrates could alternatively be heated directly) and could be positioned directly above the aperture in the anode by a rotatable holder externally driven. A number of different substrates were used among which were single-crystal Si, SiC, Al_2O_3 (sapphire) and vitreous SiO_2. Where possible, substrate dimensions were 10 mm x 8 mm x 2 mm. Both the sapphire and silica substrates could be used when both optical and electrical measurements were required.

When a pressure of 10^{-9} torr had been attained, the experimental chamber was isolated from the ion pump and "Research Grade" argon (impurity conc. < 5 p.p.m.) was admitted until a discharge was established. Using a static argon pressure of 80 x 10^{-3} torr, an anode-cathode potential of 2500v and a current density of 1 ma/cm^2, the cathode was sputtered until Al was observed to be deposited on a monitor silica slide. A partial pressure of about 5 x 10^{-3} torr of nitrogen (impurity conc. < 1 p.p.m.) was admitted through a needle valve, and with the discharge intact, the leak rate was adjusted until the total chamber pressure remained constant. Under these conditions, the rate of consumption of N_2 in the discharge was balanced by its rate of replacement via the needle valve.

It was reasoned that optimum stoichiometry in the films would be achieved by using substrate conditions favoring condensation only of the AlN composition. In this case, since N_2 is a permanent gas, it was necessary simply to use a chemically inert substrate and to maintain its temperature high enough to prevent the aluminum condensing alone. Most depositions were made, therefore, at temperatures higher than 550°C

which from Rhodin's (Ref. 51) earlier data on "critical temperatures" for aluminum might be expected to ensure at worst only a very small condensation rate for the metal.

3.1.2 Structure Studies - Using thin films (<1000 Å average thickness) deposited at T_s = 1100°C, 900°C, and 600°C, respectively on polished silicon, a TEM study was made to assess growth characteristics. The lateral size of crystallites was observed to increase with temperature. Typical micrographs are shown in Fig. 19 where average crystallite dimensions are 270 Å (600°C), 470 Å (900°C) and 950 Å (1100°C). The growth trend is unlike that reported for AlN prepared by chemical vapor deposition, CVD (Ref. 52); rather it conforms to established concepts of nucleation and growth by the capture of atoms or molecules at preferred substrate sites (Ref. 53,54). The trend suggests, but does not require, that the depositing species is the reaction product of aluminum and nitrogen. Electron diffraction patterns, Fig. 20, show almost complete epitaxy in the films deposited at 900° and 1100°C, the orientation relationship being $(0001)_{AlN}||(111)_{Si}$, $[11\bar{2}0]_{AlN}||[1\bar{1}0]_{Si}$. The films deposited at 600°C showed only a strong (0001)-fiber texture. In all cases the bulk hexagonal form (Ref. 55) is observed.

Substrates were heated prior to positioning above the anode aperture. Thicknesses of deposited AlN films were measured interferometrically. Some supplementary test data indicated that, with the voltage, current density and argon pressure values used to reactively sputter AlN, pure Al could be sputtered on unheated substrates at rates in excess of 200 Å/min. The AlN growth rates under these conditions were only 50-100 Å/min. At high temperatures, rates ranged between 10-30 Å/min.

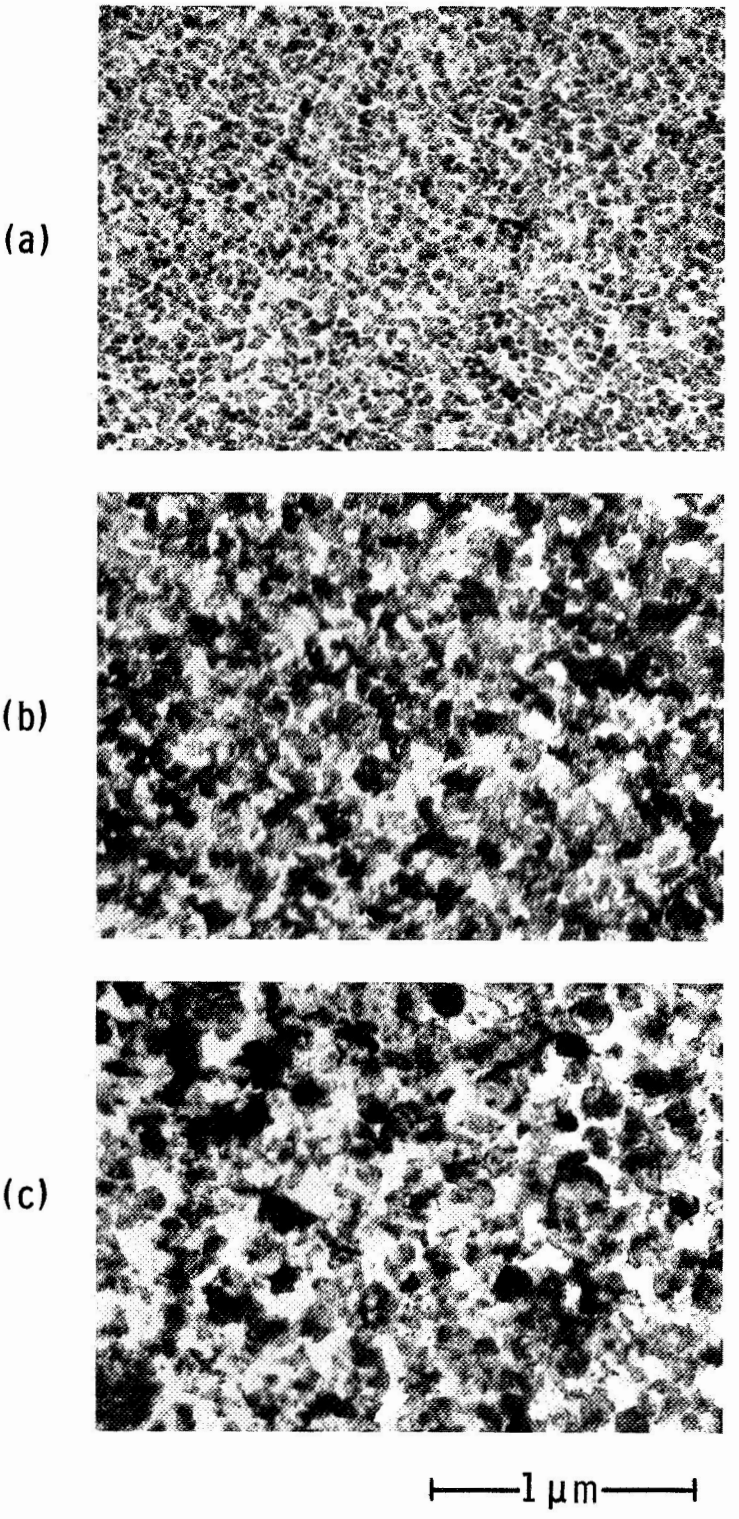

Fig. 19 Electron micrographs from reactively sputtered films of AlN on resistively heated Si substrates, (a) T_s = 600°C; (b) T_s = 925°C; (c) T_s = 1150°C. Average film thicknesses = 1000 Å. 61

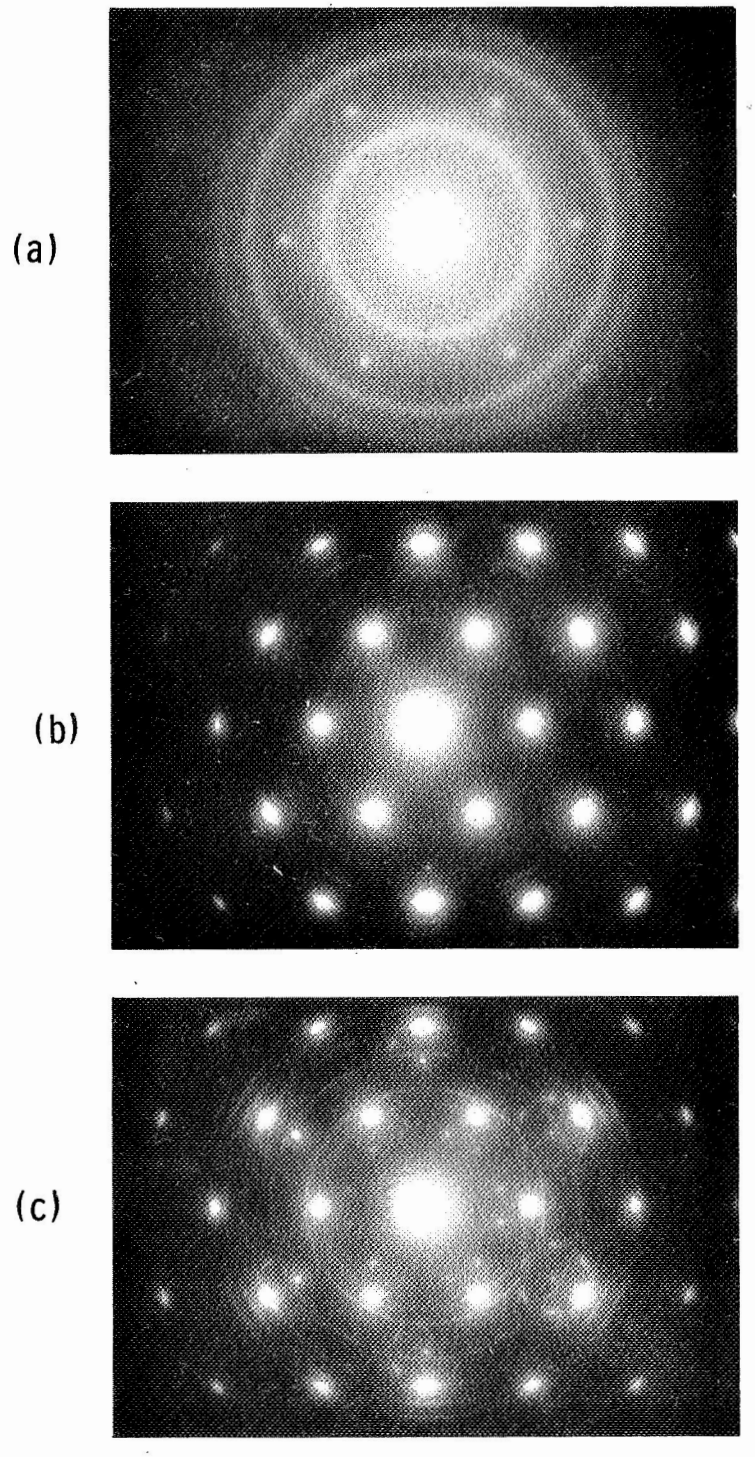

Fig. 20 Electron diffraction patterns from reactively sputtered films of AlN on resistively heated Si substrates, (a) T_s = 600°C; (b) T_s = 925°C; (c) T_s = 1150°C. Average film thicknesses = 1000 Å.

Orientations on substrates which could not be so easily thinned were examined by a reflection diffraction technique. These included SiC, CaF_2 and Al_2O_3 and results are summarized in Table IV.

Epitaxy is observed in deposits on SiC, Fig. 21, and sometimes on Al_2O_3. The former occurs near 1300°C, the orientation of the epitaxial component being:

$$(00.1)_{AlN} \;//\; (001)_{SiC}$$

$$[11.0]_{AlN} \;//\; [11.0]_{SiC} \;.$$

The latter (AlN/Al_2O_3) relationship is discussed in Sec. 3.3.5.

3.1.3 Chemical Stability - In view of the rapid deterioration observed in the structure and optical properties of the AlSb films on exposure to the atmosphere, it was decided to check on the chemical resistance of AlN films to high temperature oxidation. Film samples prepared on Si substrates were allowed to age for several weeks then were re-examined by reflection electron diffraction and by glancing-angle X-ray diffraction. They were found still to display well-crystallized and oriented single-phase structures. The films were then heated in air for periods typically between 15 and 30 minutes at temperatures ranging from 250°C to 750°C. No change in the electron or X-ray diffraction patterns was observed until the temperature exceeded 700°C, when the electron diffraction pattern showed an increase in the diffuse background scattering. The structure change appeared to have been confined to the film surface, however, since the X-ray pattern showed only slight broadening in the diffraction lines. Moreover, the X-ray pattern was

Table IV Electron Diffraction Data for Reactively Sputtered AlN Films

Sample No.	Substrate	T_s(°C)	Thickness (Å)	Remarks
185	Si(111)	27	2500	Crystalline but no orientation
186-2	Si(111)	∿500	600	weak (0001)-fiber texture
188-2	Si(111)	800	5000	(0001)-fiber texture
188-3	Si(111)	1000	5000	epitaxial AlN(0001)
191-1	Si(111)	950	2500	strong (0001)-fiber te: ture (tending towards epitaxy)
191-2	Si(111)	900	2500	(0001)-fiber texture (Not epitaxial)
192-1	SiC(0001)	1300	1900	mostly epitaxial AlN(0(--some ring component
192-2	CaF_2(111)	800	600	(0001)-fiber texture
192-3	CaF_2(111)	600	2500	(0001)-fiber texture
284A	Al_2O_3	875	1200	(0001)-fiber texture
305B	Al_2O_3	760	1200	epitaxial AlN(0001) but with some relative azimuthal variation

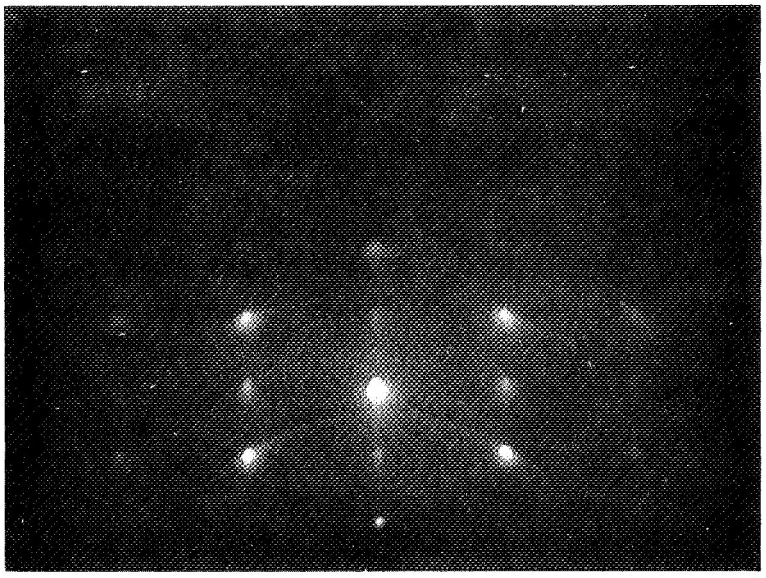

(a)

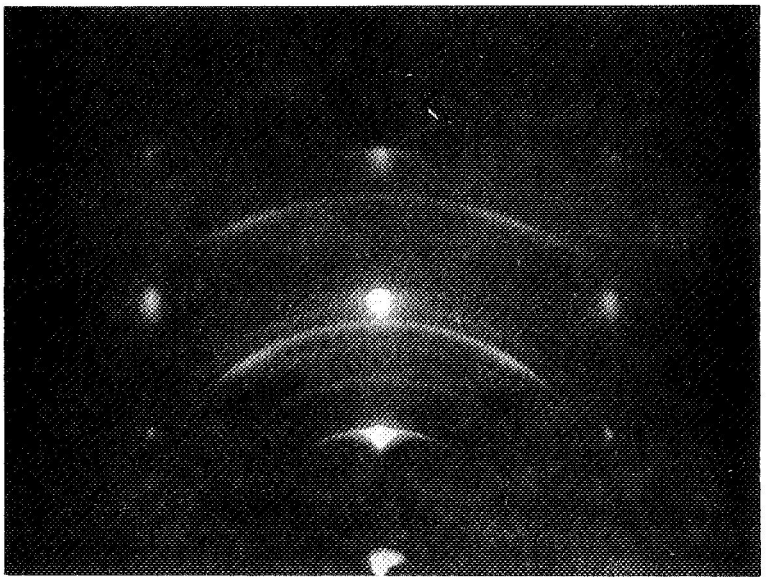

(b)

Fig. 21 Electron diffraction patterns of AlN films reactively sputtered on (0001) faces of 6H-type SiC crystals: electron beam along (a) [11.0] and (b) [10.0]. 65

essentially unchanged even after oxidizing for several hours at 750°C. AlN films thus possess a far higher resistance to chemical attack than do the other Al-V compounds.

3.1.4 Optical Measurements I - Ultraviolet - In general, qualitative examination of the optical spectra confirmed that the films were AlN. Quantitative comparisons, however, indicated that certain prominent features of the spectra were influenced by effects due to impurities or structural disorder in the films.

Data from sample Z-192-3, AlN/CaF_2, deposited at 600°C are presented in Fig. 22. A Cary Spectrophotometer was used to obtain the data. The absorption is seen to rise monotonically as a function of energy. Various values for the energy gap could be obtained for this film, depending on the energy function plotted. More meaningful, however, is a comparison to the data of Cox et al. (Ref. 56) who measured the absorption spectra for thin AlN single crystal platelets. Their data, shown in Fig. 23, give the absorption spectra for an as-grown AlN single crystal together with an absorption trace for the same crystal after annealing for 2 hours at 1100°C in argon. The data in Fig. 22, when normalized to the same value as that of Cox et al. at wavelengths greater than 3600 A, show an increasing absorption that closely parallels that of their Ar-annealed crystal, although the correspondence is not exact. Cox et al. (Ref. 56) interpret the absorption-increase caused by argon annealing as being due to nitrogen vacancy formation. In Fig. 23, we also show the absorption spectra of two films of reactively sputtered AlN which have been prepared to nearly identical thicknesses on silica, after

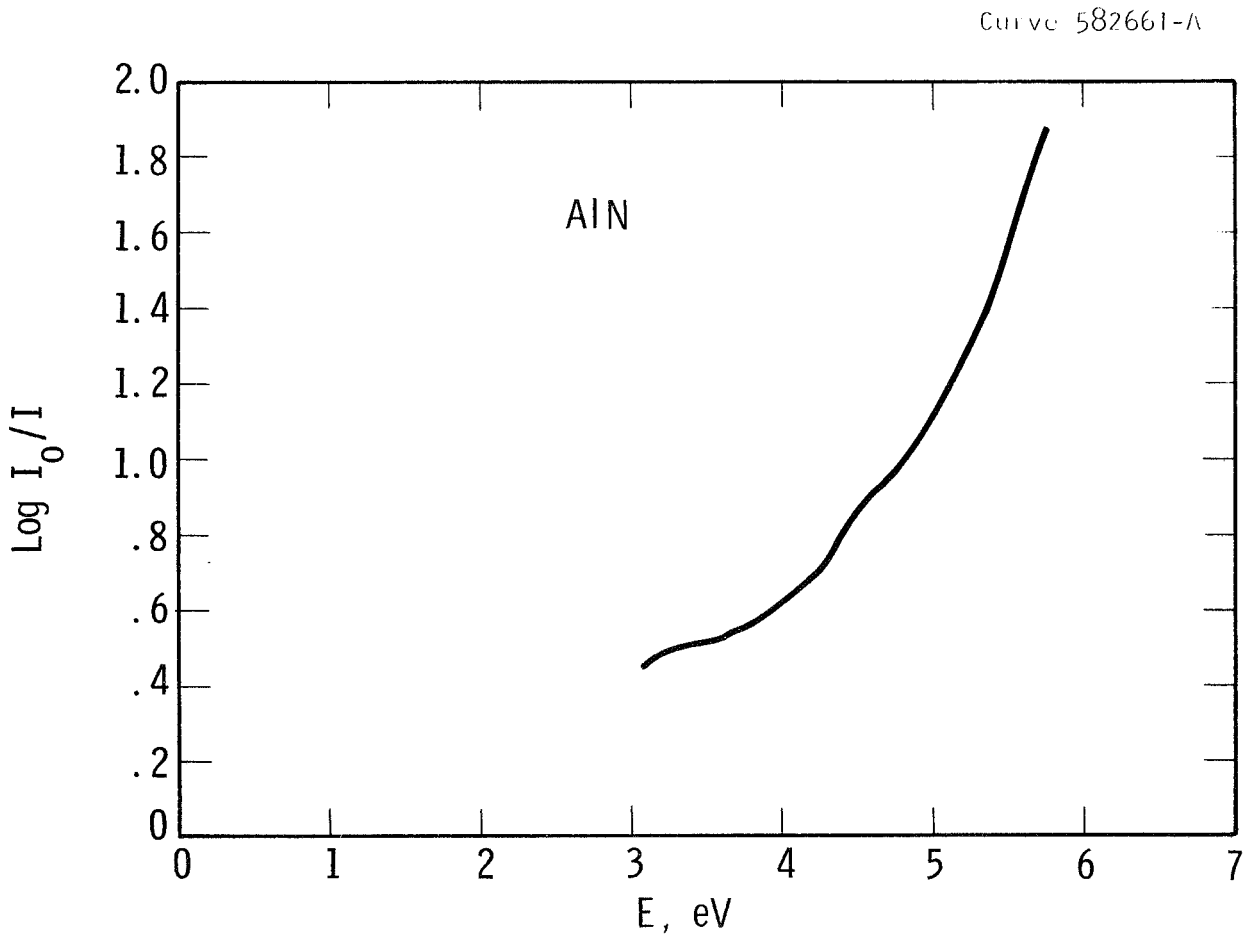

Fig. 22 Absorption spectrum of AlN film on CaF_2.

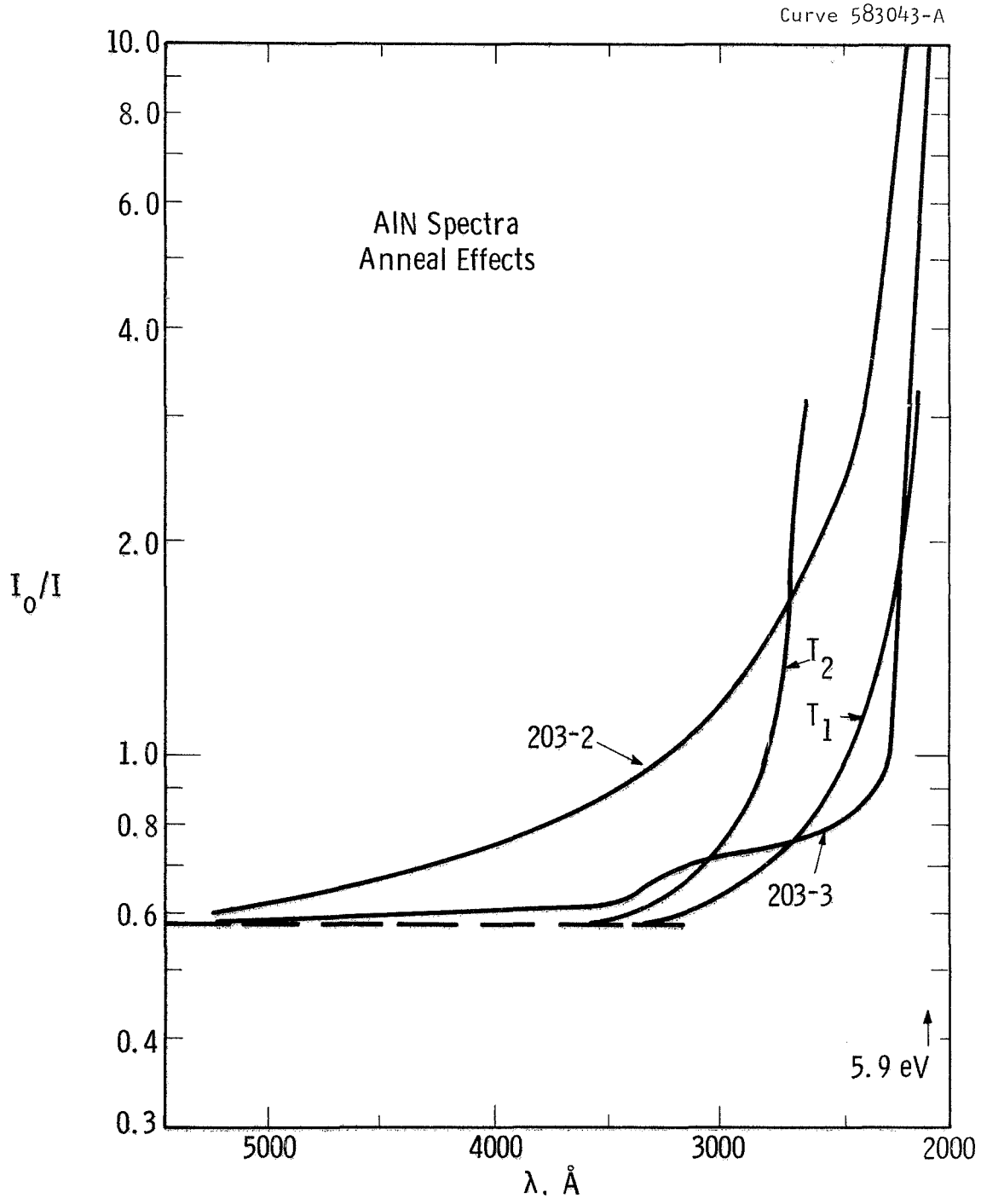

Fig. 23 Optical absorption data comparing properties of reactively sputtered AlN to bulk single crystals. Film Z-203-2 is an as-grown film; film Z-203-3 has been similarly deposited but has been annealed at 900°C in N_2. T_1 is an as-grown crystal (Cox, et al.). T_2 is a crystal annealed in Argon.

which one was annealed in nitrogen at 900°C for 2 hours. The data showed that, after annealing, the absorption of energies less than E_g (bulk) decreased and that a bulk spectrum was observed.

Changes in the spectrum were emphasized by obtaining a differential spectrum by placing the N_2 annealed film in the reference compartment of the Cary, and the unannealed film in the regular sample compartment, Fig. 24. It can be seen that there are significant changes at 4.42, 3.75, and 2.8 eV. The feature of 5.05 eV may be an instrumental artifact, since the slits are opening rapidly in this wavelength region.

The differential spectrum shows that the number of mid-gap states is significantly reduced by the nitrogen anneal. It also shows that a significant ordering of the structure takes place. The reduction in state density is indicated by the reduction of the absorption, while the ordering is indicated by the appearance of discrete absorption thresholds rather than the monotonically increasing absorption found in the as-grown films.

To insure that the shift of band-edge position in the N_2 annealed films was not due to an effect generated by a particular type of substrate a set of four AlN films were deposited to a thickness of 8000 Å at about 800°C, two on the (0001) face of sapphire (Al_2O_3) and two on vitreous silica, and examined optically in annealed and unannealed states. The results are shown in Fig. 25, and indicate that these substrate materials did not affect the position of the absorption edge nor the general details of the absorption curves. We thus were led to conclude that the shift was associated with a built-in surplus of Ar trapped during

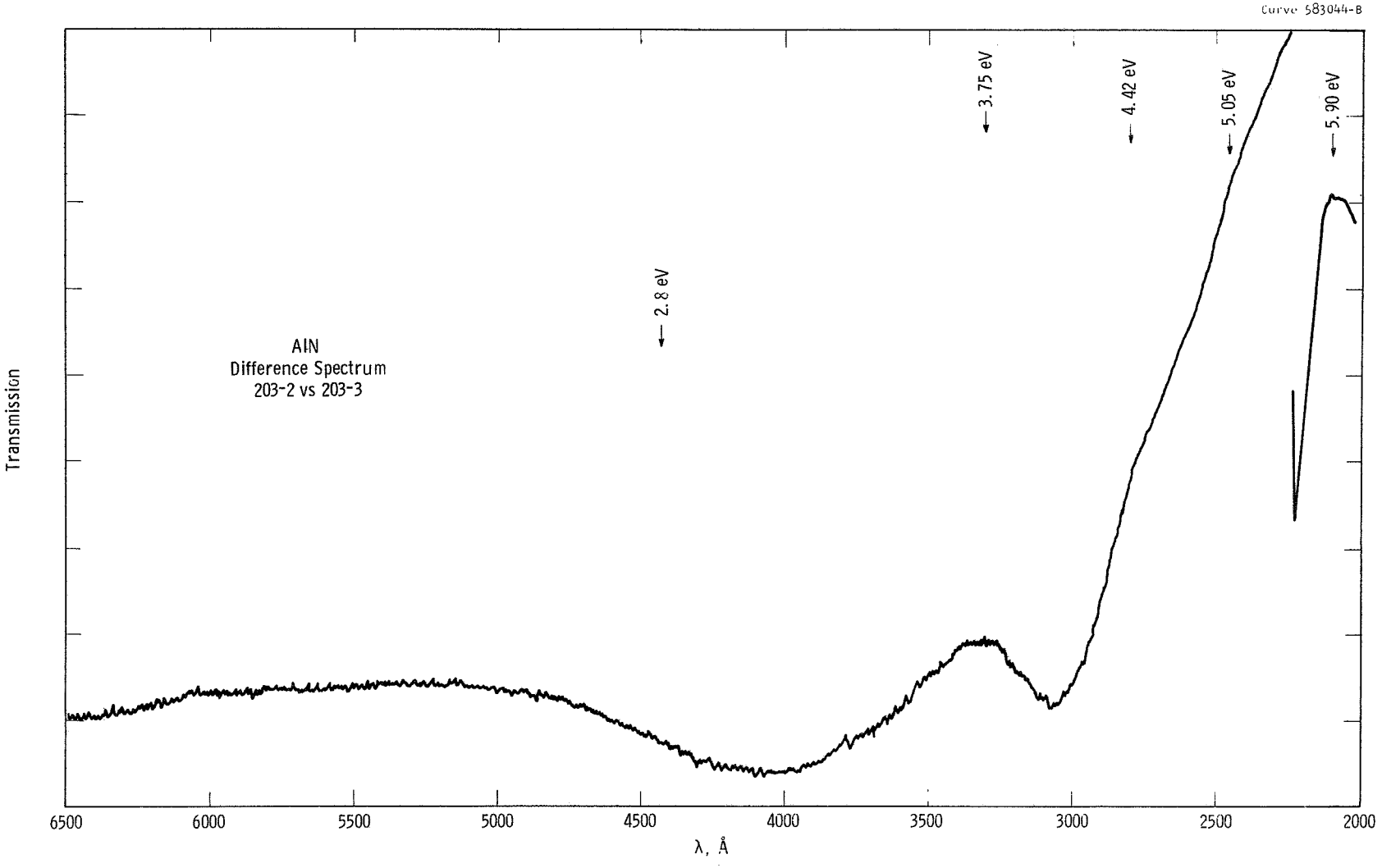

Fig. 24 Absorption difference spectrum obtained from nitrogen anneal of sputtered AlN film.

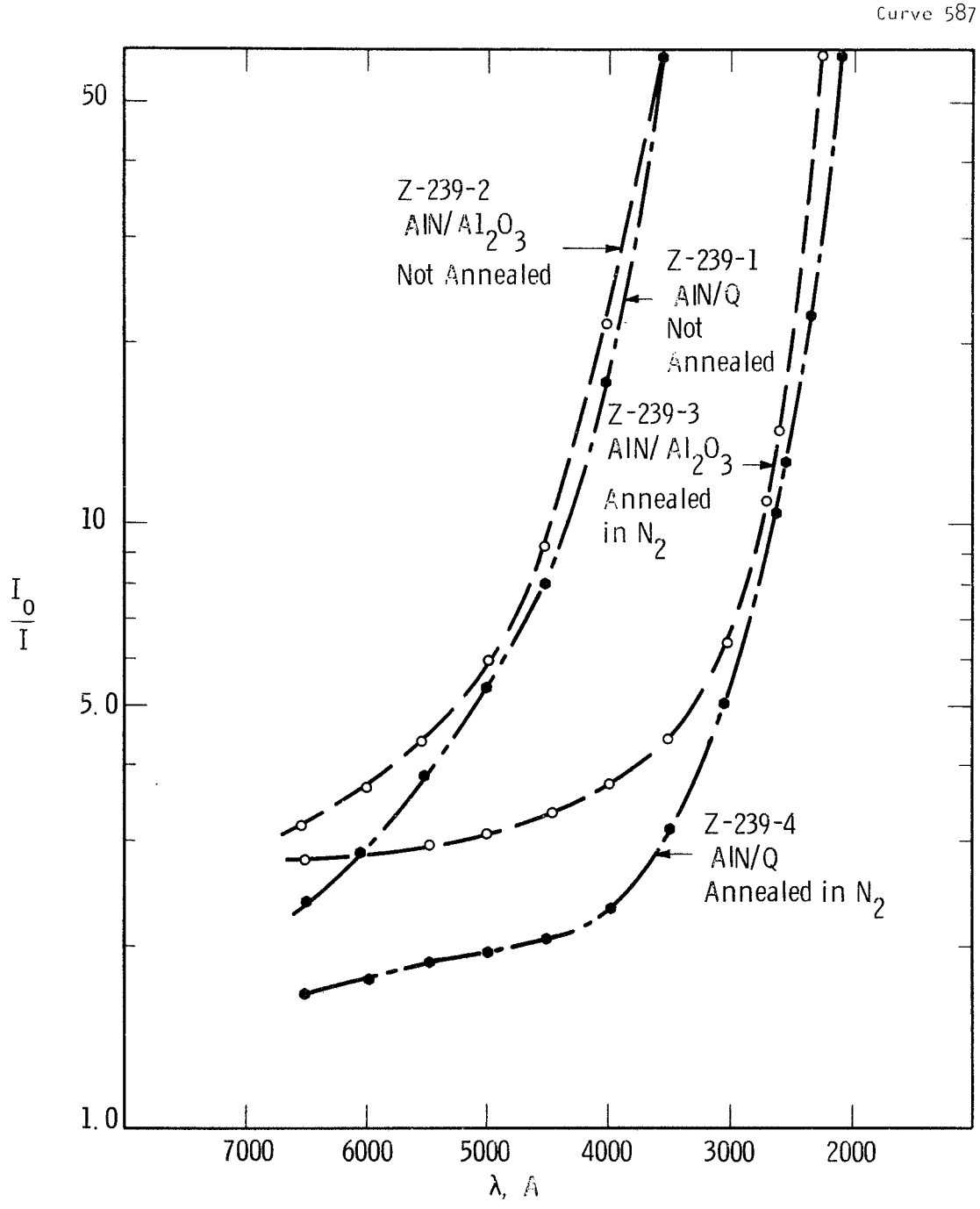

Fig. 25 Optical absorption in four AlN films, thickness 8000 A, deposited on vitreous silica and sapphire under same sputtering conditions. One film on each substrate was given standard annealing treatment in nitrogen.

deposition in the growing film. The excess Ar may partly replace nitrogen and produce a nitrogen deficiency condition not dissimilar to that reported for Ar annealed bulk crystals (Ref. 56).

Determination of an accurate value for the absorption edge of AlN films was made by evaluation of measurements performed in a precision ultraviolet spectrophotometer. The apparatus was capable of detecting I/I_o ratios of 10^{-6}. In the present experiments detection of a ratio of 10^{-4} was sufficient. The substrates in each case were high purity silica ("Suprasil") which is not absorbent in the near ultraviolet. Figures 26 and 27 show transmittance data for 3000 Å and 4500 Å films, respectively. Deposition temperatures were 950°C. The position of the absorption edge was determined by the intersection of the almost horizontal (negligible absorption) curve with an extension of the curve at maximum slope (strong absorption). Figures 28 and 29 show transmittance data from a pair of 1 μm films. The data indicate a negligible shift ($\pm$ 0.03 eV) of the absorption edge in the "as-deposited" state. The absence of the absorption edge shift is puzzling but we believe it is associated with the high deposition temperature ($\sim$950°C) used during these experiments; we note in later experiments on BN that a maximum shift occurs in as-deposited room temperature deposits. The shift appears less pronounced in as-deposited films prepared at higher temperatures. The average absorption edge, making use of the data contained in Figs. 26 through 28, is located at 5.90 $\pm$ 0.08 eV. A replotting of the steeply sloping portions of the curves in Figs. 26 through 29 using $\alpha \propto (h\nu - E_g)^{1/2}$ as the ordinate where α is the absorption coefficient, $h\nu$ is the photon energy and E_g is the band gap, resulted in linear plots and indicated

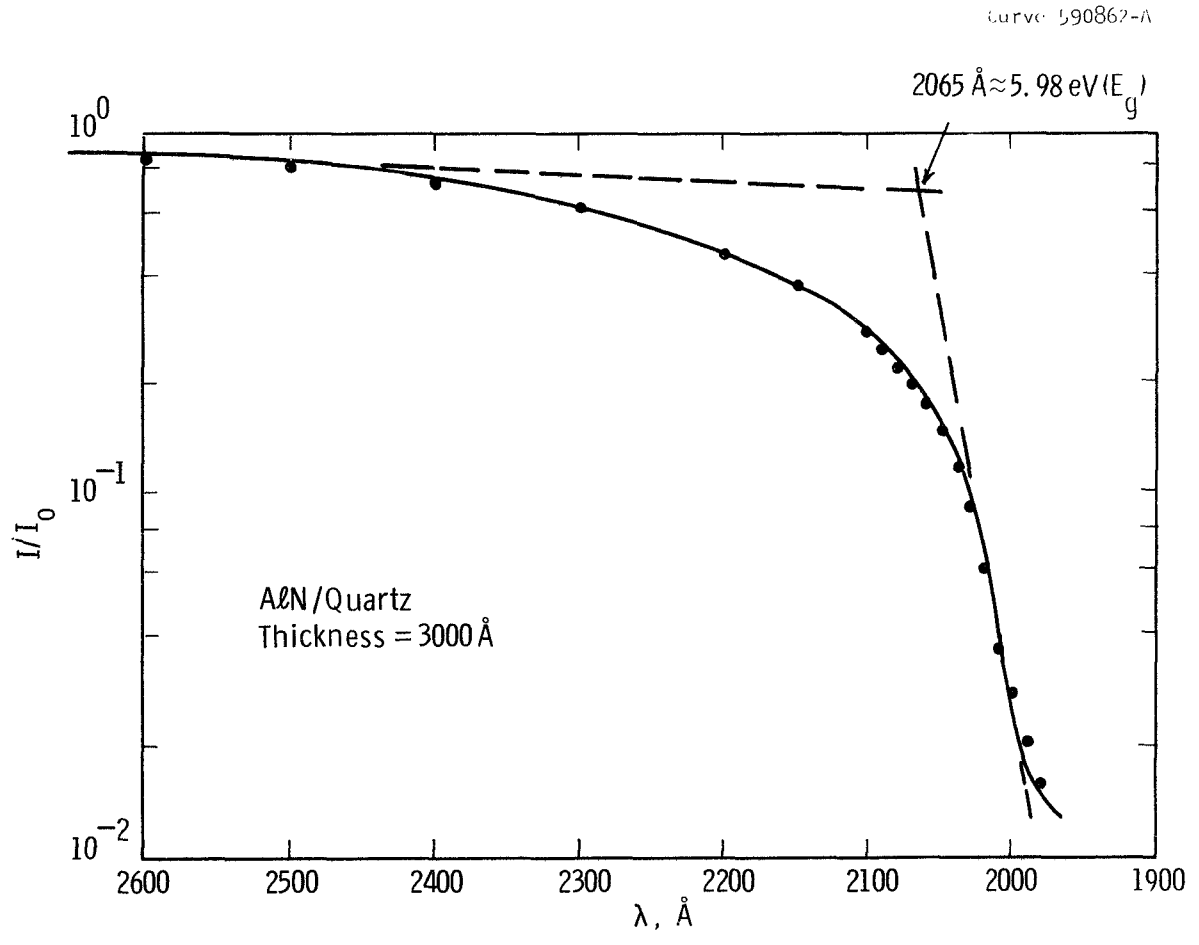

Fig. 26 Transmittance data (uv) for unannealed AlN film; thicknesses = 3000 Å. Data normalized so that $I/I_o = 1$ at λ = 3000 Å.

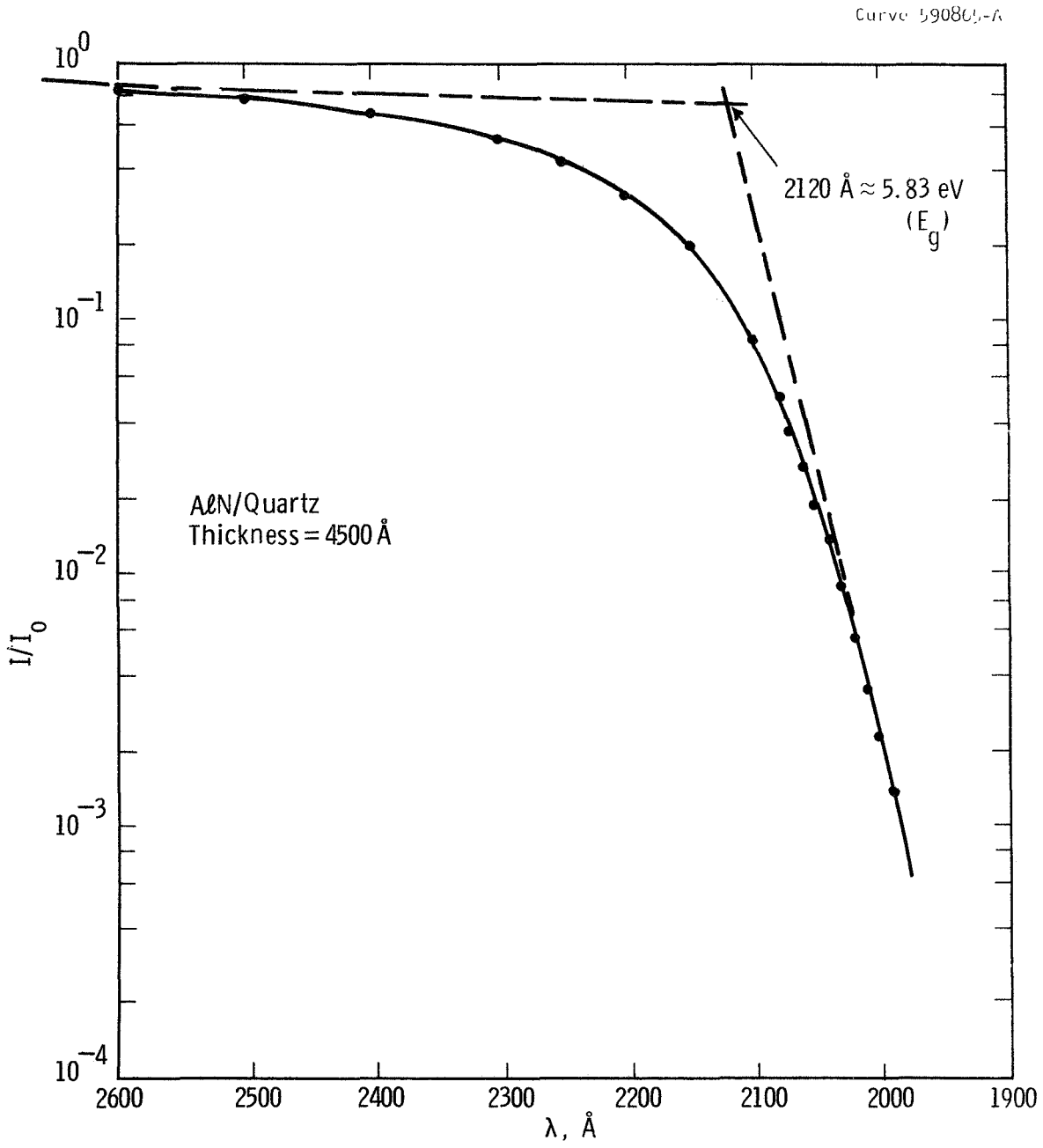

Fig. 27 Transmittance data (uv) for unannealed AlN film; thickness = 4500 Å. Data normalized so that $I/I_o = 1$ at $\lambda = 3000$ Å.

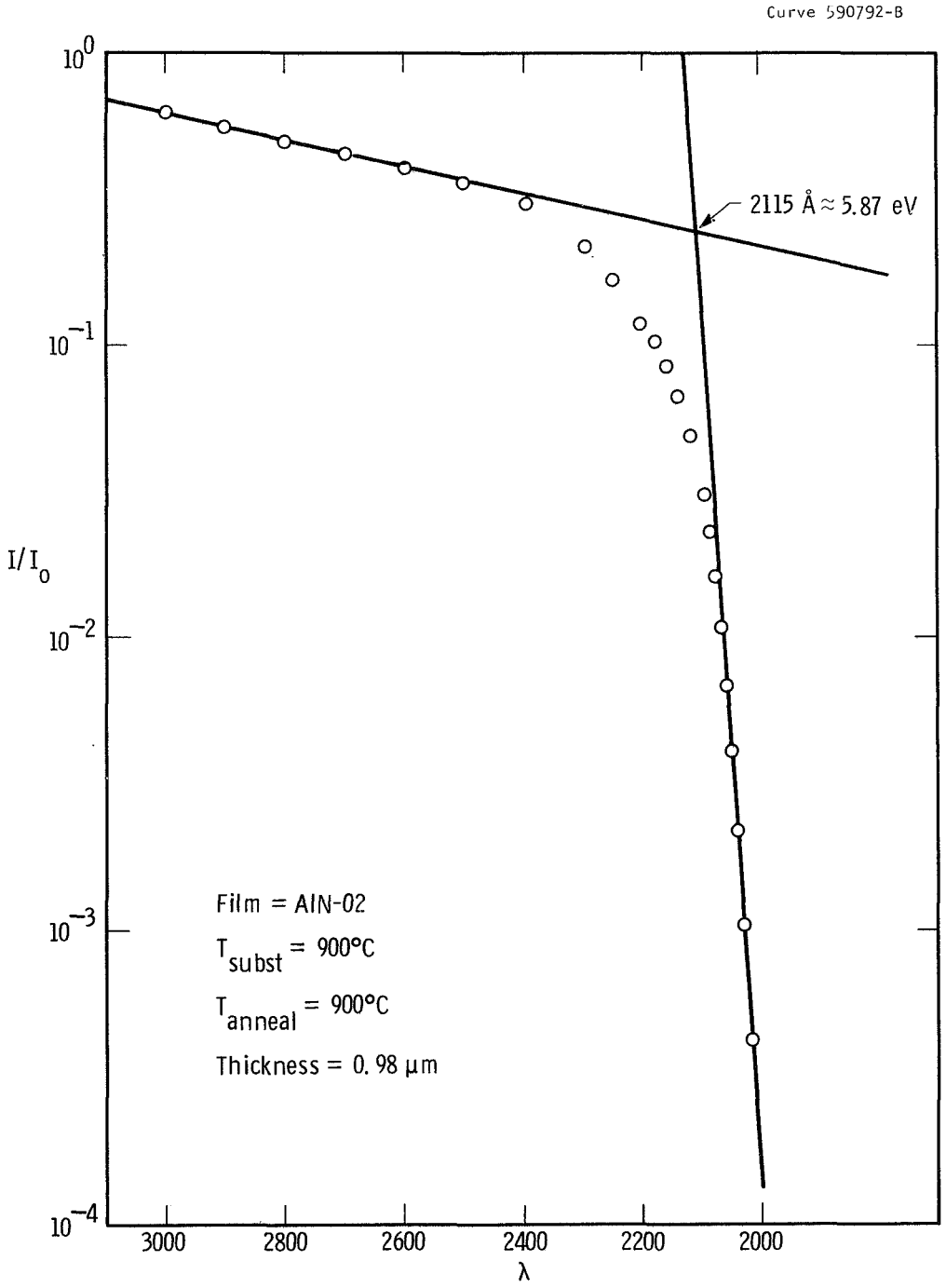

Fig. 28 Transmittance (ultraviolet) curve of AlN film deposited on "Suprasil" ultra-pure quartz. Annealed in N_2.

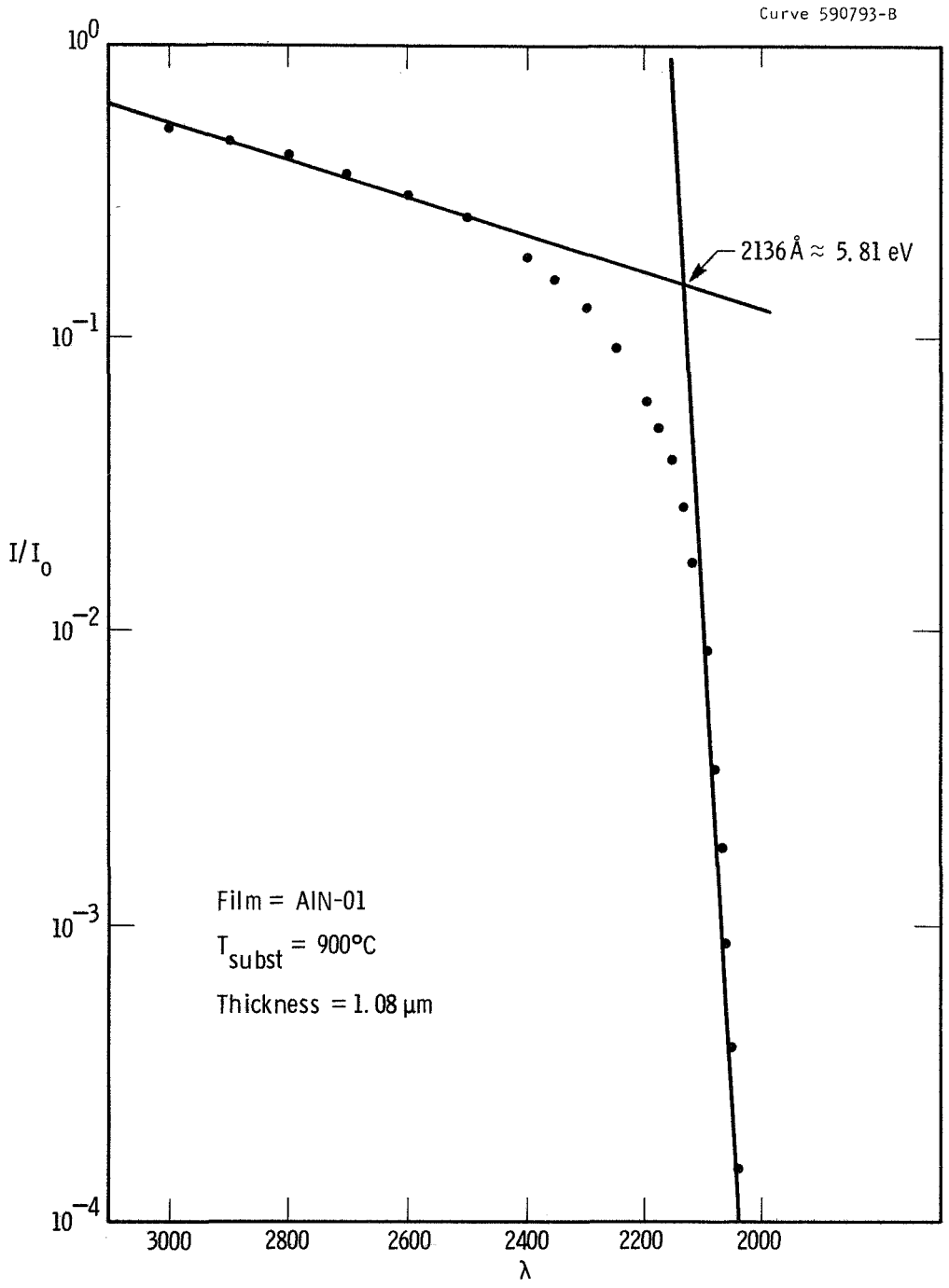

Fig. 29 Transmittance (ultraviolet) curve of AlN film deposited on "Suprasil" ultra-pure quartz. No anneal.

that the associated electronic transitions were of the direct type (Ref. 57). Figure 30, the transmittance data from a relatively thick film, ∿3 μm, showed negligible transmittance ($I/I_o < 10^{-6}$) at wavelengths slightly greater than the previously measured (thin film data) absorption edge. The film has a considerable thickness, however, and much of the absorption effect is considered as due to light scattering within the film. When film uv transmittance data is compared to bulk single crystal data, an obvious discrepancy is noted, viz., that the value of absorption coefficient at a given thickness is greater in the films by an order of magnitude or more. This discrepancy is almost certainly the result of scattering at grain boundaries which are inherent to the mosaic structured films. It is thus concluded that data relating absolute values of absorption coefficient cannot be obtained from such deposits.

Figure 31 shows reflectance data from a deposit (at 950°C, 1 μm thick) prepared on a silicon web surface. Such surfaces are considered atomically smooth. This experiment was a minor disappointment since some absorption structure was anticipated in the wavelength range below 2000 Å. Instead, only a broad peak is observed at 1600 Å (7.7 eV). This peak is likely to be associated with strong reflection (analogously, SiC shows a strong peak at 7.8 eV) (Ref. 58), but the amplitude I_R/I_o is, in this case, greatly attenuated by scattering in the mosaic-like structure. The peaks at longer wavelengths are due to interference effects at the nitride-silicon interface (functions of film thickness). Attenuation of these peaks in a wavelength range lower than the absorption edge is evident.

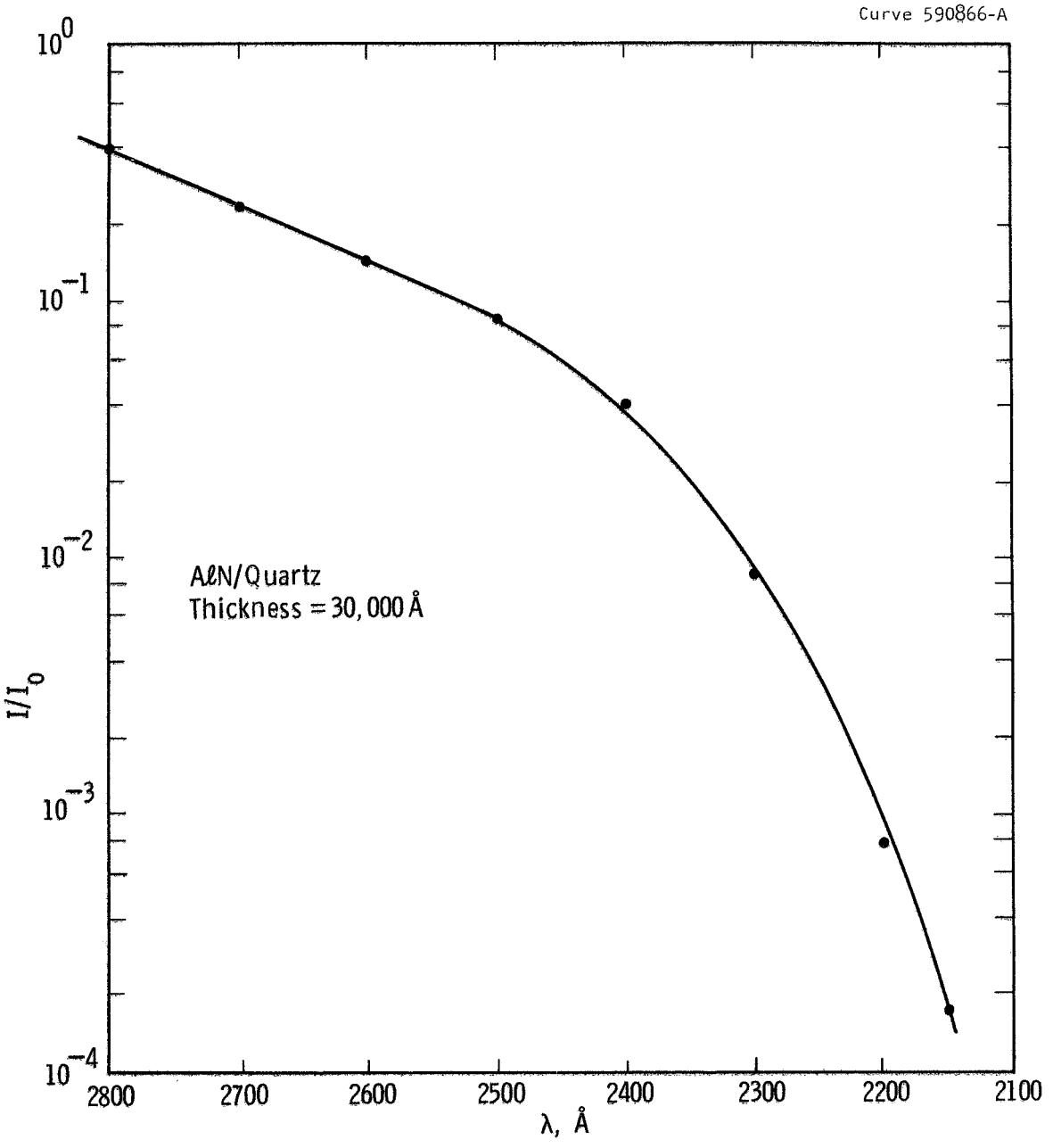

Fig. 30 Transmittance data (uv) for unannealed AlN film; thickness = 30,000 Å. Data normalized so that $I/I_o = 1$ at $\lambda = 3000$ Å.

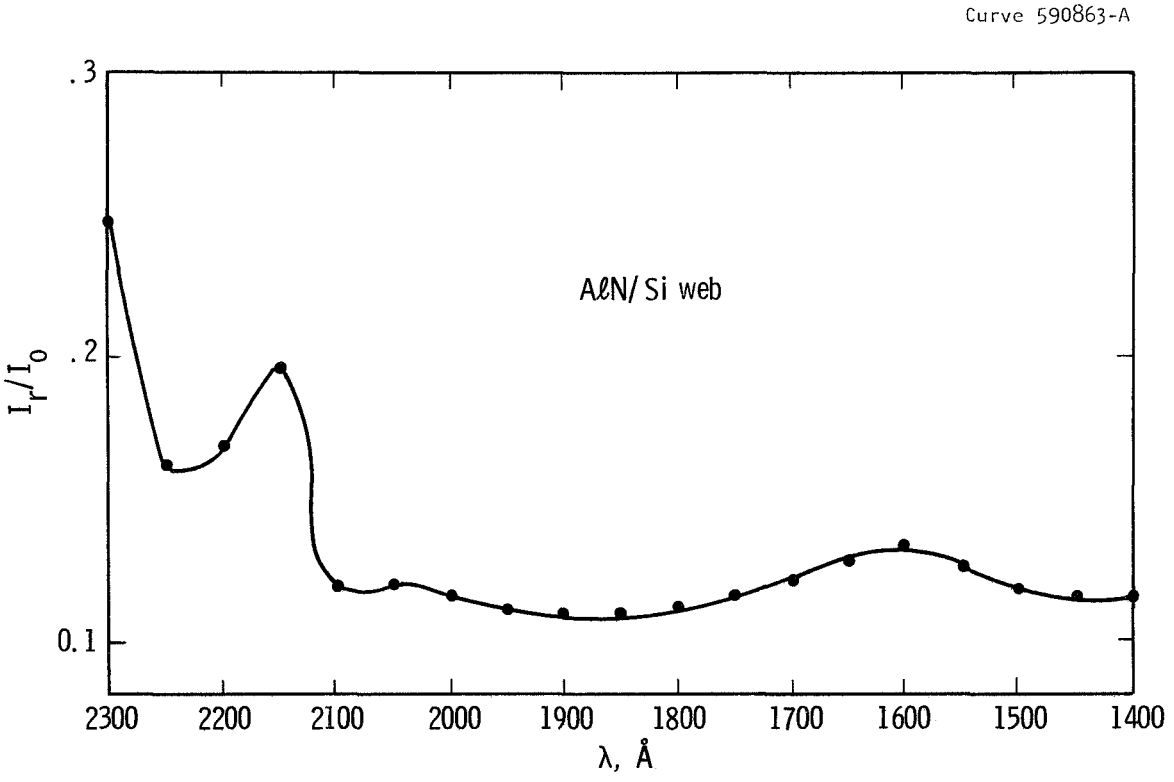

Fig. 31 Reflectance spectra taken from AlN film deposited on Si web substrate. Broad peak (1600 Å) is characteristic of mosaic film structure.

3.1.5 Optical Measurements II - Infrared - When the films described in preceding section were examined in an infrared spectrophotometer, no prominent absorption bands were observed over a wavelength range 4 to 14 μm. The relative absence of absorption spectra is due to the small thicknesses of the films; bulk data (Ref. 7) indicate that optimum crystal thickness for the measurement of absorption coefficient in this wavelength range is 25 μm.

3.1.6 Dielectric Properties - A comparison was made of the capacitive properties of reactively sputtered AlN films with those of the bulk material. To obtain a representative result for given deposition conditions, capacitor structures based on a metal-nitride-metal sandwich arrangement were constructed. These consisted of base electrodes, those in immediate contact with the substrate, of sputtered Ta, 2500 Å thick. Such films either covered the entire substrate or only part of it, the latter configuration being chosen to permit optical evaluation. After an AlN film was deposited, no intentional heating of substrates was attempted during the electroding schedules. The counter-electrode configuration was an hexagonal array of 0.3 mm dots on 0.5 mm centers, thus approximately 200 individual test samples were available on a given substrate.

Capacitance measurements were made over a frequency range between 1 and 100 kHz with an impedance bridge (General Radio Type 1608-A). When Ta/AlN/Ta sandwiches were examined the effects the temperature change could be observed between 25° and 500°C, heating taking place in a 10^{-5} torr vacuum to prevent oxidation of the electrodes. Attempts

to use gold or aluminum electroded sandwich structures in similar experiments were unsuccessful, the main difficulty being caused by peeling of the counter-electrode as the temperature was raised. Room temperature measurements were also made using the Au/AlN/Ta and Al/AlN/Ta sandwiches and were in excellent agreement with those using the Ta electrodes.

Reproducible measurements were obtained from films in the thickness range 0.15 to 5 microns. Films with thicknesses less than 0.15 micron demonstrated an erratic behavior under applied voltages, the breakdown being attributed to leakage at grain boundaries. The following dielectric data thus are based on the properties of the thicker films.

At 25°C and 1 kHz, measurements of capacitance yielded a dielectric constant, $\varepsilon/\varepsilon_o$, of about 8.5 in good agreement with that for the bulk. The film dielectric proved to have a slight frequency dependence and variations of $\varepsilon/\varepsilon_o$ with temperature up to 500°C for several frequencies are shown in Fig. 32. Some comparative selected bulk data (Ref. 5) are also shown. The temperature dependence of $\varepsilon/\varepsilon_o$ for the film differed from that for the bulk, the former being insensitive to temperature up to 350°C and at this limit still retaining a room temperature value. The dielectric constant for the bulk material at 350°C and 1 kHz shows a three-fold increase over the room temperature value.

The dissipation factor, D, as a function of temperature is shown in Fig. 33. Again, there is little temperature variation up to 350°C whereas the bulk data (Ref. 5) indicate approximately two orders

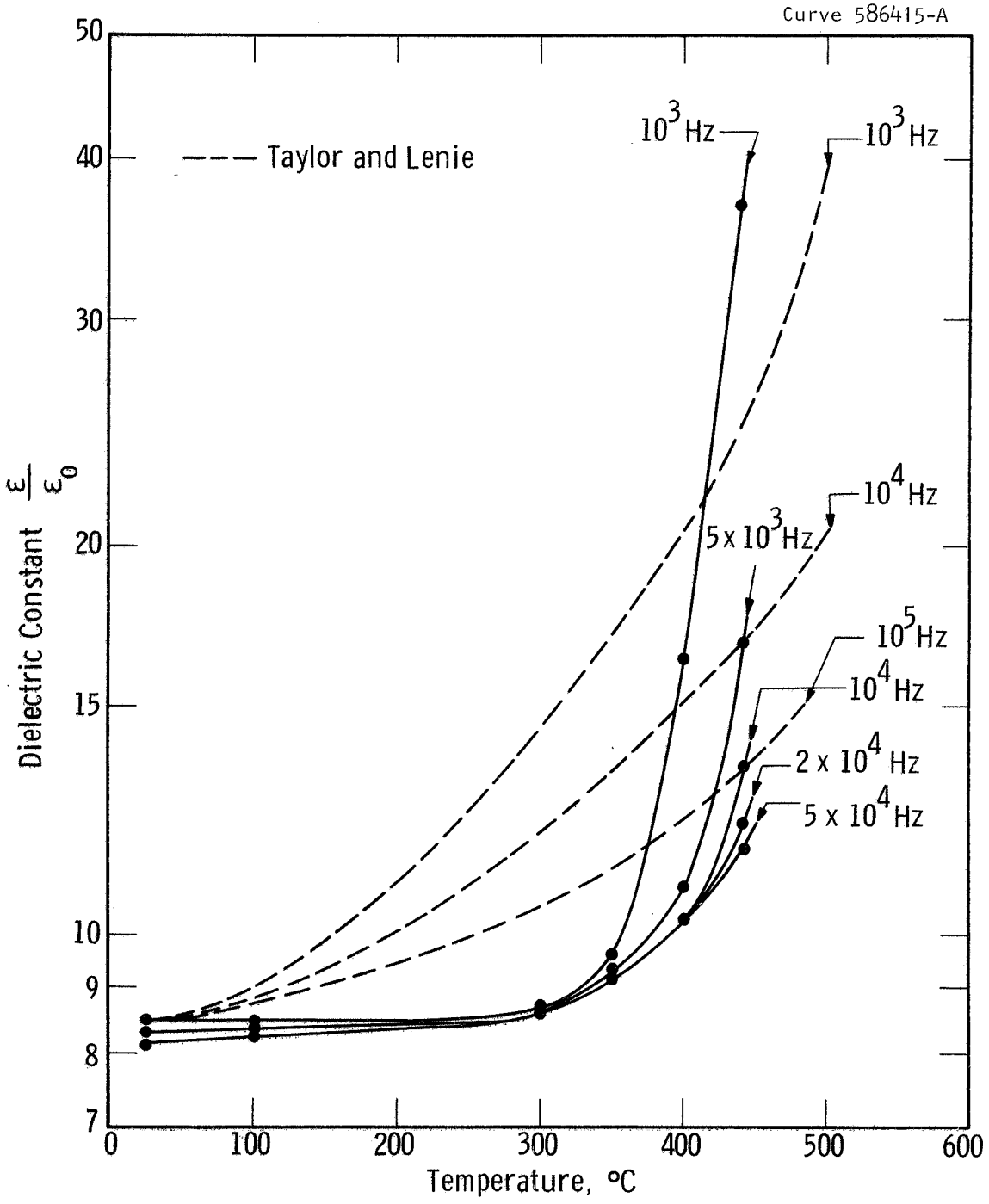

Fig. 32 Variation of dielectric constant, $\varepsilon/\varepsilon_o$, with temperature at several frequencies.

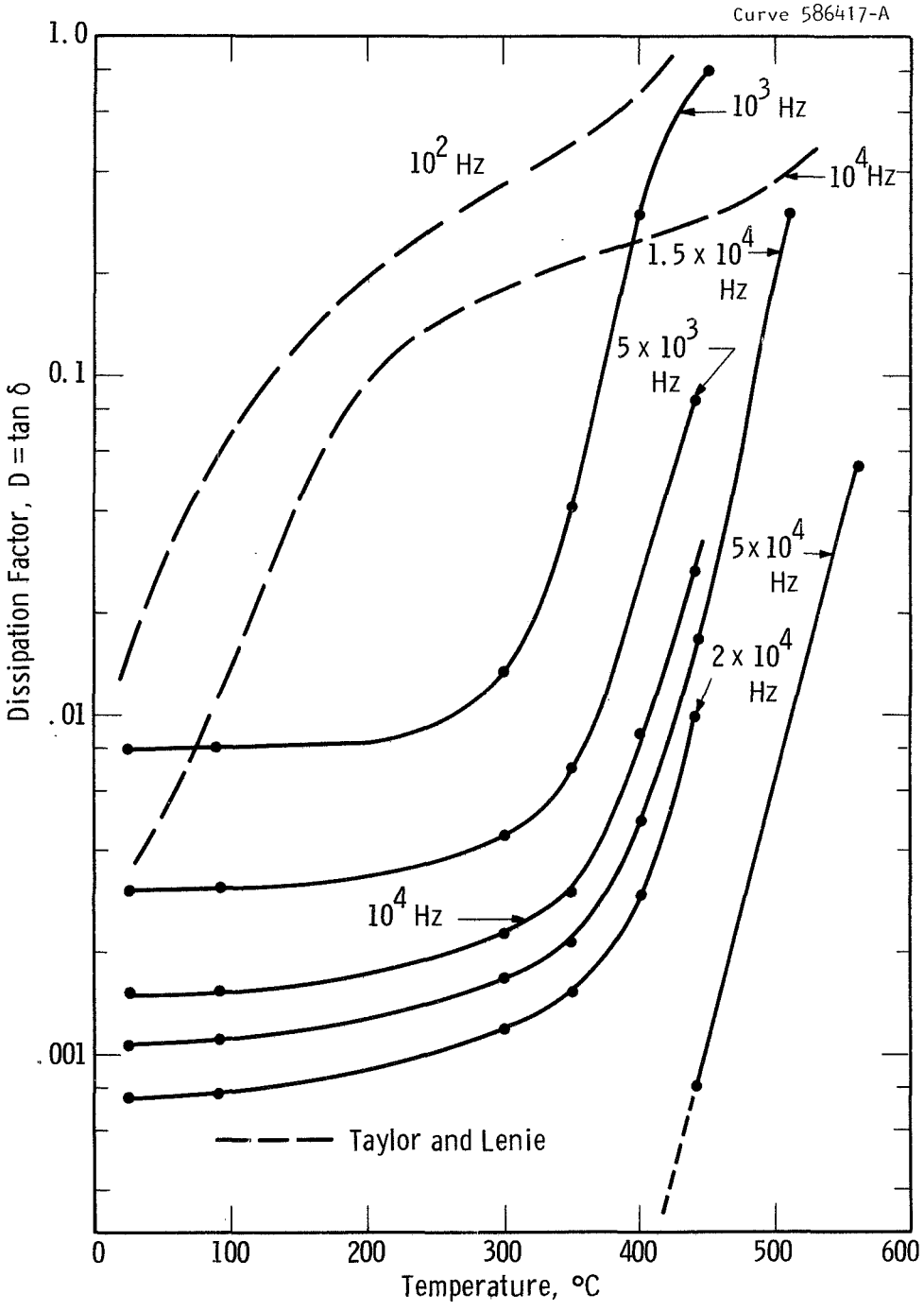

Fig. 33 Variation of dissipation factor, D, with temperature at several frequencies.

of magnitude change, referred to the room temperature value, when measured at 350°C and 10 kHz.

It is noteworthy, that the thin film configurations using the Ta electrodes are structurally stable even after thermally cycling several times to 500°C. This stability implies that no significant diffusion of the electrode material has occurred. The thermal insensitivity of capacitance and loss data also appears to suggest that the films contain fewer or less conductive impurities than the bulk ceramic.

Volume ac resistivities, as calculated from C and D values, Ref. 5, were plotted as a function of temperature for several frequencies and are shown in Fig. 34. At frequencies less than 10 kHz, the resistivities of both the AlN films and the bulk material decrease for a corresponding increase in frequency, the effect in the bulk being more pronounced. The resistivity-frequency dependence for the bulk ceramic is also retained at frequencies greater than 10 kHz. The resistivity trend in the films, however, in the higher frequency range is reversed, resistivity increasing with frequency. No satisfactory explanation is as yet available to account for the differing resistivity-frequency relationships. It is probable, however, that more than one polarization and conduction phenomenon is operative and the the observed data, especially in the films, are due to a combination of superposed effects (Ref. 59).

The resistivity-temperature variations in both the films and the bulk show decreasing resistivities as temperatures are raised. However, at comparable frequencies, the film material exhibits higher resistivities in the temperature range below 400°C. Those for the films show an additiona frequency dependence at temperatures near and above 350°C.

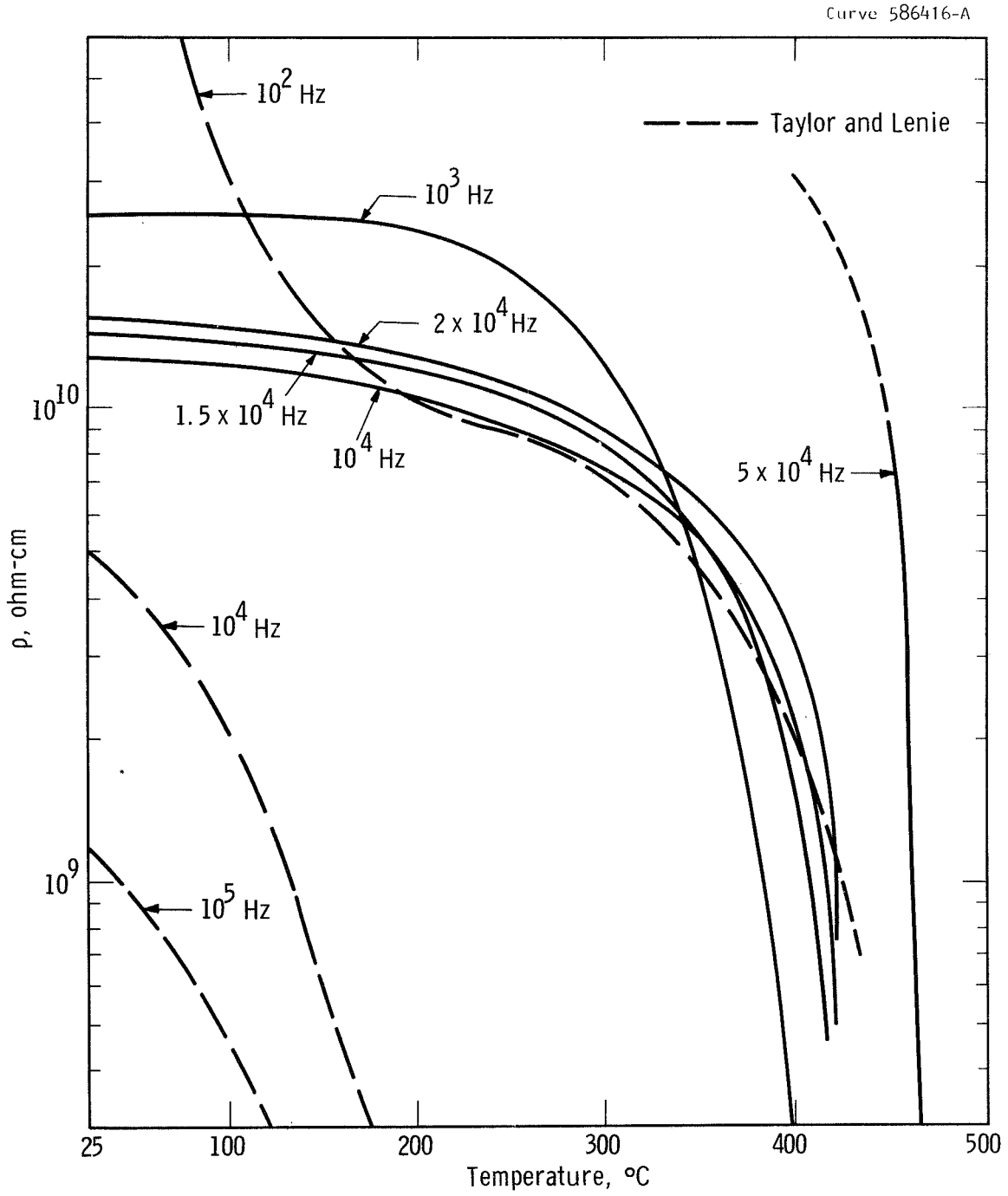

Fig. 34 Variation of ac resistivity with temperature at several frequencies.

3.1.7 Properties of Annealed Films - In addition to the data referred to in Sec. 3.1.6, results were obtained during temperature cycling of several test specimens. (The tests were coincident with I-V measurements which will be reported in Sec. 3.1.9.) A typical result appears in Table V.

Table V

Frequency Variation of Capacitance and Loss Values Of Some Annealed AlN Films

f(kHz)	before 220°C - 20 hr. anneal C (F x 10^{-12})	D	after 220°C - 20 hr. anneal C (F x 10^{-12})	D
1	8.6	.04	8.7	.025
2	8.6	.0175	8.6	.0045
5	8.45	.004	8.5	.0015
10	8.3	.0017	8.5	.0005
15	8.1	.001	8.4	.0005
20	7.9	.001	8.4	.0005
50	7.9	.001	8.3	.0005
100	7.9	.0005	8.1	.0005

Measurements in the 1 to 100 kHz frequency range on annealed samples show no significant change in capacitance but display an apparent reduction in loss. This suggests that the ac resistivity at frequencies above 1 kHz has been increased after annealing. At first sight, these results conflict with an increase in current (and therefore in the dc conductivity) found in the I-V data after annealing. The apparent disagreement can be resolved by considering the observed increase in the dispersion of the dissipation factor after anneal relative to that

in the as-grown films (see Fig. 35; these data are extracted from Table V). If the data in Fig. 35 are extrapolated to frequencies less than 1 kHz, one notes that the loss for annealed films soon becomes greater than for the unannealed films. Thus, low frequency loss characteristics would still be consistent with a lowered dc resistivity (the latter suggested by the I-V data of Fig. 40).

3.1.8 I-V Measurements - To assess the potential usefulness of the AlN films as dielectric layers in, for example, semiconductor field effect devices, it was desirable to study their behavior under applied fields. Since the high preparation temperatures used in these experiments had limited the choice of base electrodes, only films deposited on bulk Si or on to sputtered Ta films were investigated. Data were obtained using the sandwich arrangements described previously. In some cases, large area counterelectrodes were also used.

Figs. 36 to 39 illustrate some of the results. In general, with Au and Ta counterelectrodes, data are reproducible in form. This is illustrated in Fig. 36 which shows a plot based on measurements from four 0.5 mm diameter electrode areas on the same film. Each capacitor structure was measured up to about 70 V and one was taken to a maximum voltage of 115 V. The I-V characteristic up to about 60-70V was reversible. However, when the current was taken to high values a new characteristic was followed on reducing the voltage. This plot approximates to a square law; i.e., the observed dependence is

$$J = k\ (V)^{2.2} \ . \qquad (5)$$

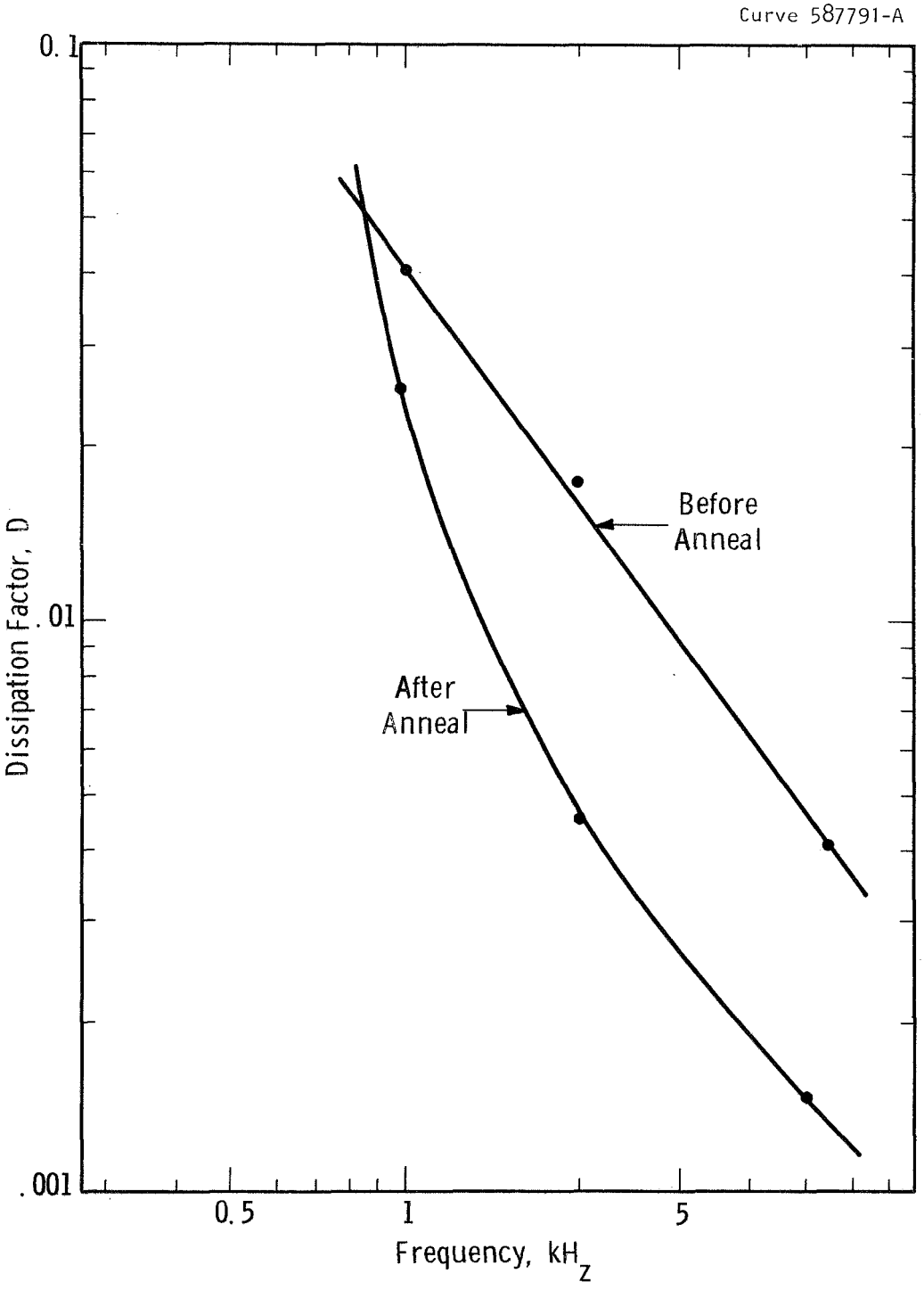

Fig. 35 Effects of thermal anneal on dissipation factor (loss) of reactively sputtered AlN films.

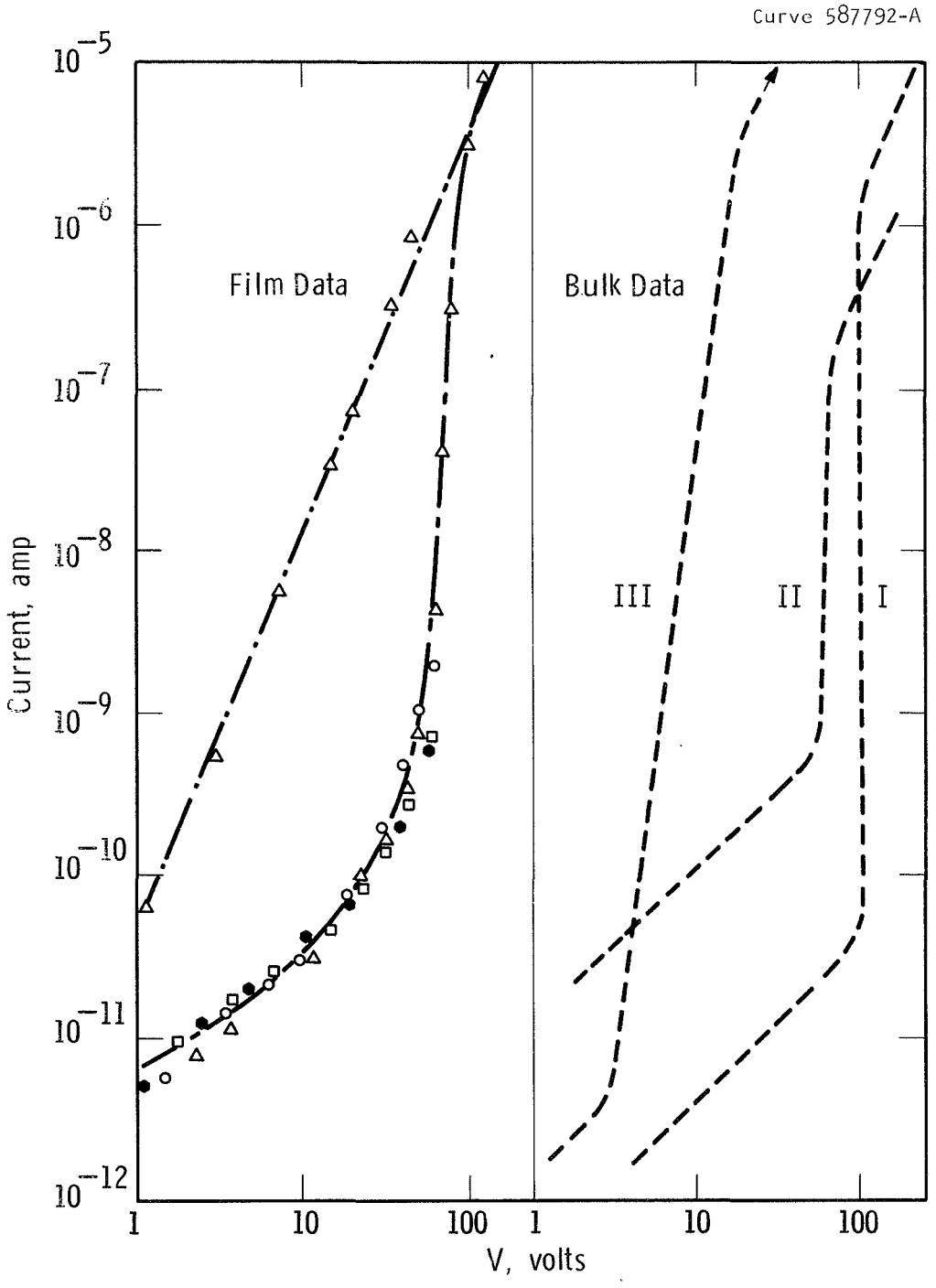

Fig. 36 Current-voltage data for Al/AlN/Ta film sandwich structure, AlN film thickness 8000 A. Also shown are data of Kawabe, et al. for single crystal AlN.

The slope of the low voltage segment of the initial plot on all films tested is approximately unity indicating that Ohm's law is followed.

It is interesting to compare our results with the data of Kawabe (Ref. 60) et al. for single crystal platelets of AlN fitted with Au electrodes on opposite faces. These workers explain their results on the basis of a space-charge limited current mechanism of the type outlined in the theory of Lampert (Ref. 61). At low applied voltages where any excess injected carriers are trapped, the carriers "n" normally present, thermally will generate an ohmic current of the form

$$J = e\, n\, \mu\, V_a/d \qquad (6)$$

where V_a is the voltage applied to an insulator of thickness d, and μ is the carrier mobility. When the traps are filled at an applied voltage V_{TFL}, the injected carriers are available for conduction and a steep rise in current occurs until the I-V characteristic meets a line represented by Child's law, i.e.,

$$J = 9\, \theta\varepsilon\, \mu\, V_a^2/8\, d^3, \qquad (7)$$

where θ is the fraction of the total charge available for conduction, and ε the dielectric constant of the insulator.

The results of Kawabe et al. (Ref. 60) for Au electrodes are reproduced at the right of Fig. 36 and demonstrate the extreme sensitivity of the I-V characteristic to thermal history of the crystal, and presumably to a number of traps. Curve I is the result obtained initially, Curve II after the crystal has been heated to 160°C and cooled slowly, and Curve III after heating to 160°C and quenching. These treatments produce significant

changes in V_{TFL} and hence in the voltage ranges over which Ohm's law (equation (6)) and Child's law (equation (7)) are obeyed.

Our data for the Au electroded AlN film are not inconsistent with the space-charge limited model, although they are open to alternative interpretations. If this model is assumed, the approximate value of V_{TFL} can be used in the theoretical expression,

$$V_{TFL} = e\, d^2\, N_t / 2\, \varepsilon \qquad (8)$$

to calculate the trap density N_t. Taking V_{TFL} as 75 V, from Fig. 36 d as 8×10^{-5} cm. and ε as 8.5, the value of N_T is about $10^{18}/cm^3$. This is about 5 orders of magnitude higher than Kawabe et.al. (Ref. 60) find for single crystals but is a reasonable estimate for a polycrystalline film. Incidentally this value of N_T corresponds very closely to the number of crystallites/cm^3 in the film (i.e., $2.5 \times 10^{17}/cm^3$) based on the micrographic data in Fig. 19.

Some results obtained with Al electrodes on the same AlN film are shown in Fig. 37. A much wider variation of the I-V characteristics from sample to sample was found in this case and the current was more erratic at lower voltages. This behavior could mean a variation in the number and energy of traps between samples, but in view of the consistency in the results with Au electrodes, it is more probable that the effect is spurious, and arises from a chemical interaction or perhaps an oxide film at the Al/AlN interface.

Rather strong photoconductivity effects were observed with the Al/AlN/Al sandwiches although none were observed when other electrode materials were used. Using visible radiation from a tungsten lamp,

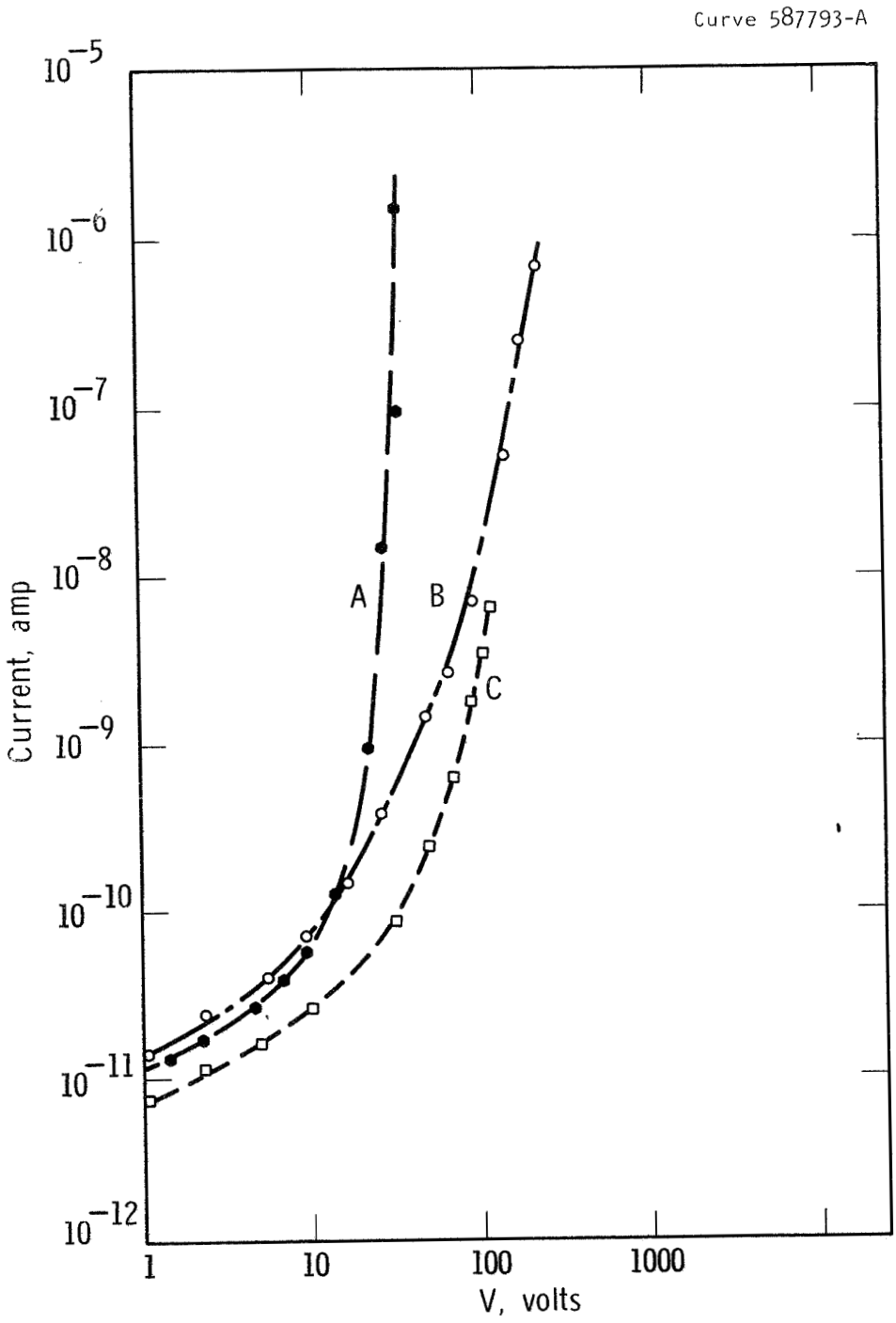

Fig. 37 Current-voltage data for Al/AlN/Ta film sandwich structure, AlN film thickness 8000 A. Curves A, B and C obtained from adjacent test samples on same film.

focused with an internal parabolic reflector, no photoconduction was detected. However, with a 2 watt mercury-argon lamp placed about one inch from the sample, the results shown in Fig.38 were obtained. Although the spectral dependence of the effect was not measured, it seems probable that the photoconduction is a maximum at about 2.8 eV, which Cox, et.al. (Ref. 56) and Kawabe et.al. (Ref. 60) report for Al-doped AlN crystals.

Figure 39 shows a fairly typical I-V characteristic for a Ta/AlN/Ta sandwich. This result is somewhat different from those found with Al and Au electrodes. Thus, despite the fact that a thinner sample was used (approximately 4000 Å) the current values are reduced compared with those for Al and Au, except at low applied voltages in the near-ohmic range. Also, the effective field for breakdown was relatively high, corresponding to a voltage of 350 V, giving a dielectric strength of about 9×10^6 V/cm.

3.1.9 I-V Data for Annealed Films - Because efforts to fully explore the complete I-V behavior were impeded by erratic behavior at high voltage, the currents in this region being strongly time dependent, several test specimens were examined at elevated temperatures. The purpose of an increased temperature was to possibly facilitate a complete filling of traps at lower voltage thus permitting observation of the trap-filled voltage limit before the onset of instability.

Some results from heated films appear in Fig. 40. The 25°C curve depicts typical behavior for an as-grown film. Data in this case were taken from Ta/AlN/Ta sandwiches in which the nitride thicknesses

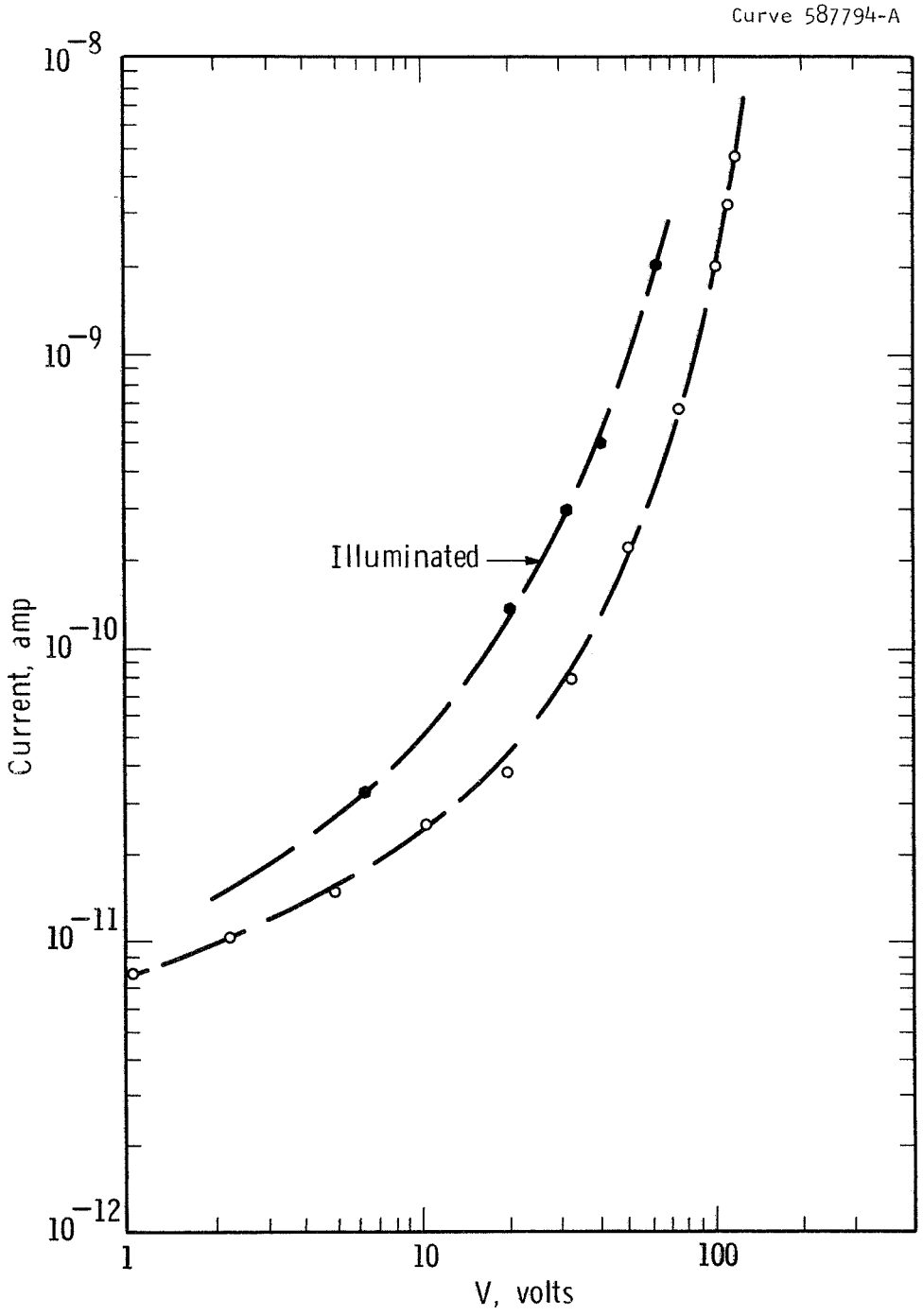

Fig. 38 Photoconductivity effect for Al/AlN/Ta film sandwich (sample illuminated with mercury-argon lamp).

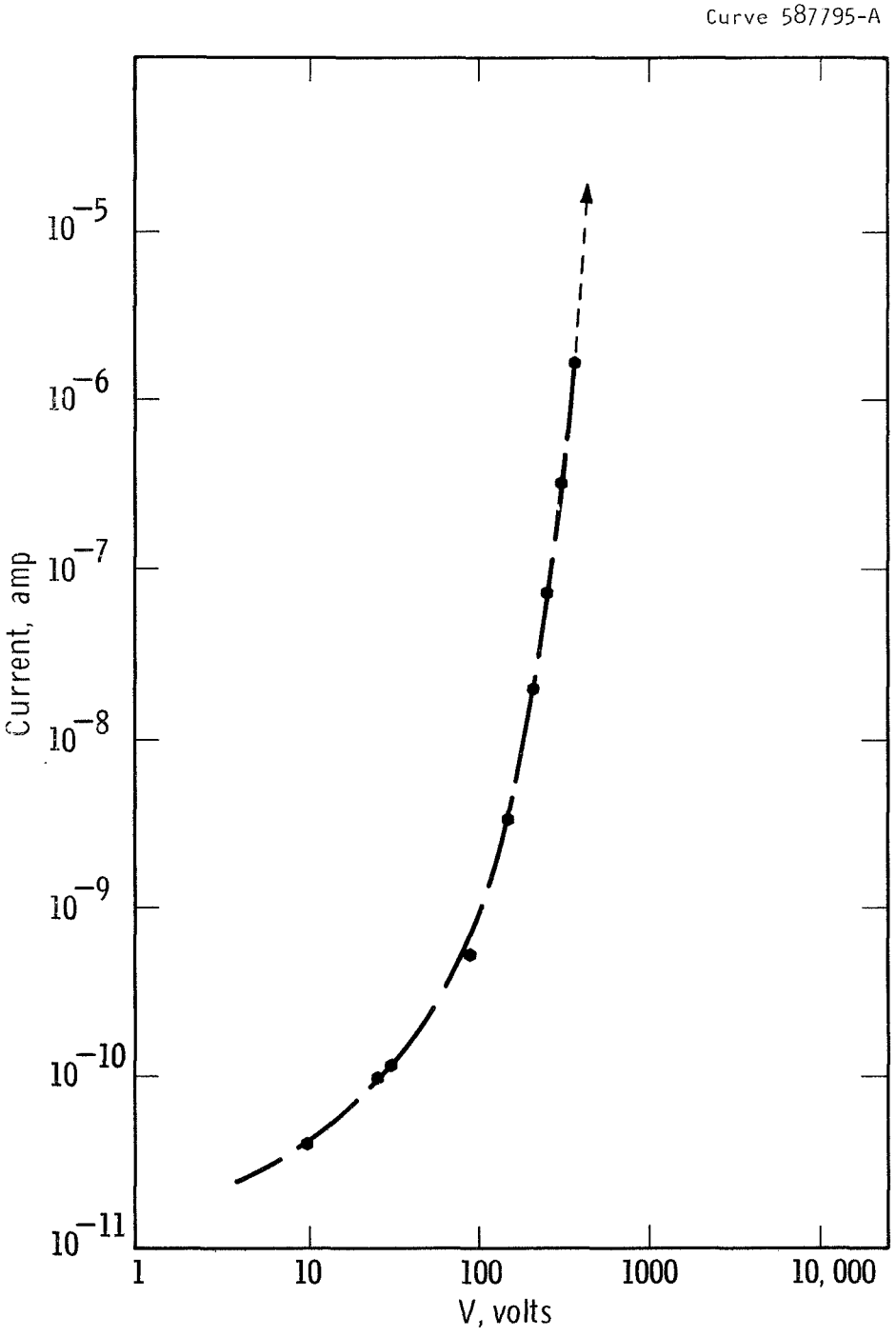

Fig. 39 Current-voltage data for Ta/AlN/Ta film sandwich structure, AlN film thickness 4000 A.

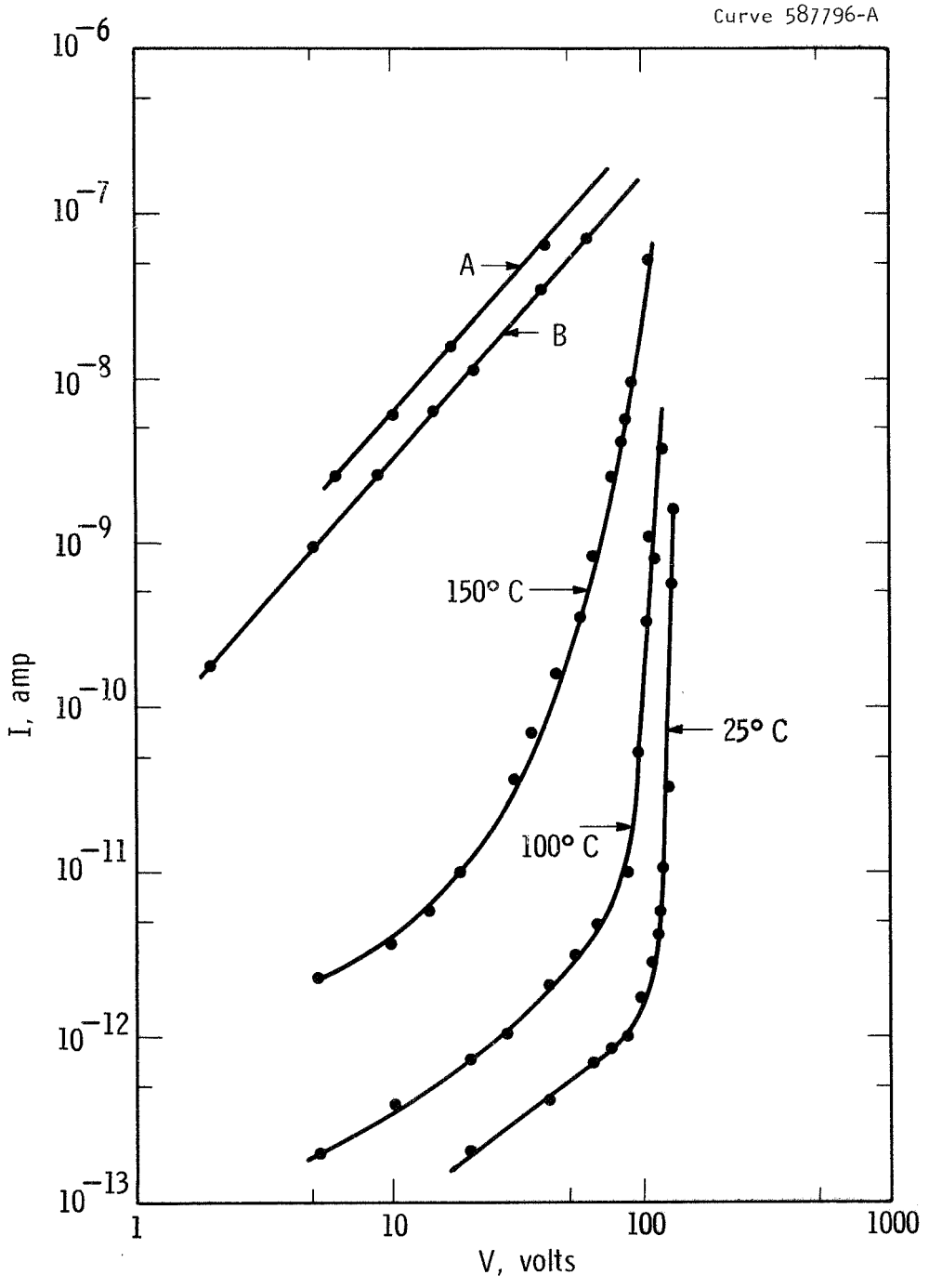

Fig. 40 I-V relationships of an AlN film at various temperatures. The dielectric is part of a Ta/AlN/Ta structure. AlN thickness is 4500 A.

were approximately 4500 Å. On raising the temperature, a progressive decrease in dc resistivity was observed. At 150°C, the rapidly rising current region is no longer prominent. The anticipated filling of traps and observance of reversible transition to a Child's type, square law I-V relationship, however, had not occurred even at an applied potential of 100 volts. At 150°C, and with 120 volts applied, the square law dependence was finally observed but it had occurred irreversibly, Curve A, Fig. 40. Moreover, a 20 hr. anneal at 150°C of similar sandwiches with no applied voltage produced identical irreversible square law behaviors, Curve B, Fig. 40 (measured at room temperatures after anneal).

The mechanism which has produced the new I-V characteristic is, as yet, uncertain. In effect, the behavior suggests that all traps are filled or no longer available. Diffusion of Ta from electrodes seems unlikely since the original deposition of AlN took place at 950°C (on one electrode). To test the possible effects of diffusion from a surface electrode, however, I-V measurements were made on several Al/AlN/Ta sandwiches, the Al being deposited on an unheated AlN film (thickness 6000 Å). After a 20 hr., 220°C anneal, departure from the space-charge limited, trap-filled behavior was observed and is shown in Fig. 41. The curves, in fact, tend to resemble those produced by a 150°C anneal of the 4500 Å Ta/AlN/Ta structure (Fig. 40). The specimens were then submitted to a further 60 hr., 220°C anneal. Both previously electroded and unelectroded regions were subsequently examined, the latter now receiving Al electrodes. These results are also incorporated in Fig. 41. The square law characteristic is not observed, possibly

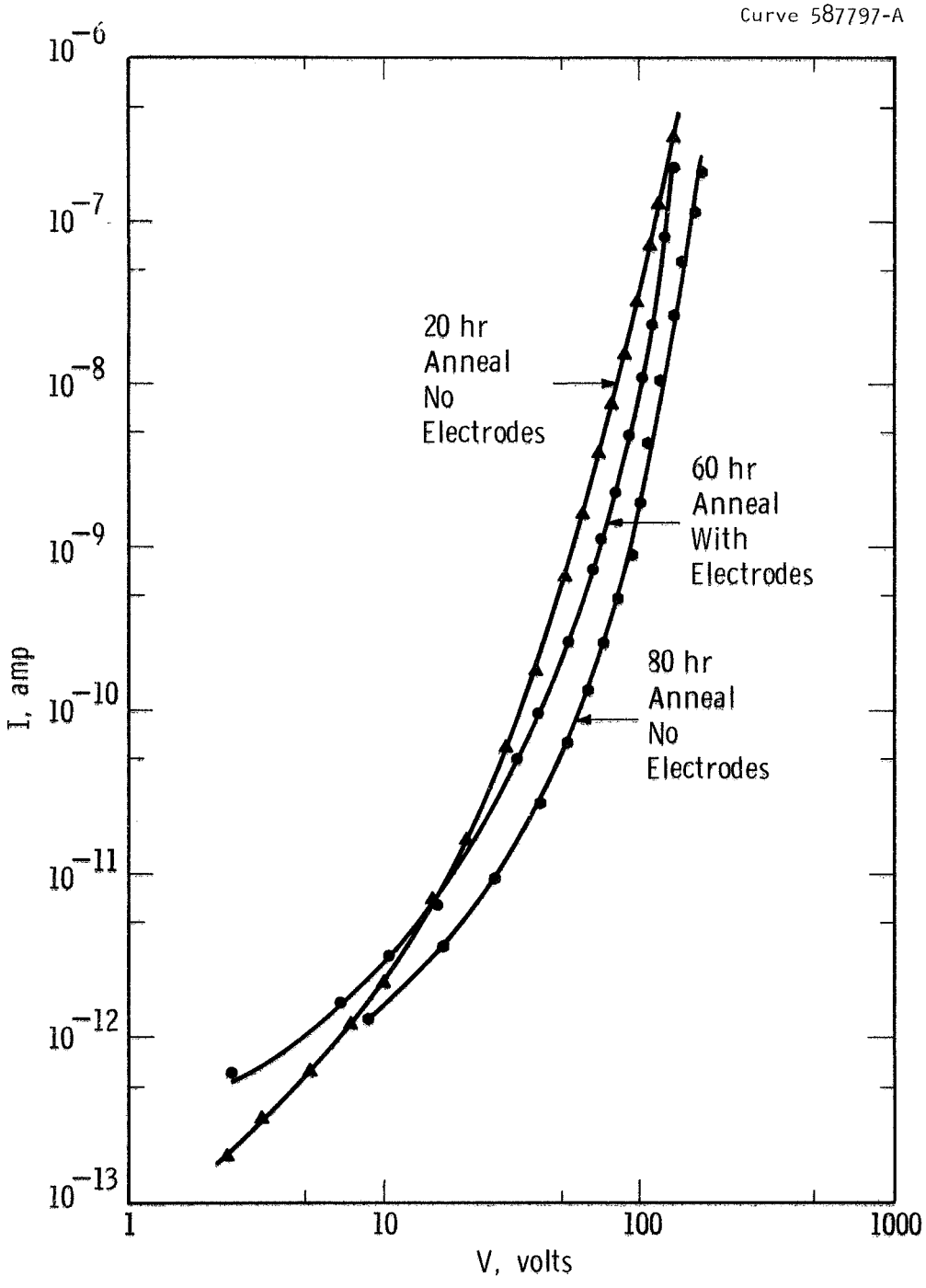

Fig. 41 I-V relationships of an AlN film for various annealing schedules. Annealing temperature is 220°C; AlN thickness is 6000 A.

a higher temperature is required for the 6000 Å AlN film. Diffusion seems even more unlikely, at this point, since unelectroded areas (during diffusion) showed similar behavior to previously electroded and annealed regions.

3.1.10 C-V Measurements - Capacitance-voltage studies, viz., those which relate to some properties of MIS devices, were made on several AlN films sputtered onto silicon substrates.

The films fell into several categories, depending on the temperature at which they were deposited, and the technique used to heat them during the deposition. In an early series, in which substrates were heated resistively by passing current through the silicon, two films were prepared at 1000°C and 800°C respectively. The 1000°C sample did not suffer dielectric breakdown for voltages < 100 volts and the C-V study of this film is described below. The other (800°C) film broke down at $\sim$ 4 volts, obviating any study of its C-V characteristics. Later sets of films were prepared on silicon substrates heated inside tantalum envelopes. For films held in envelopes at a nominal 800°, 900° or 1000°C temperatures, breakdown was observed at 5 to 15 volts when film thicknesses were less than 1500 Å. When thicknesses exceeded 1500-2000 Å results were reproducible and similar to those for a dilute mixed nitride as shown in Fig. 57 of Sec. 3.4.1.3.

For the resistively heated film on which C-V measurements were made, the substrate was p-type, and the accumulation mode capacitance at large negative potentials across the sample (silicon grounded) varied from 3.0 to 3.9 picofarads as the AlN film thickness varied from the

the center of the sample to its edges. The AlN film dielectric constant calculated from these values lies between 8.0 and 9.4; these numbers bracket the published values. The uncertainty arises from the method used to determine the film thickness, that is, counting the interference fringes observed under monochromatic light. Dielectric loss in these 1000 Å films was negligible at 100 kHz.

In the tracing of a typical C-V plot (Fig. 42), the bias voltage was swept from zero to +60 volts, then from +60 to -60 volts and back by a 0.025 Hz saw-tooth sweep generator.

On the initial sweep, from 0 to +60 volts, the capacitance of a typical unit was 2.4 pF, its lowest value. The capacitance remained at 2.4 pF on the sweep from +60 volts to about -25 volts, when it rose to 3.3 pF. This value was maintained as the sweep continued to -60 volts, and back to +30 volts when a decrease to 2.4 pF was observed. On continued sweeping, the point of increase in capacitance shifted from -25 to -37 volts, while the point of decrease remained at +30 volts. In all, the mid-point of the capacitance change, that is the voltage at which $C = \frac{3.3 + 2.4}{2} = 2.9$ pF, shifts by 75 volts with each sweep to $\pm$ 60 volts. Using the relationship given by Grove, et.al. (Ref. 62) to calculate the charge induced in the semiconductor by the charges in the dielectric, viz.,

$$\frac{Q_s'}{q} = \frac{(-V_{FB} + \phi_{ms})\ C_O}{1.6 \times 10^{-19}\ A} \qquad (9)$$

where Q_s' is the number of induced charges per unit area, V_{FB} is the flat-band voltage, C_O/A is the capacitance per unit area and ϕ_{ms} is the

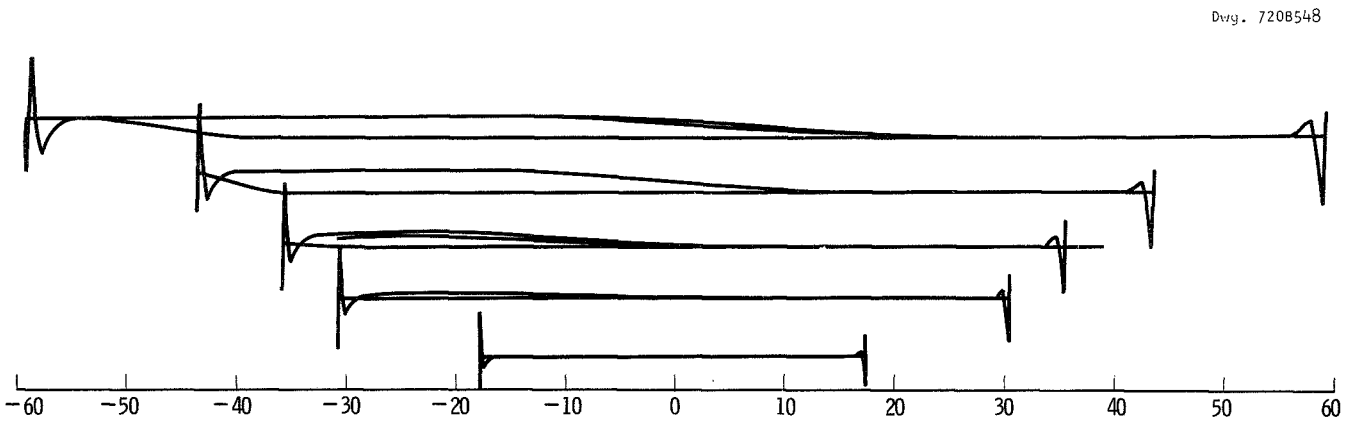

Fig. 42 Capacitance-voltage traces of Al-AlN-Si with varying sweep voltages. The transient at the ends of the sweep is an instrumental artifact.

metal-semiconductor work function difference (usually neglected), we note that a charge of 7×10^{12} charges/cm^2 thus occurs in the surface state density with each sweep.

The sense of this hysteresis in the C-V behavior is that of ions moving in the oxide under the drive of the $\pm$ 60 volt sweep. Reduced sweep voltages generate smaller loops. Flat-band conditions occur at smaller voltages in both directions. Motion of ions of only a single charge type cannot account for the change of the flat-band voltage from large positive to large negative values: it is necessary that both positive and negative ions be present. An alternate explanation is that the AlN film is polarizable, and that the degree and direction of the polarization are determined by the sweep voltage.

In films prepared in heated Ta envelopes, deposits on p-type Si similarly display a charge associated movement with a change of bias. C-V data for films on n-type substrates are remarkably dissimilar showing no loop characteristic. A possible doping of the substrate surface, thus forming a p-type layer and junction, is believed influential in the suppressed characteristics of these films. Interposition of thin, thermally grown SiO_2 layers are possible remedies to the doping effect.

3.2 Reactively Sputtered AlN (Triode System)

During the course of the present investigation, it was noted that after a period of many hours the growth rate of AlN would decrease due presumably to the formation of a passivating layer of the compound

on the cathode. In a particular experiment, a drop in the N_2 partial pressure occurred inadvertently and was associated with a significant increase in the total sputtered AlN yield. The effective deposition rate in this experiment was, in fact, some five to six times greater than that normally observed.

Reference to an earlier work by Krikorian and Sneed (Ref. 63) on the reactive sputtering of Al_2O_3 suggested that both increased sputtering rates and a more highly oriented deposit might be obtained by using low partial pressures of oxygen (cited pressures necessary for epitaxy of stoichiometric films are between 10^{-5} and 2×10^{-5} torr). It is possible that similar effects might occur in the reactive sputtering of AlN. Exploration of such parameters in detail is a time consuming exercise in an ultra-high vacuum facility, however, since a wide range of growth temperatures of N_2 partial pressures should be studied. Therefore, it was decided that a systematic study of film structures and growth rates should be undertaken in a more flexible triode sputtering system capable of base pressures in the 10^{-7} torr range. Previous studies with such a system had indicated that both pure Al and AlN films could be deposited with this arrangement.

3.2.1 Preparation - The experimental arrangement basic to the supported discharge facility consists of a filament (tungsten wire), anode, target and grounded substrate support. The latter pair are positioned in a vertical plane parallel to one another. The target-substrate spacing is 4 cm. An axial magnetic field is applied parallel to the electron current which flows from the filament to the anode, and

helps to enhance the probability of ionizing collision in the target-substrate region. Sputtering is carried out by accelerating the ionized species, argon, onto a negatively biased (1500-2000 V) Al target.

Substrates are heated in Ta strip heater envelopes and the working arrangement permits sequential heating and exposure to the discharge of one of four substrates.

3.2.2 Composition and Growth Rate Evaluation - Some data obtained by electron and X-ray diffraction analyses which are representative of AlN films sputtered reactively in the triode sputtering facility are shown in Table VI. The sputtering voltage in all experiments except those marked with an asterisk was -1500 V. The marked values were prepared with the target at -2000 V. Ar pressures were fixed at 5×10^{-3} torr.

Table VI Data for Triode Reactively Sputtered AlN Films

Temp. °C	N_2 Press. (torr)	Film Composition	Thickness (Å)	Growth Rate (A/min)
300°C	5×10^{-5}	Al	3000 Å	100
560°C	---	Al	1000 Å	34
560°C	5×10^{-5}	Al	1000 Å	34
560°C	10^{-5}	Al & AlN	1000 Å	34
560°C	5×10^{-4}	AlN	3000 Å	100
700°C	5×10^{-4}	AlN	2000 Å	100
900°C	5×10^{-4}	AlN	3000 Å	∿50
*800°C	5×10^{-4}	AlN	3000 Å	100
*900°C	5×10^{-4}	AlN	1500 Å	80

We assume that thickness and growth rates associated with deposition at 300°C reflect, to a fair approximation, the sputtering

rate of Al at -1500 V dc. Thus, the growth rates of AlN near 560°C seem to represent complete reaction of all incident Al atoms when the N_2 pressure exceeds 5×10^{-4} torr. At higher temperatures, a sticking factor correction must be accounted for.

Optical and electrical measurements were made on films deposited on vitreous silica substrates partly metallized with sputtered Ta electrodes ($\sim$ 1000 Å thick). The first set of four films (Z-270) were grown with target voltages of -1500 Vdc, a N_2 partial pressure of 5×10^{-4} torr and at temperatures which ccvered the range 6C0° to 900°C. For the second set (Z-271), the target voltage was altered, in this case being -2000 Vdc. Film thicknesses ranged from 1500 Å to 3000 Å. As judged from electron diffraction data, the film structures were, in all cases, consistent with that expected for pure AlN. No addition phase, e.g., Al, was detected. Both the degree of crystallinity and orientation, however, were observed to increase markedly as the substrate temperature was increased from 600° to 900°C.

3.2.3 Optical Properties - The optical absorption data for these films differed significantly from that obtained from AlN films prepared in a glow discharge environment. In the latter conditions, the partial pressures of Ar and N_2 were 80×10^{-3} and 5×10^{-3} torr, respectively. The triode sputtered films displayed a sharp absorption edge and irrespective of the substrate temperature (within the 600° to 900°C range) the position of the edge corresponded to an energy gap of 5.95 ± 0.5 ev (Fig. 43). It should be emphasized that these films were not subjected to a N_2 anneal yet displayed the bulk AlN optical spectrum in the

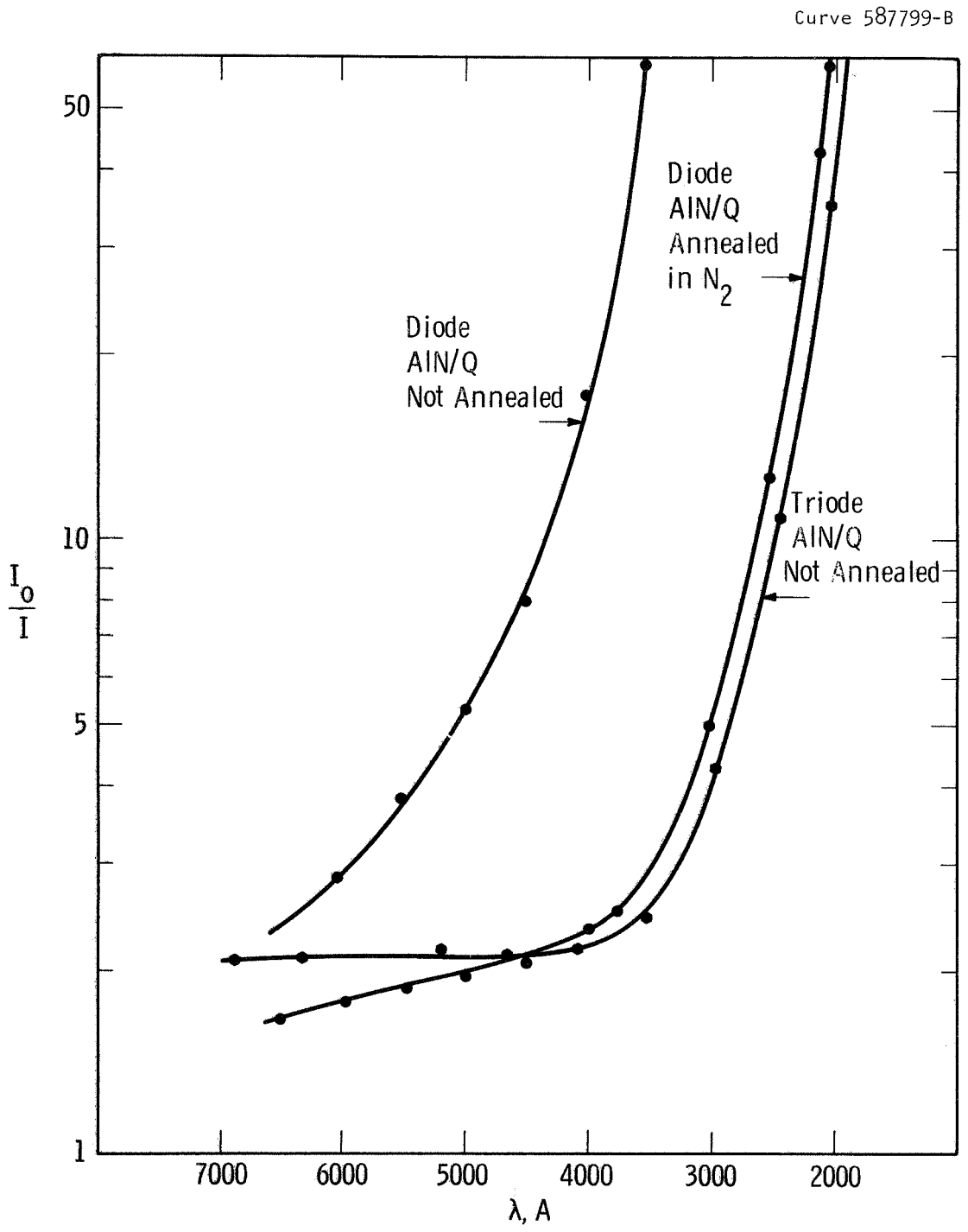

Fig. 43 Optical absorption in three AlN films deposited on vitreous silica, two having been prepared by diode reactive sputtering, the third by triode reactive sputtering. The shift toward higher wavelength for the unannealed diode-prepared film is likely due to a N_2 deficiency in the film. The triode prepared film does not suffer in a like manner.

as-deposited condition. This behavior had not been evident in the glow discharge deposited films which, as-deposited at lower temperatures, showed significant shifts of the absorption edge to lower energies.

3.2.4 Electrical Measurements - Test results from experimental capacitor configurations, i.e., films fitted with 0.3 mm evaporated Al counterelectrodes, indicated that even for films only 1400 Å thick, the dielectric loss was low, lying typically at about .02 at 500 Hz, decreasing to .003 at 1 kHz and becoming less than .001 at frequencies greater than 5 kHz. The dielectric constant showed no perceptible dispersion with frequency and capacitances of 50 picofarads were measured.

The behavior of the very thin films on application of dc fields was far less erratic than for some of comparable thickness prepared by glow discharge sputtering. The I-V data showed conduction consistent with a space-charge limited mechanism with breakdown occurring at about 35 to 60 Vdc corresponding to breakdown fields greater than 3×10^6 V/cm. Room temperature, dc resistivities measured with an applied field of 3×10^5 V/cm were approximately 10^{13} ohm-cm.

Several AlN films of two thicknesses, $\sim$ 1000 Å and 3000 Å, were deposited on both n- and p-type Si substrates. MIS measurements (at 1 MHz) revealed that the former were leaky and suffered breakdown at applied fields of approximately 3×10^6 V/cm. The latter, however, exhibited a behavior not unlike that reported for nitride films prepared by diode reactive sputtering. The hysteretic behavior indicates the movement of charge in the dielectric on the p-type substrate. Measurements carried out for an identical film on an n-type substrate were, again similar to those for the diode sputtered nitride, apparently insensitive to any movement of charge.

3.3 Transducer Application

3.3.1 Preparation - A triode, reactive sputtering facility based on that described in Sec. 3.2 was used for the deposition of oriented AlN films on cylindrical sapphire (Al_2O_3) rods, the latter measuring an inch in length with a one-quarter inch diameter. To hold and heat the rods, a furnace of tubular design was fabricated first of .005 inch tantalum sheet and later of .005 inch platinum. The furnace is shown in Figs. 44 and 45. Chemical cleaning of the substrates (in a series of HNO_3, NaOH and methanol baths) preceded each deposition. During the course of the experiments both new and used Al_2O_3 rods were used as substrates. Some difficulty in reconditioning the latter was experienced, however, and these were eventually discarded. Following the insertion of a substrate rod in the tubular furnace, the sputtering chamber was evacuated and baked. When a 10^{-9} Torr vacuum had been obtained, argon, and then nitrogen, were introduced and their partial pressures adjusted to approximate those normally used for deposition onto silicon or silica substrates, viz., p(total) = 5.7×10^{-3} Torr, and $p(N_2) = 7 \times 10^{-4}$ Torr. A sputtering potential of -1500 V dc and current density of 0.1 mA/cm^2 gave a growth rate of about 50 Å/min. Thickness adequate for piezoelectric property evaluation ranged between 1.0 and 3.0 μm.

Development of the sputtering apparatus proceeded through two stages. In the first stage a single aluminum cathode positioned parallel to one face of the substrate rod was used. Deposits Z-284A, B and C and Z-285 A and B were prepared in this way, the two faces of the rod being coated in sequential depositions. The later stage of development comprised a twin cathode arrangement, Figs. 46 and 47, and permitted

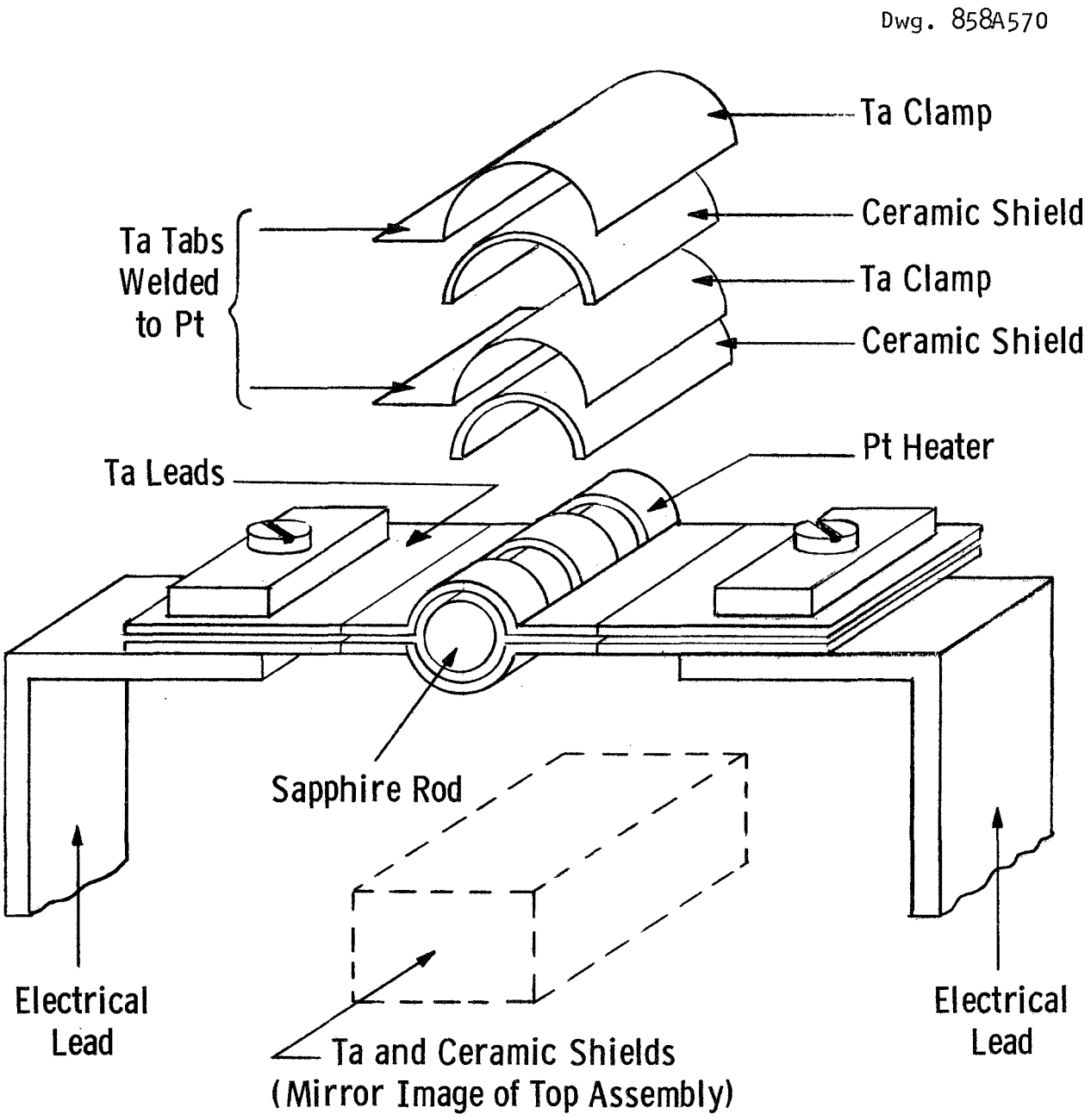

Fig. 44 Exposed view of heater assembly used to heat Al_2O_3 (sapphire) rods during simultaneous deposition of AlN on the end faces.

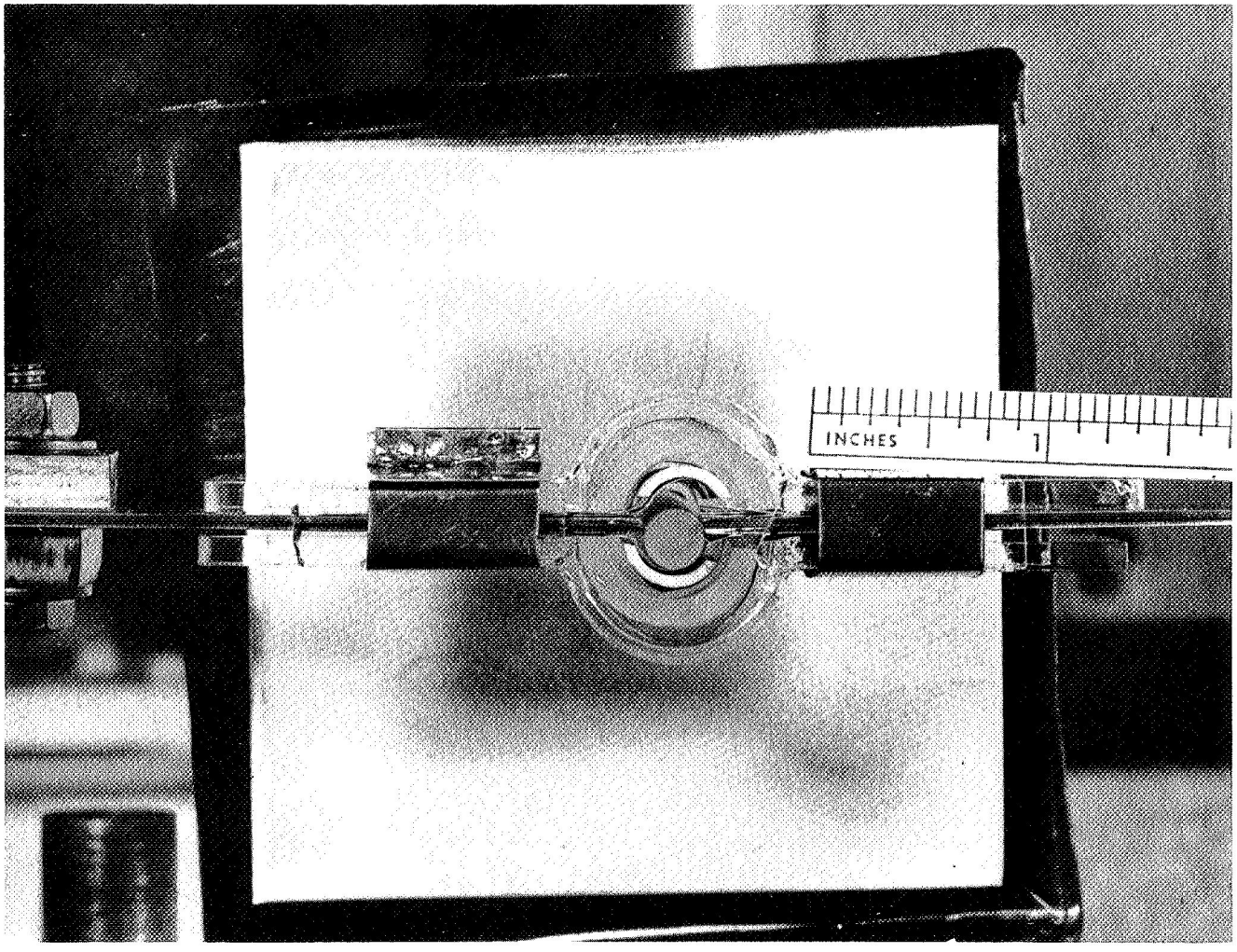

Fig. 45 Close up view of a tubular Pt heater used to heat cylindrical sapphire rods.

simultaneous deposition onto both substrate faces. Films so deposited were Z-291A and B, Z-292A and B, Z-296A and B, Z-297A and B, Z-298A and B, Z-300A and B and Z-305A and B.

3.3.2 Coupling Relationships Between Substrates and Films - In the present experiments the Al_2O_3 substrate rods are oriented so that the crystallographic c-axis lies parallel to their long axis. Such an orientation favors propagation of compressional (longitudinal) acoustic waves. The faces of the rods are, as a result of the axial orientation constraint, (0001) planes. To insure maximum coupling between transducers and substrates, a parallel orientation, viz., (0001), and intimate contact is required of the AlN films. Coupling in film-rod configurations with these orientations is then related by the longitudinal piezoelectric coefficient (modulus) d_{33}. The first subscript of the coefficient notes the direction of the E-vector and the second, the component of elastic stress. In films in which the c-axis is constrained to the plane of the film, coupling is related via d_{31} or d_{32}, the shear wave mode coefficients.

3.3.3 Pulse-Echo Measuring Technique - A block diagram of the apparatus (Ref. 64) which generates and detects the microwave impulses is shown in Fig. 48. Two triggering pulses, both at repetition rates of 100 pps, are produced by a sync. generator and alternately trigger a transmitter and delay generator, the latter, in turn, triggering a pulse comparator. Pulses from the transmitter, at the cavity resonant frequency (in this instance 1 GHz) are introduced into the transmitter cavity at the maximum H-field end. Corresponding E-field pulses are

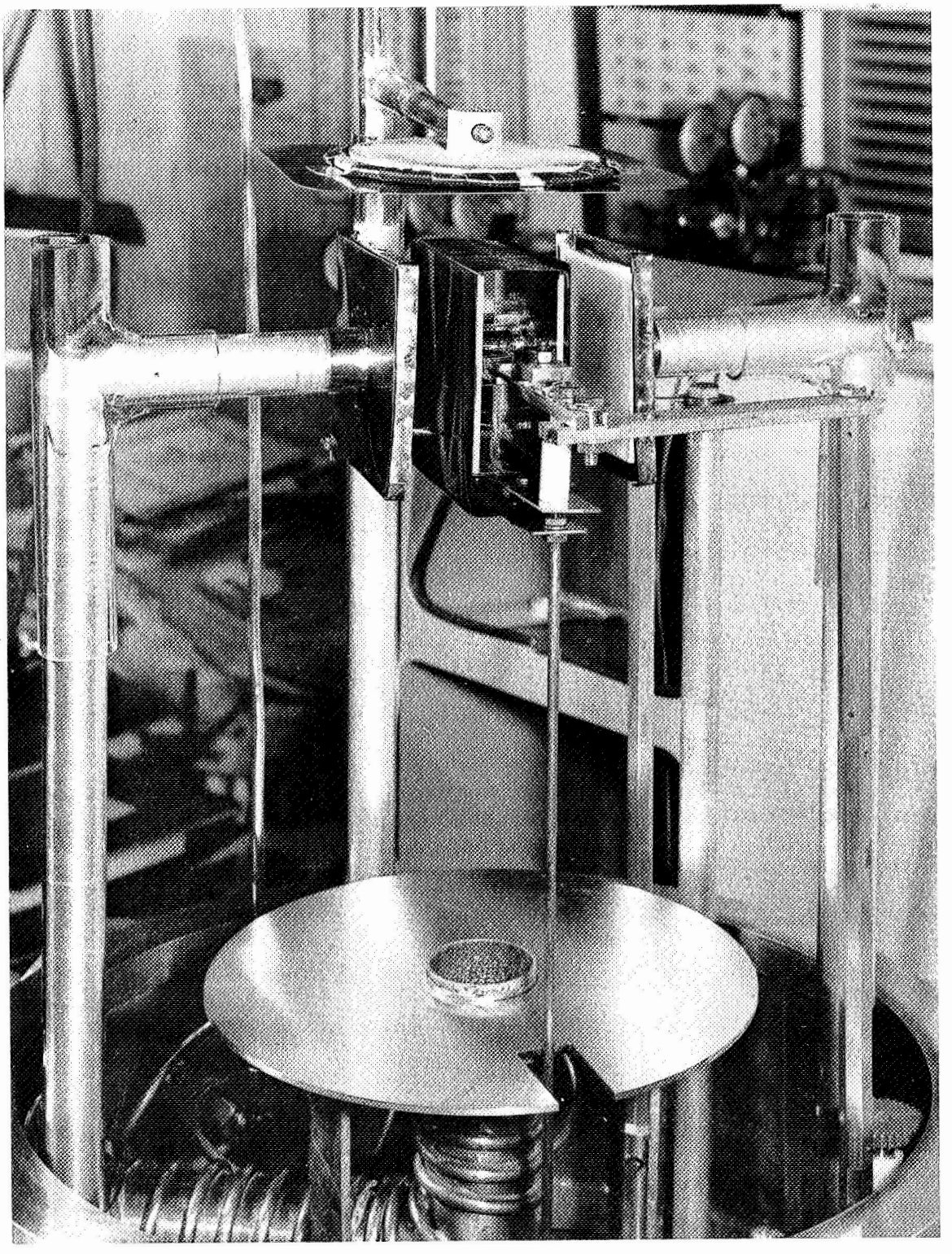

Fig. 46 Twin-cathode, triode sputtering system for the simultaneous reactive sputtering of AlN films on the end faces of a sapphire rod.

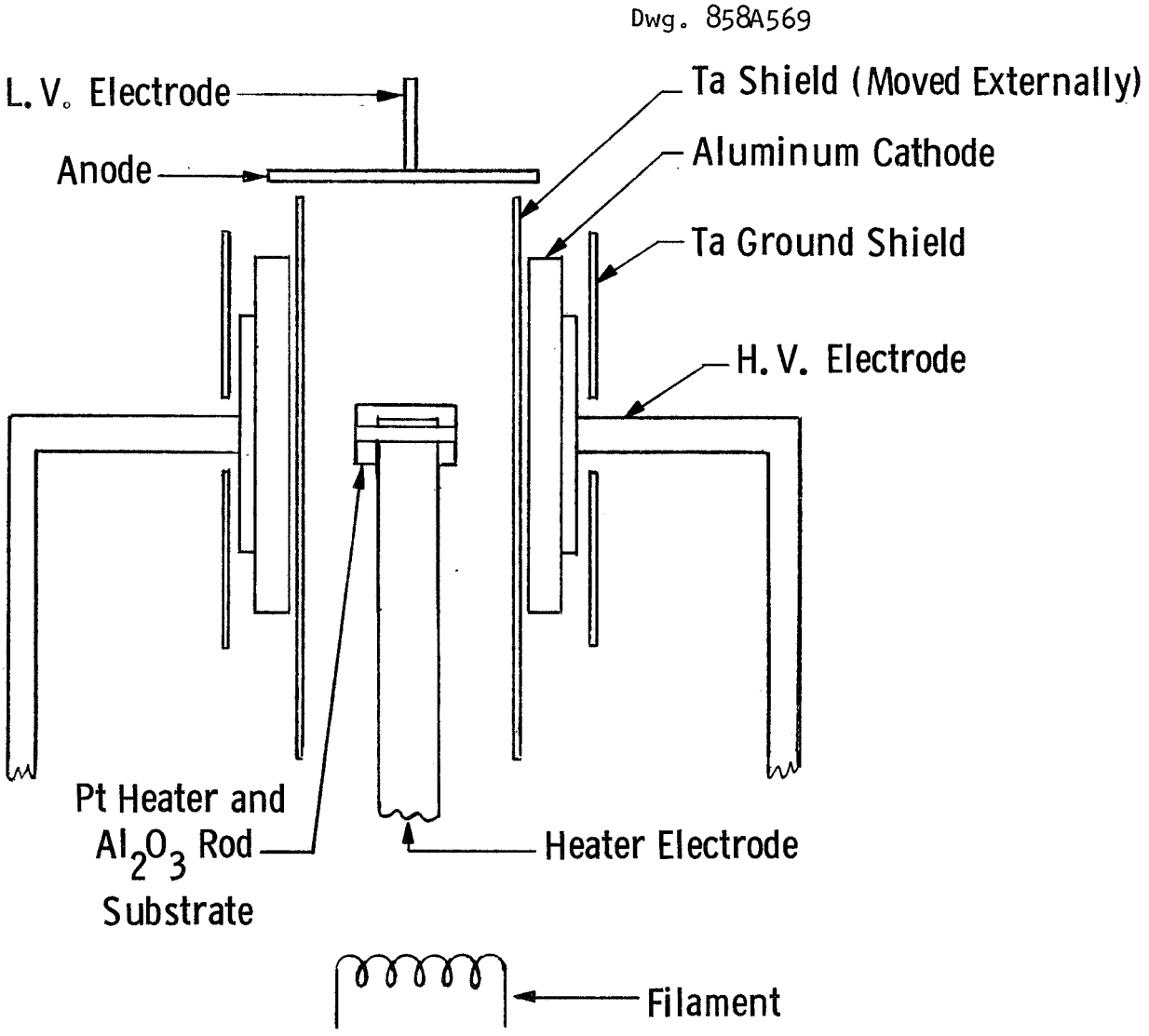

Fig. 47 Schematic diagram of double-ended triode (filament supported discharge) sputtering apparatus for depositing AlN films simultaneously on two faces of a heated Al_2O_3 (sapphire rod.

DWG. 623A009

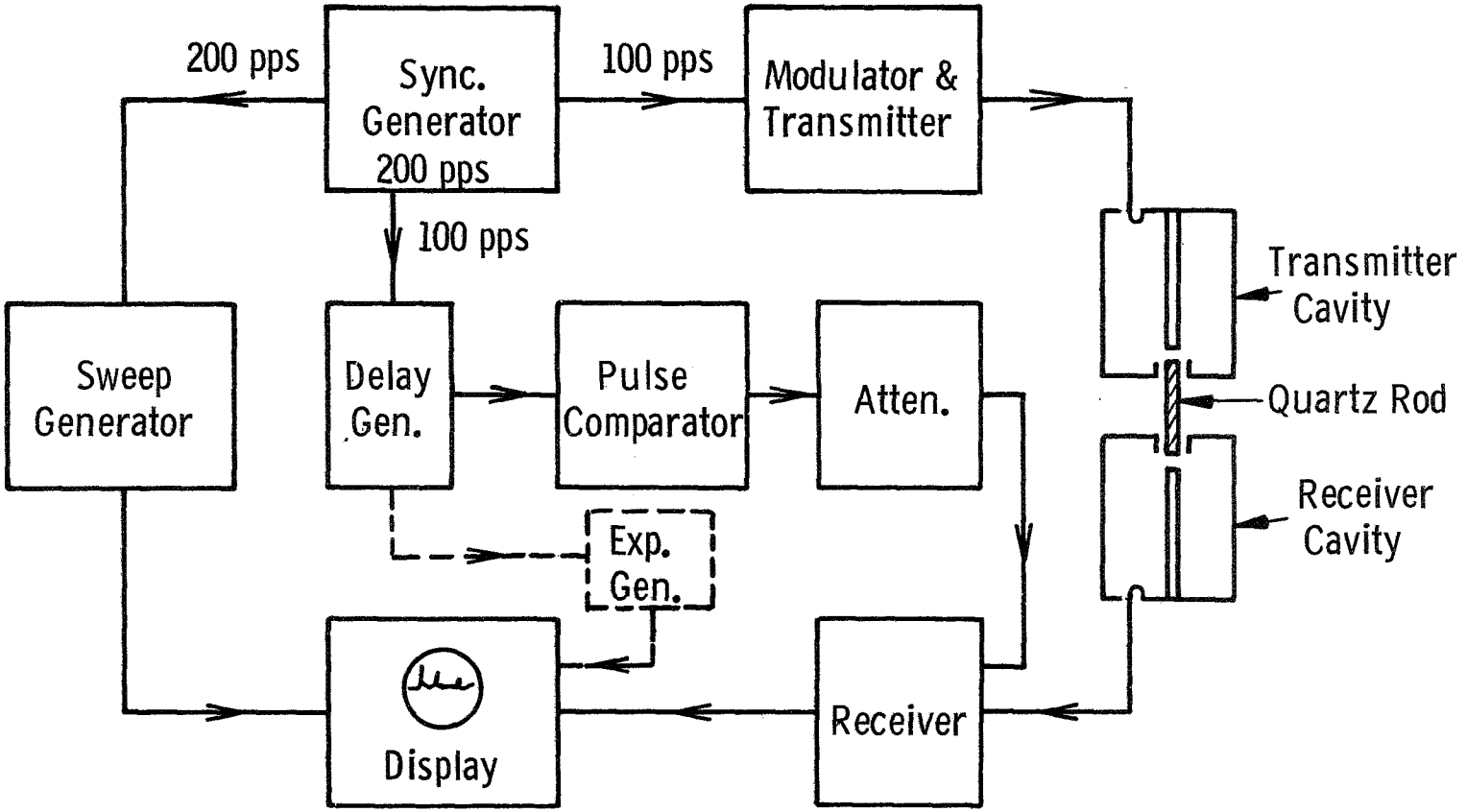

Fig. 48 Block diagram of pulsed hypersonic equipment.

produced in the small gap at the opposite end of the cavity. One end of a sapphire rod, one inch long and one-quarter inch in diameter, is placed in this E-field, so that the field is parallel to the axis of the rod. Acoustic pulses are generated in the sapphire as a result of its piezoelectric character and travel along its length. At the opposite end of the rod, which extends into the receiver cavity, the acoustic pulses generate E-field pulses which are detected at the far end of this cavity in an H-field loop. Since a fraction of the acoustic signal is reflected at the film-rod interface, a series of periodic pulses is received, the number and amplitude of which denote the relative electromechanical conversion. Pulses from both the receiver cavity and from the pulse comparator, the latter via a calibrated attenuator, are alternately displayed on a CRT. By displaying these signals simultaneously and attenuating the comparator signal to match that of the receiver signal, a direct measure of the electromechanical coupling is obtained. Since both signals are of the same frequency and are amplified by the same receiver, all errors due to receiver distortion are automatically compensated. The pulse comparator and attenuator can be replaced by a calibrated exponential generator (shown by the dotted lines) when low loss materials are being studied.

3.3.4 Cavity Design - Figure 49 shows schematically the design of a non-resonant, tunable cavity, (Ref. 64) the type in which the present measurements were made. In this design each physical cavity is merely a termination to a stub stretcher impedance matching unit, the latter representing the true cavity. Thus, the frequency band over which such

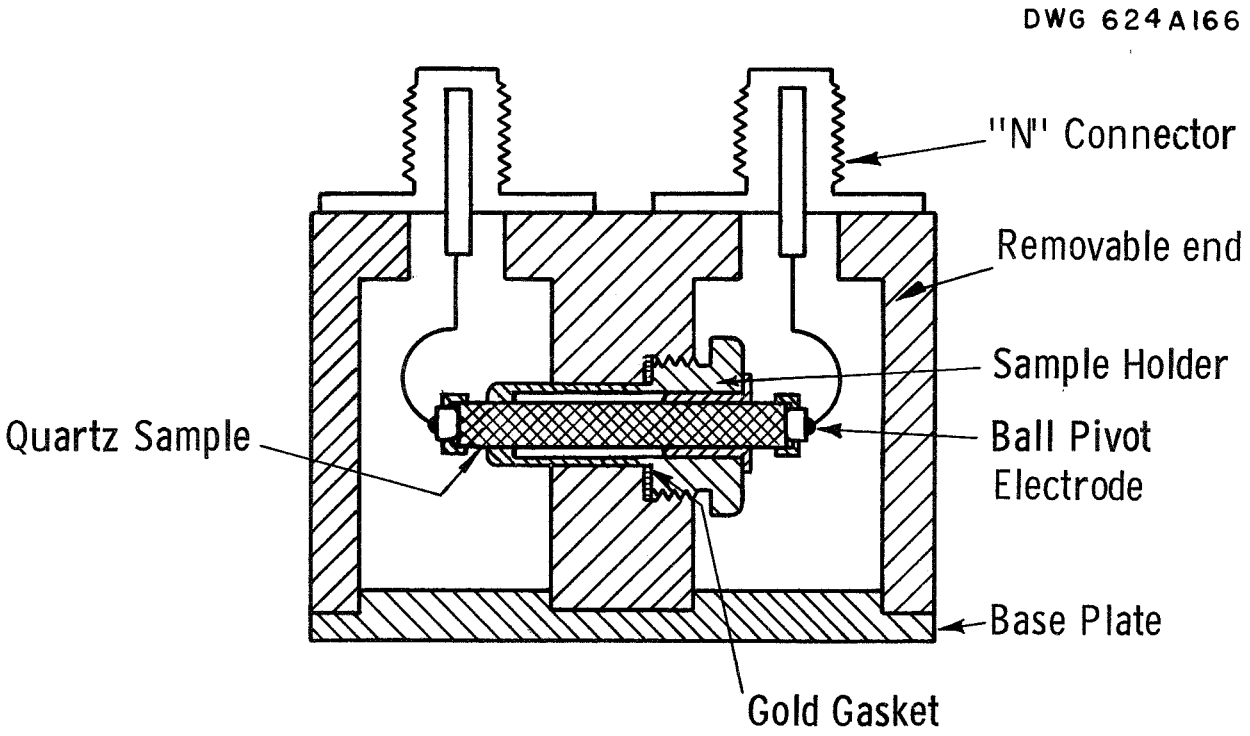

Fig. 49 Nonresonant hypersonic cavity tunable from 250 MHz to 2500 MHz.

cavities can operate is determined by the tuning range of the matching stub stretchers. Figure 50 shows an exploded view of the cavity enclosure. When oblique fields are to be generated, the circular (ball pivot) electrodes, attached to the N-type connectors, are replaced by knife-edge elements.

3.3.5 Results

3.3.5.1 Transducers Z-284A-B-C - Figures 51a and 51b show oscillograms of compressional acoustic pulses at 1 GHz, set up in two $AlN/Al_2O_3/AlN$ test structures (Z-284A-B and Z-284A-C). The results are seen to differ; Fig. 51a exhibits a longer pulse train than Fig. 51b. When the films on the faces of the former film-rod combination, Z-284A-B, were examined by reflection electron diffraction, the diffraction patterns shown in Figs. 52a and 52b were obtained. Fig. 52a is characteristic of AlN showing a (0001)-fiber texture; Fig. 52b indicates a $(11\bar{2}0)$-fiber texture, i.e., with the c-axis in the plane of the film. Later diffraction from set Z-284-C (the film labeled Z-284B ($(11\bar{2}0)$-orientation) was removed chemically and Z-284C was deposited in its place) indicated that both film orientations were of the (0001)-fiber texture type.

Although bulk values of the piezoelectric coefficients have not been reported for AlN, they are believed similar to other class 6 mm crystals such as CdS. Thus, one expects d_{31} and d_{32} to be smaller by a factor of 3 to 5 times than d_{33}. The electromechanical conversion efficiency for film pair Z-284A-C will, according to this premise, be greater than that for pair Z-284A-B by this factor and will be seen as an apparent increase in acoustic loss (attenuation) in the pulse echo

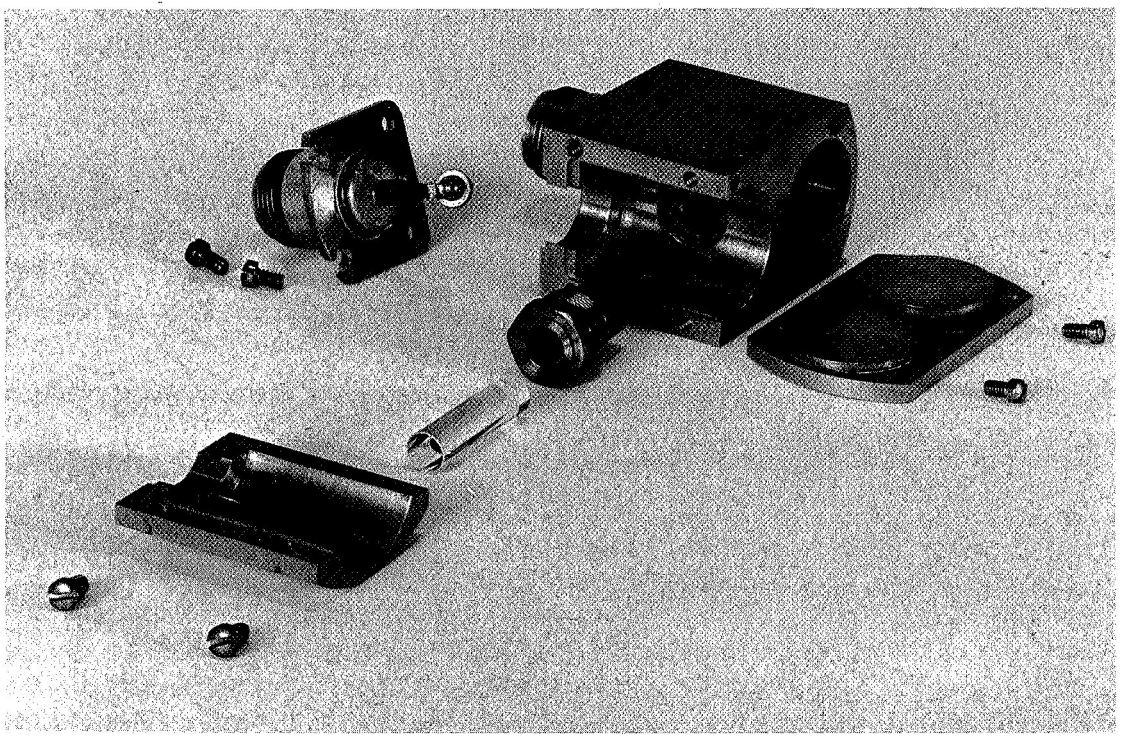

Fig. 50 Exploded view of the cavity used for the pulse echo measurements.

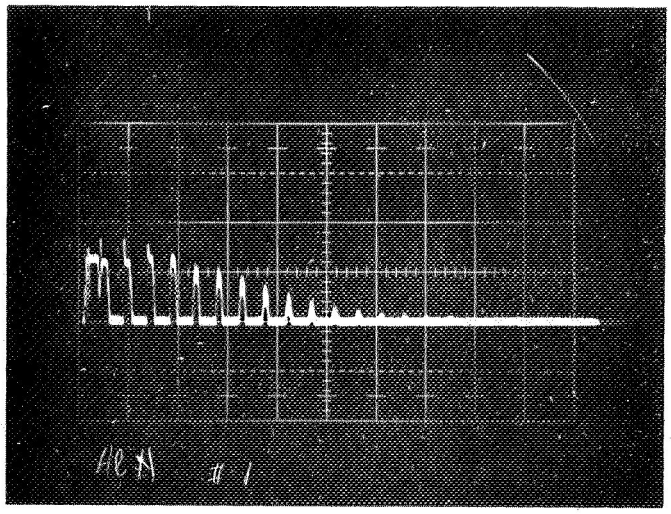

(a)

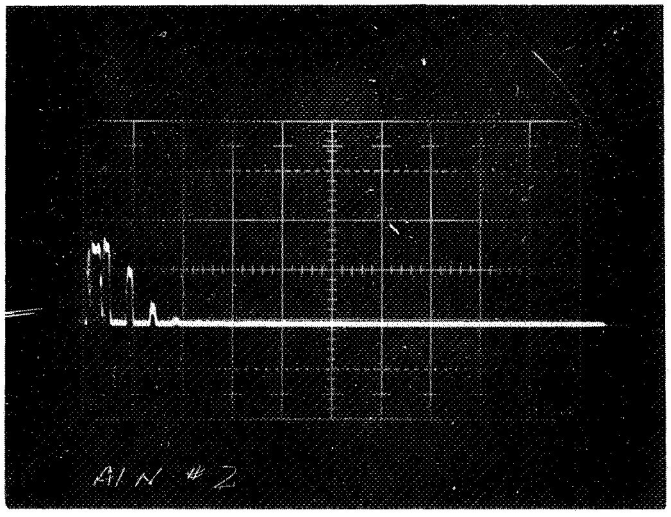

(b)

Fig. 51 Oscillograms of compressional acoustic pulses generated in AlN-Al_2O_3-AlN film-test rod combinations. The trace shown as (a) shows poor electromechanical coupling; trace (b) shows good coupling.

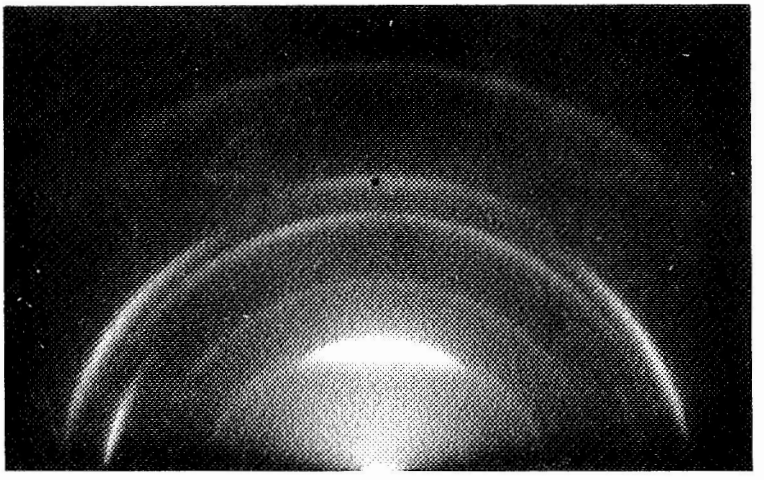

(a)

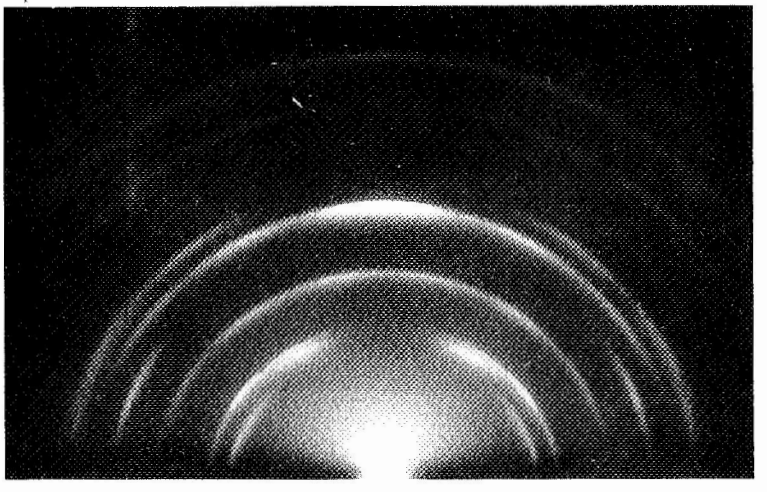

(b)

Fig. 52 Reflection electron diffraction patterns of AlN films deposited on opposite faces of a sapphire rod; (a) (00.1) orientation and (b) (11.0) orientation.

measurements. The sixteen echoes in Fig. 51a thus represent low loss (poor coupling) and show a property comparable to that observed for oriented ZnS films when they were used in this type of experiment. The four echoes in Fig. 51b represent a higher conversion efficiency (factor of 4) and show the coupling dependence on orientation. As potential device transducers, they favorably compare to films of CdS (Ref. 65) evaluated in similar fashion.

3.3.5.2 Transducers Z-285 - Another AlN film (Z-285) was deposited, this time at a slightly higher temperature, 925°C. The temperature adjustment was made to facilitate an increase in the degree of orientation adopted by the film. (Such an effect is observed in epitaxial AlN films deposited on Si.) The initial deposit of this series, Z-285A, was oriented but possessed a $(11\bar{2}0)$-fiber texture. This film was subsequently chemically dissolved and another film (Z-285B) was deposited in its place. The result was identical. Inspection of the furnace element, tantalum, showed considerable erosion and suggested that tantalum or a nitride of tantalum may have inadvertantly condensed at the substrate surface during a predeposition interval which is used to sputter-clean the aluminum cathode and to thermally stabilize the substrate heater. The layer if it exists, however, is not detectable by electron diffraction since examination of the uncoated face of the sapphire rod showed no obvious foreign phase. The attack on the tantalum furnace elements led to replacement by platinum.

3.3.5.3 Transducers Z-291, Z-292, Z-296 - These film/substrate combinations were deposited in the twin-cathode arrangement shown previously in Fig. 46. Deposits on both substrate faces were thus

made simultaneously. The substrate temperatures during deposition were as follows: 800°C (Z-291), 620°C (Z-292), and 950°C (Z-296). Deposition rates in all films were similar, viz., $\sim$ 40 Å/min. Strong (0001) and $(10\bar{1}2)$-fiber texture orientations were observed in both the 800°C films. These orientations were repeated although less pronounced in the 620°C deposits. The pair deposited at 950°C were not identical, one film showed a strong (0001)-fiber texture, the other a $(11\bar{2}0)$-fiber texture. The latter behavior is similar to that observed in deposits Z-284A-B.

When tested acoustically at 1.0, 1.25 and 1.6 GHz, none of the three film pairs functioned as efficiently as the well-oriented (0001) deposits of set Z-284A-C. The occurrence of the several unwanted orientations, however, can account for the poorer results.

3.3.5.4 Transducers Z-297, Z-298, Z-300, Z-305 - Films Z-297 and Z-298, deposited at 830°C, provided no electromechanical attenuation when subjected to the standard microwave pulse-echo measurements. These results were not anticipated since electron diffraction examination of the films showed good (0001)-fiber orientation. Since the Al_2O_3 test rods in both experiments had been used in previous experiments and considerable difficulty was experienced in restoring their surfaces to a newly-polished state, the results implied poor, possibly graded, interfaces. One of the rods was mechanically, then chemically, polished and Z-300 (770°C) was deposited. The acoustic traces are shown in Fig. 53. We note the attenuation to be weaker than that for films Z-284A-C. An x-ray investigation of the surfaces of Al_2O_3 rods subsequently

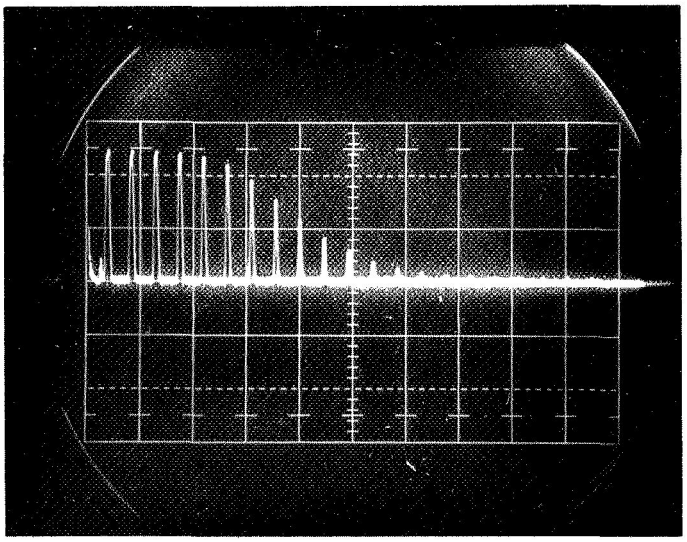

Fig. 53 Oscillogram of compressional pulses generated in Z-300 (A,B) an AlN-Al_2O_3-AlN experimental microwave acoustic pulse attenuator.

was made and revealed that a newly polished rod retained surfaces which showed considerable strain. Thus, the interfaces in Z-300 may have been sharp enough to permit some electromechanical coupling but the strain which remained in the vicinity of the rod faces inhibited a maximum effect. A second rod was repolished and etched for several days in a saturated NaOH solution. X-ray evaluation indicated surfaces with a lesser degree of strain. Deposits on this substrate at 760°C (Z-305), however, proved disappointing. Film Z-305A characteristically displayed a (0001)-fiber texture. Film Z-305B was more strongly oriented having reached a virtual epitaxial state, Fig. 54. There was some relative misalignment of the orientations of the various crystallites but good azimuthal alignment had been achieved. The orientation relationship between film and substrate was parallel, i.e., $(0001)_{AlN}||(0001)_{Al_2O_3}$; $[11\bar{2}0]_{AlN}||[11\bar{2}0]_{Al_2O_3}$. The acoustic traces Fig. 55, however, indicated that regardless of the degree of orientation, signal attenuation was again limited. The envelope modulation observed in the trace is due to slight ($\sim 6 \times 10^{-6}$ radian) relative non-parallelism of the film-rod interfaces.

3.4 Mixed Nitrides

The electrical instabilities (erratic breakdown) encountered in thin, < 1500 Å, AlN films were attributed to grain boundary conduction, the grains in many cases having linear dimensions comparable to the thickness. In an effort to suppress the crystalline habit of AlN, mixture with a less crystalline, but no less refractory, dielectric was sought. Si_3N_4 and BN were thus introduced as diluents. (It is reported that pyrolytically deposited films of these compounds are virtually amorphous) (Refs. 30,66).

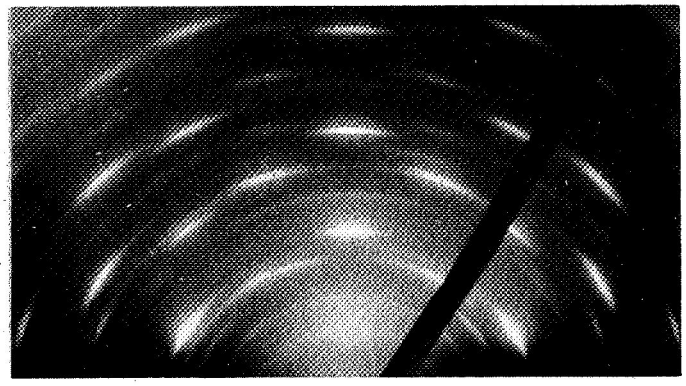

a

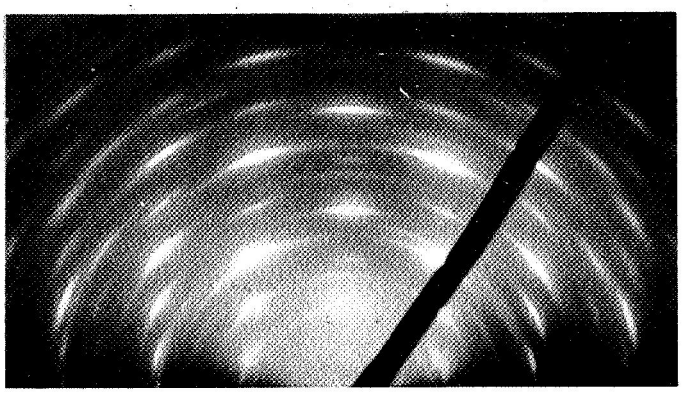

b

Fig. 54 Electron diffraction patterns of highly ordered AlN transducer film. There is finite misalignment of crystallites but the azimuthal dependence of orientation indicates epitaxy; (a) electron beam along [21.0]; (b) electron beam along [11.0].

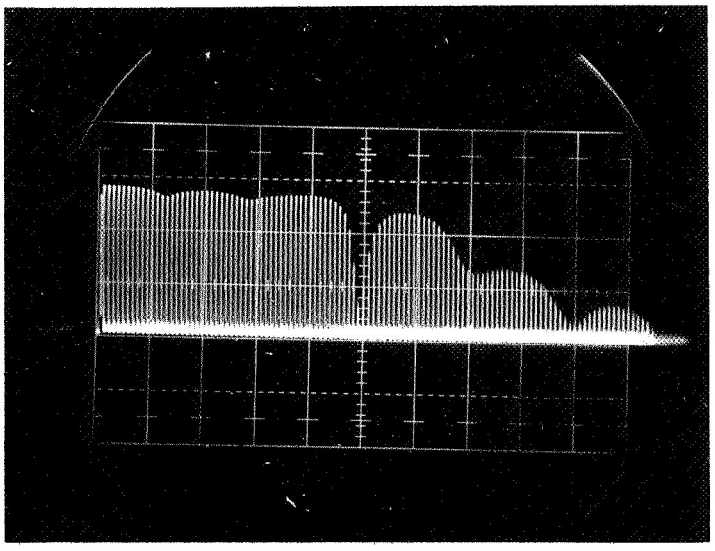

Fig. 55 Pulse train generated in Z-305(A,B). The large number of pulses show poor attenuation by the transducer films. Envelope modulation is due to nonparallelism of the film-rod interfaces.

3.4.1 Mixed Al-Si Nitrides

3.4.1.1 Preparation - Preparation of two sets of films, with nominal Al/Si ratios of 6/1 and 1/1 was accomplished. The ratios cited are related to the target areas of the respective elements and do not necessarily indicate the true compositions of the films. Films were deposited in the optimized conditions used for the diode sputtering of pure AlN (see Sec. 3.1.1). Substrates included Ta coated vitreous silica and n- and p-type Si wafers.

3.4.1.2 Structural and Optical Properties - When films prepared by sputtering a cathode with a 6/1, Al/Si area were examined by electron diffraction, it appeared to consist primarily of a polycrystalline AlN-type phase, Fig. 56. The diffraction data, however, showed some evidence of an additional component, one which caused diffuse scattering of diffracted electrons. When the 1/1, Al/Si target was used, the diffuse diffraction component became far more prominent. The partly resolved diffraction rings which were measured, however, indicated that a phase consistent with poorly crystallized AlN was still present.

Optical absorption measurements were made on both sets of AlN-Si_3N_4 films. The as-deposited films showed a diffuse absorption edge occurring in the approximate wavelength range as for pure, as-deposited, AlN films. Annealing at 900°C in N_2 caused a sharpening of the edge and a shift to higher energies, again in a manner similar to that for annealed AlN films.

While the shift for the 6/1, Al/Si nitride films matched that for the pure form, the edge of the 1/1, Al/Si nitride films shifted to energies greater than 5.9 eV, viz, to an absorption edge value of

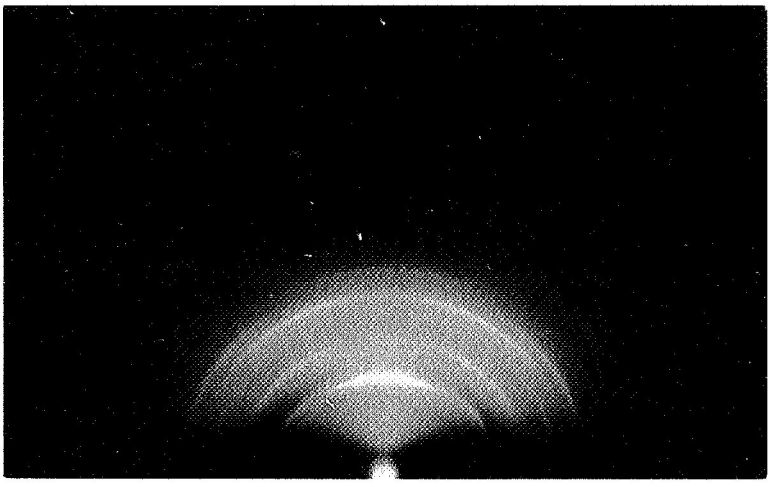

Fig. 56 Electron diffraction patterns of mixed AlN-Si_3N_4 film. Substrate temperature, 900°C; thickness 6000 A.

approximately 6.35 eV. The effect is unexpected since the energy gap of the added component, Si_3N_4, is reported to be 4.35 eV (Ref. 67). Other studies, however, have recorded conflicting values, e.g., 5.0 eV (Ref. 66) and 6.35 (Ref. 68).

3.4.1.3 Electrical Measurements - The results of capacitance vs voltage measurements at 1 MHz made for deposits on the Si substrates are shown in Fig. 57. The sandwich configuration, after Al counter-electrodes have been deposited is that of a MIS (metal-insulator-semiconductor) structure.

The symmetrical shift of the C-V plot for films deposited on p-type substrates indicates that a polarization effect probably is generated within the dielectric by the application of a field; such an effect is observed in the pure AlN films (see Sec. 3.1.10) and has also been observed in Si_3N_4 (Ref. 69). As for the pure AlN films, the polarization may be due to the orientation of dipoles in the AlN component by the applied field or by a stress-induced polarization inherent in it (AlN is strongly piezoelectric). The charge induced in the Si by the charges contained in the dielectric is $8.75 \times 10^{11}/cm^2$, a value intermediate between those reported for vapor deposited Si_3N_4 and SiO_2.

Deposits on n-type substrates showed no tendency to display loop-type characteristics, the flat band voltage exceeding 100 V.

Measurements relating current and voltage characteristics in the 6/1, Al/Si nitride films were essentially similar to those made on the pure nitride films, viz., currents followed on Ohmic behavior at low voltage then rose steeply as the voltage was increased; a further

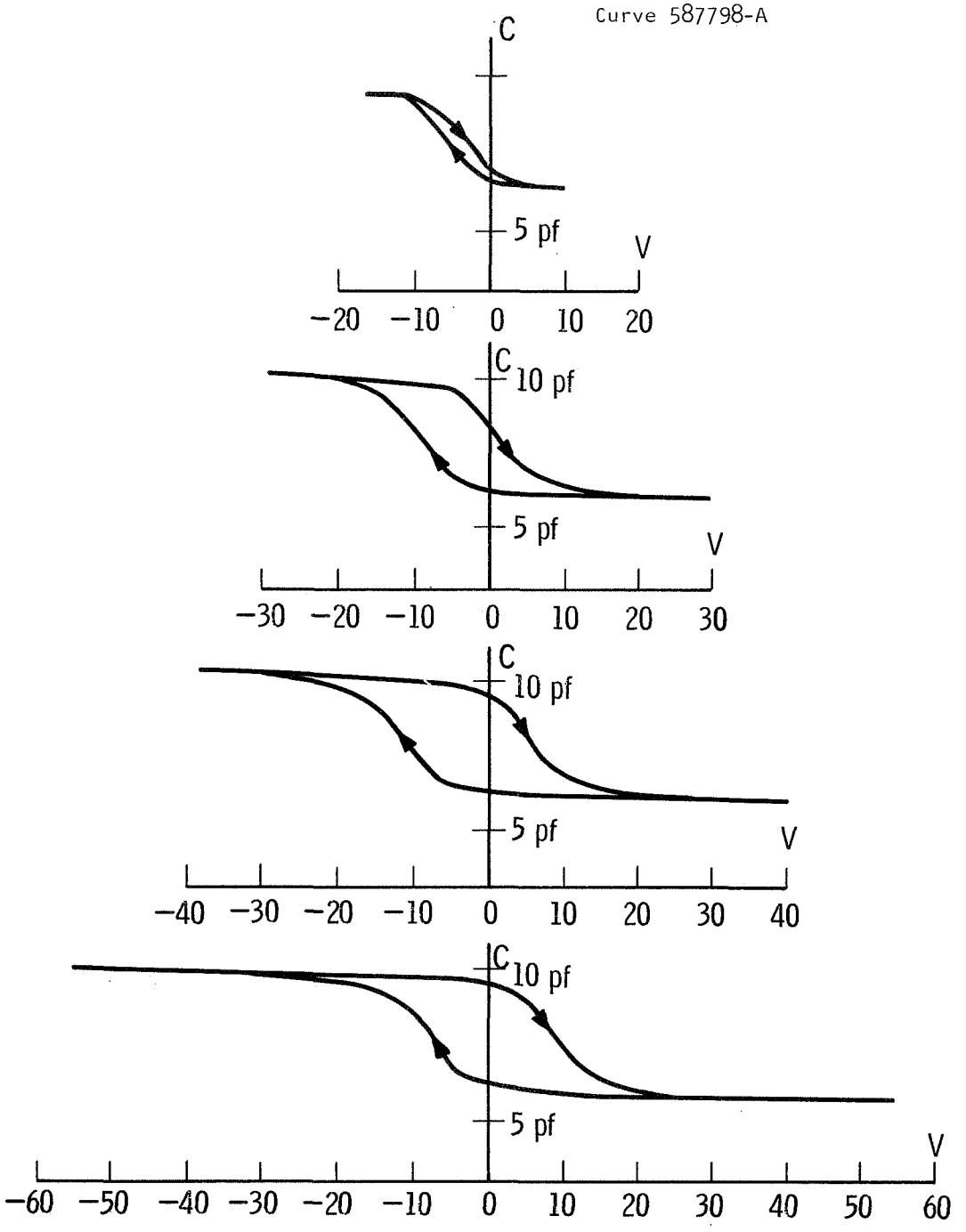

Fig. 57 Dielectric polarization effect observed in mixed AlN-Si_3N_4 films. Film thickness is approximately 4500 A.

voltage increment induced a time dependent instability followed by breakdown or a major change in the I-V characteristic.

In the 1/1, Al/Si nitride films, however, a reproducible and highly stable I-V behavior was followed, Fig. 58. The slopes of the curves at the low and high voltage values represent Ohmic and trap-filled space-charge behavior, respectively. The voltage at which the transition between the main conduction mechanisms occurred, the traps-filled-limit, was low ($\sim$ 10 V) relative to the values for pure AlN films. In addition, the slope of this transition was less steep and suggests that fewer but probably more active traps take part in conduction. Although the I-V characteristics of the 1/1 mixed Al-Si nitride films were stabilized by the mixing, dielectric measurements showed a range of dispersion with frequency. The dielectric properties of pure Si_3N_4 are unfortunately not well characterized at various frequencies. Several reports list conflicting values of dielectric constant, e.g. 12.0 (Ref. 70) and 6.2-8.5 (Ref. 71) but this property seems to be strongly influenced by the density of the deposited layers and the given values seem only relative to this property. We suggest that both the conduction behavior and frequency dispersion of the dielectric properties are attributable to a modification of the numbers and levels of trapping, or impurity sites, relative to those operative in sputtered AlN films.

The 6/1, Al/Si nitride layers displayed no obvious dispersion with frequency showing, rather, dielectric properties similar to those of undiluted AlN.

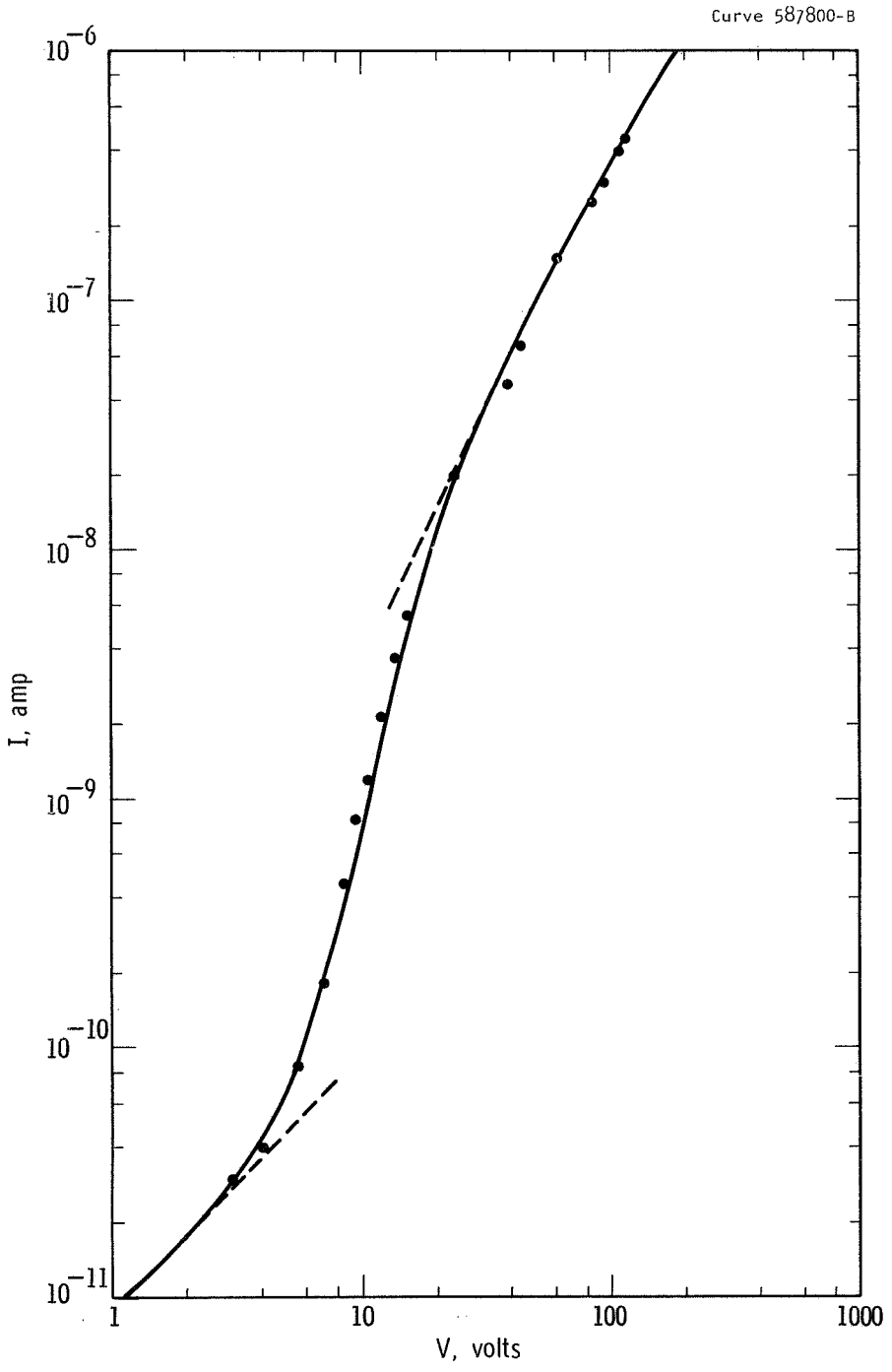

Fig. 58 I-V data for mixed AlN-Si_3N_4 film. Cathode Al:Si ratio is approximately 1:1.

3.4.2 Mixed Al-B Nitrides

3.4.2.1 Preparation - The experimental apparatus used to deposit films of a mixed AlN-BN composition is also similar to that used previously for the reactive sputtering of AlN. Figure 59 shows a schematic of the arrangement consisting of a target, target shield, and four movable substrate holders. The target is a high purity aluminum (99.999%) disk which has been milled to accommodate plugs of boron (99.9999%). The boron plugs are 8 mm in diameter. A variable Al/B sputtering area ratio was obtained merely by adjusting the number of plugs. Substrates included both polished silicon and silica which were heated resistively or via tantalum strip heater envelopes. Substrate temperatures were adjustable to 1000°C and were monitored optically with both a conventional optical pyrometer and an "Ircon" Model 300 Infra-red pyrometer. The deposition procedure was also essentially similar to that used for AlN. After evacuation of the uhv chamber to 10^{-9} torr, backfilling with 80×10^{-3} torr of argon (purity 99.995%) commenced. Sputter-cleaning of the cathode (-2750 V, 1 ma/cm^2) was then carried out for about one hour. Injection of nitrogen (purity 99.999%) followed until a 5×10^{-3} torr increase in total pressure was maintained. The substrate was heated, moved into the discharge and a deposit was collected.

3.4.2.2 Composition and Structure - Two series of films were initially prepared using substrate temperatures in the range 800-900°C and with Al/B area ratios on the sputtering target surface of 3/2 and 2/3, respectively. In each experiment the substrate was cooled rapidly after completion of film growth by turning off the input

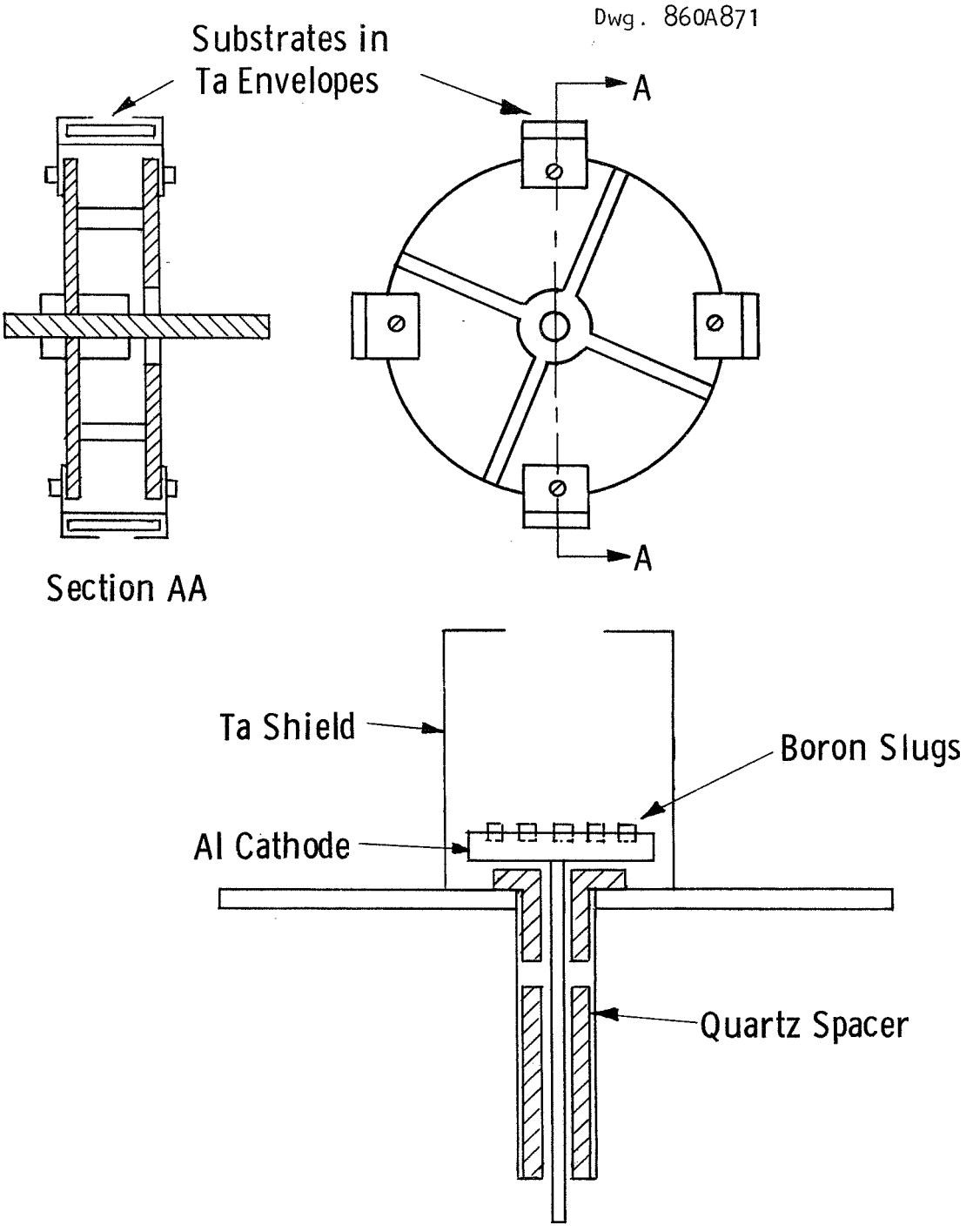

Fig. 59 Schematic for target and substrate holder assembly used in preparation of reactively sputtered films of the mixed composition (Al,B)N.

power to the heater. Electron microprobe measurements were made on the "2/3" films to determine the actual Al/B ratio of the films; (the boron detection was accomplished by the use of a lead stearate crystal and a methane-argon filled flow proportional counter). Measuring inaccuracies were introduced due to a need to coat the AlN-BN film with a conducting carbon layer during examination. The coating reduced charging effects due to the insulating silica substrate but absorbed almost 50% of the boron x-radiation. The best Al/B ratio estimates are between 2.4/1 and 4/1 (atom ratio). Structural evaluation by x-ray techniques showed only the well-resolved AlN-type phase, however, in the case of films produced from both target compositions this phase was found to possess slightly smaller lattice parameters than pure AlN, Table VII.

TABLE VII

Table of Lattice Parameters for AlN and AlN-BN

AlN			AlN-BN (900°C)		
a	c	c/a	a	c	c/a
3.11 Å	4.96 Å	1.60	3.08	4.88	1.58

Another set of films were grown, the nominal Al/B target area ratio again being 2/3, but extending the substrate temperature range to 500°-900°C. At temperatures less than 600°C the cell parameters showed no deviation from those observed for pure AlN. At higher temperatures, the shrinkage was again evident. Examination of these films by transmission electron diffraction revealed the presence of a strong BN phase in addition to the AlN one, Fig. 60, indicating that

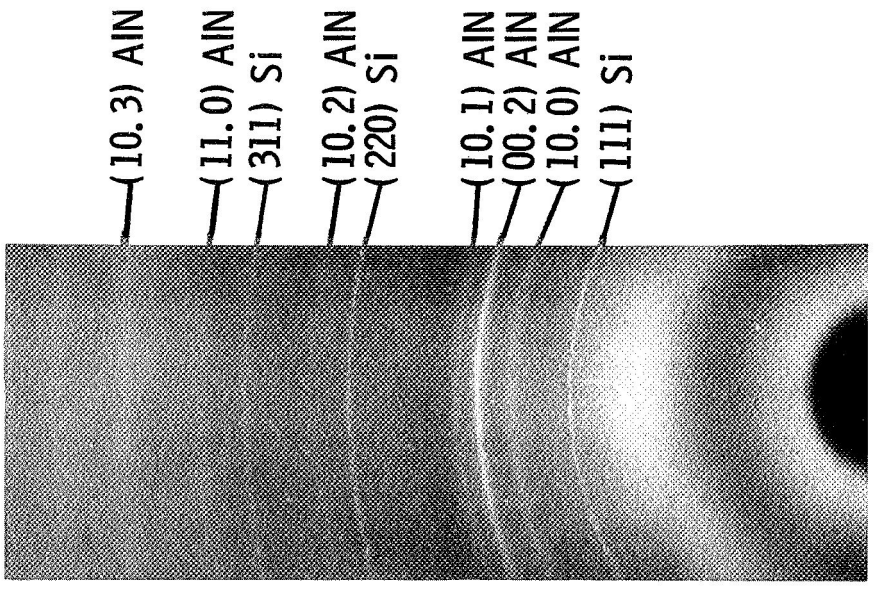

Fig. 60 Diffraction from mixed AlN-BN films; (a) glancing angle x-rays and (b) transmission electron diffraction. The BN-phase is not obvious in the x-ray pattern due to extreme line broadening. Spotty rings due to Si standard.

limiting solubility of BN in the AlN-type phase had been reached. Reference to later measurements of diffraction results on BN films indicated that the BN phase showed no noticeable lattice parameter change.

Diffraction patterns from films of the 3/2, Al/B nominal ratio, showed a greater degree of disorder, Fig. 61 (the estimated Al/B atom ratio is 1.5/1), although the AlN-phase is still evident. Direct determination of the amount of boron in solution in the "contracted" AlN-rich phase are not easily obtained. Differentiation between boron in solution and boron in the unreacted BN component, for example, cannot be achieved by the microprobe analyses. One notes also that borides of aluminum, viz., AlB_2 and AlB_{12}, are known to exist (Ref. 72) although not observed as a major component in these films. The amount of dissolved boron could presumably be determined using a "disappearing phase" approach which entails gradual reduction of the B/Al ratio until the unreacted BN phase is no longer observed by x-ray diffraction. A microprobe determination would then give the amount in solution. If it is assumed that Vegard's law is followed for the AlN-type solid solutions, then taking 1.26 Å and 0.88 Å (Ref. 73), respectively for the tetrahedral radii of aluminum and boron, the lattice parameter changes observed are consistent with a solution of approximately 6 - 7-1/2% of boron in AlN.

3.4.2.3 Dielectric and Optical Measurements - Capacitance measurements were made on large area (1 mm^2), capacitor structures of the mixed nitride films. A moderate dispersion with frequency was noted, viz., C = 74.3 pF (500 Hz), C = 61.1 pF (500 kHz); this was less apparent

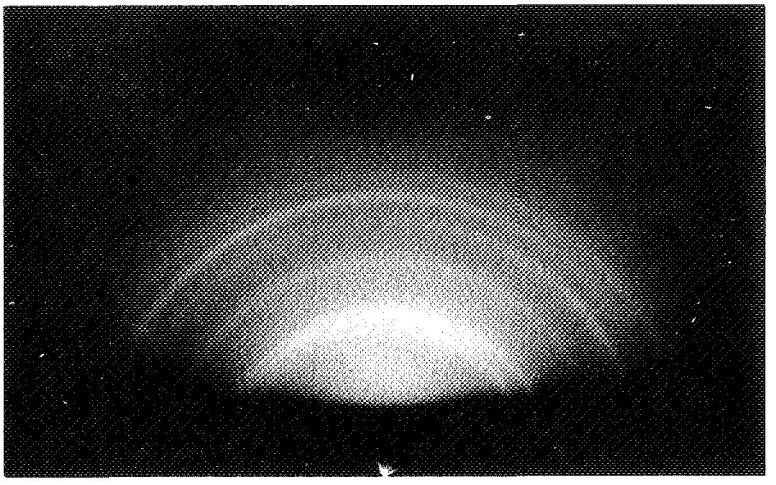

a

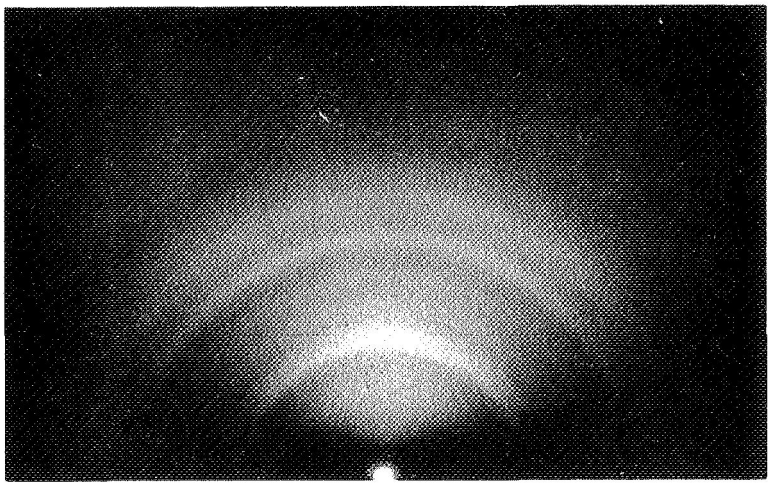

b

Fig. 61 Electron diffraction patterns from reactively sputtered films of mixed (Al,B)N composition; (a) film contains 20 to 35 atomic percent boron; (b) film contains 30 to 45 atomic percent boron.

for values of loss, viz., D = 0.03 (500 Hz), D = 0.04 (500 kHz). Values for the dielectric constant computed from these data range from 6.8 to 9.1.

In Fig. 62 optical absorption data obtained with the Cary instrument are shown in the vicinity of the absorption edge. Values for the annealed and unannealed mixed films fall within the observed energy range spanned by annealed and unannealed films of pure AlN (Sec. 3.1.4). In two-phase film structures of the type considered, we expect the spectral cut-off to be determined by the component whose absorption edge occurs at lowest energy. Thus it is probable that the unannealed film spectrum represents the AlN-type phase component and reflects, qualitatively, the amount of BN in solid solution. The absorption edge position in the annealed films lies close to the edge observed for annealed pure BN films (Ref. 74). It may be that the BN phase is setting the limit in this case, however, nothing is yet known about the possible role, if any, of solution of AlN in BN.

3.4.2.4 C-V Measurements - After Al counterelectrodes (0.3 mm diameter) were evaporated, the mixed nitride films deposited on n- and p-type Si substrates were subjected to standard C-V measurements (Ref. 75). Results are shown in Figs. 63, 64, and 65 and are unlike those in which AlN alone is the dielectric. The curves have a dual-segment appearance and show a hysteretic effect in which the trace movement is indicative of surface state charge. The interaction between the applied field and these surface states is especially apparent in Fig. 65 where the rate of application of applied field is varied. During a positive excursion,

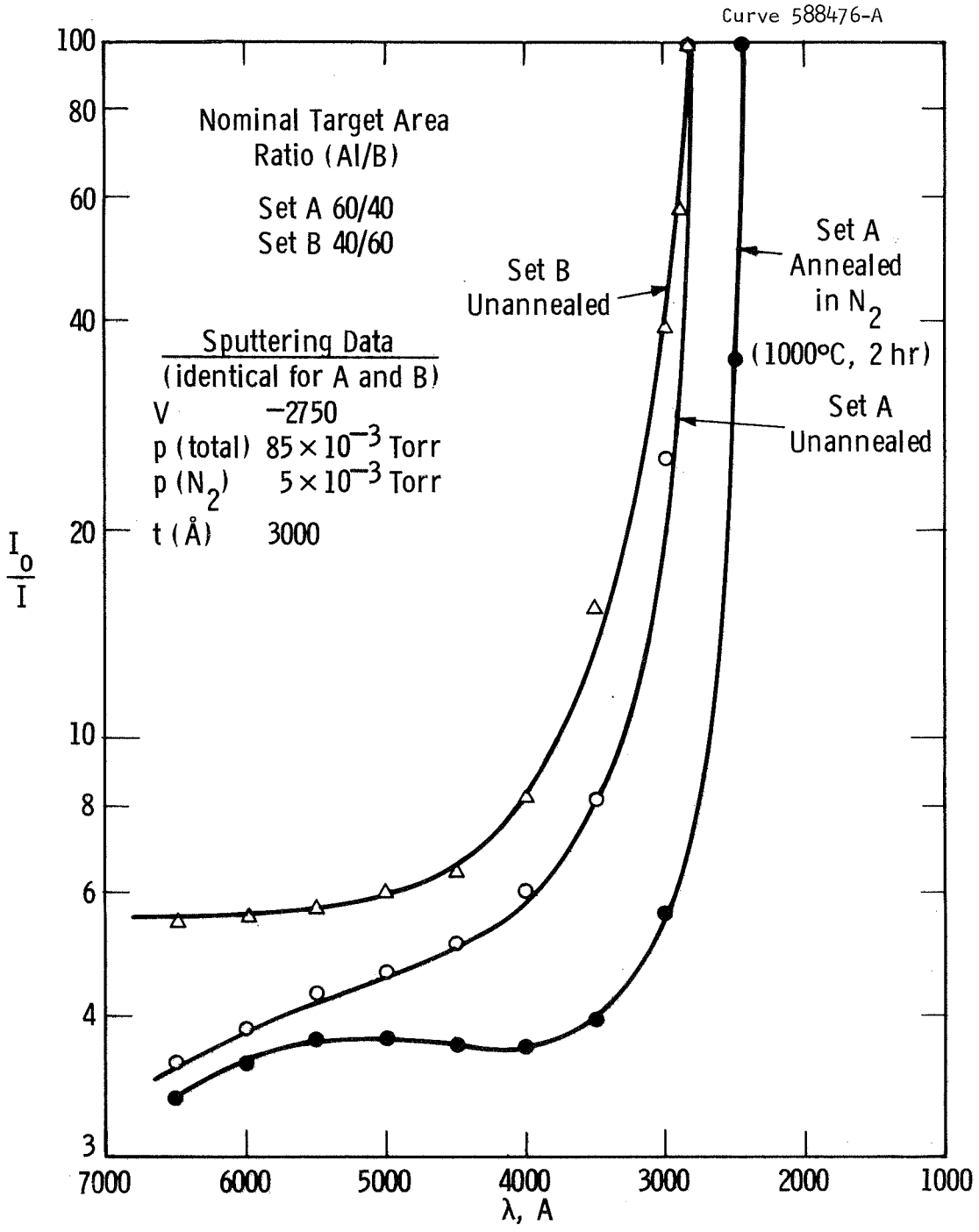

Fig. 62 Optical absorption data for mixed films of AlN-BN. Films prepared from cathodes of variable Al/B ratios.

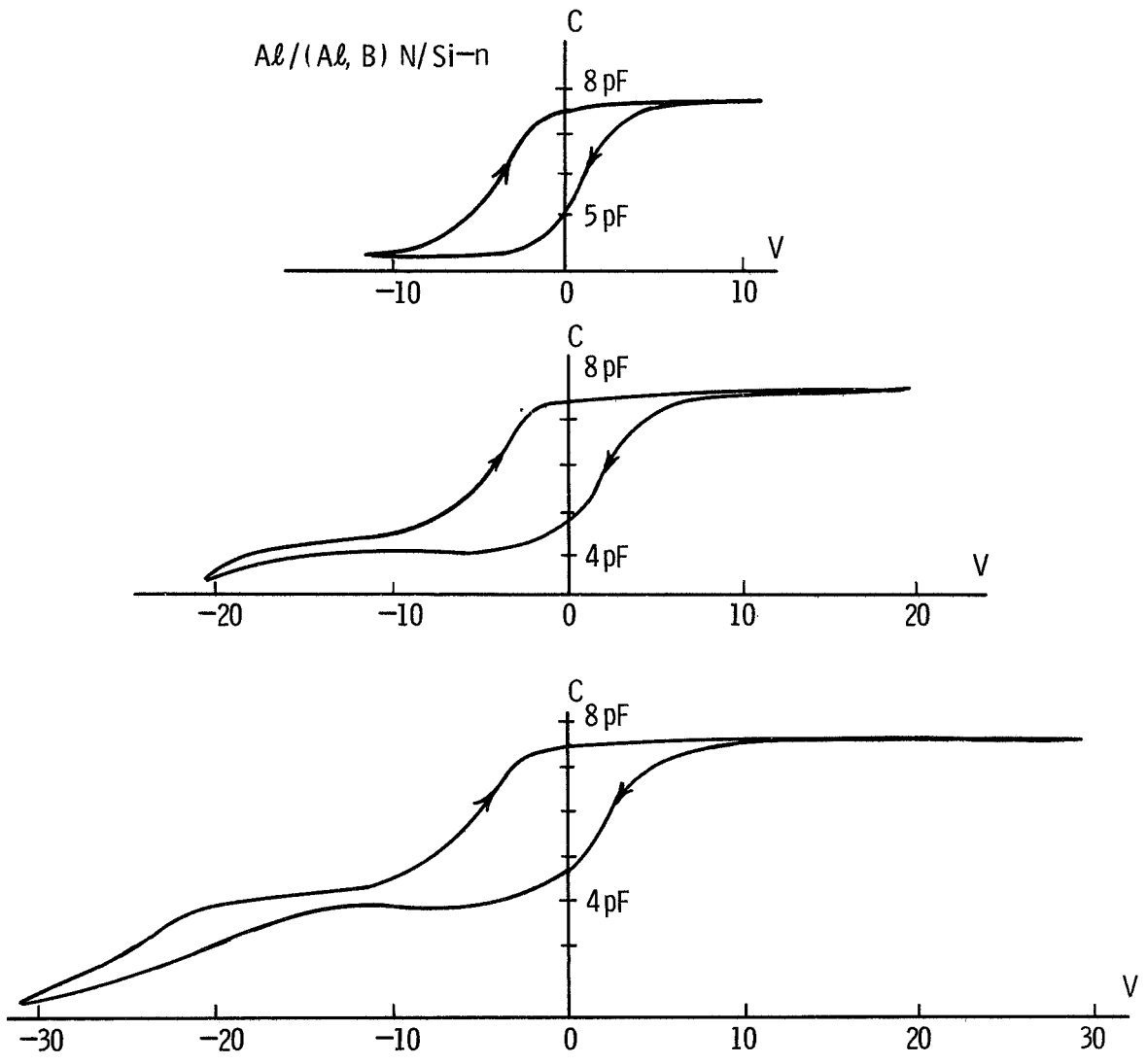

Fig. 63 C-V curves from films with a mixed AlN/BN composition prepared by reactive sputtering. Film thickness = 6000 Å.

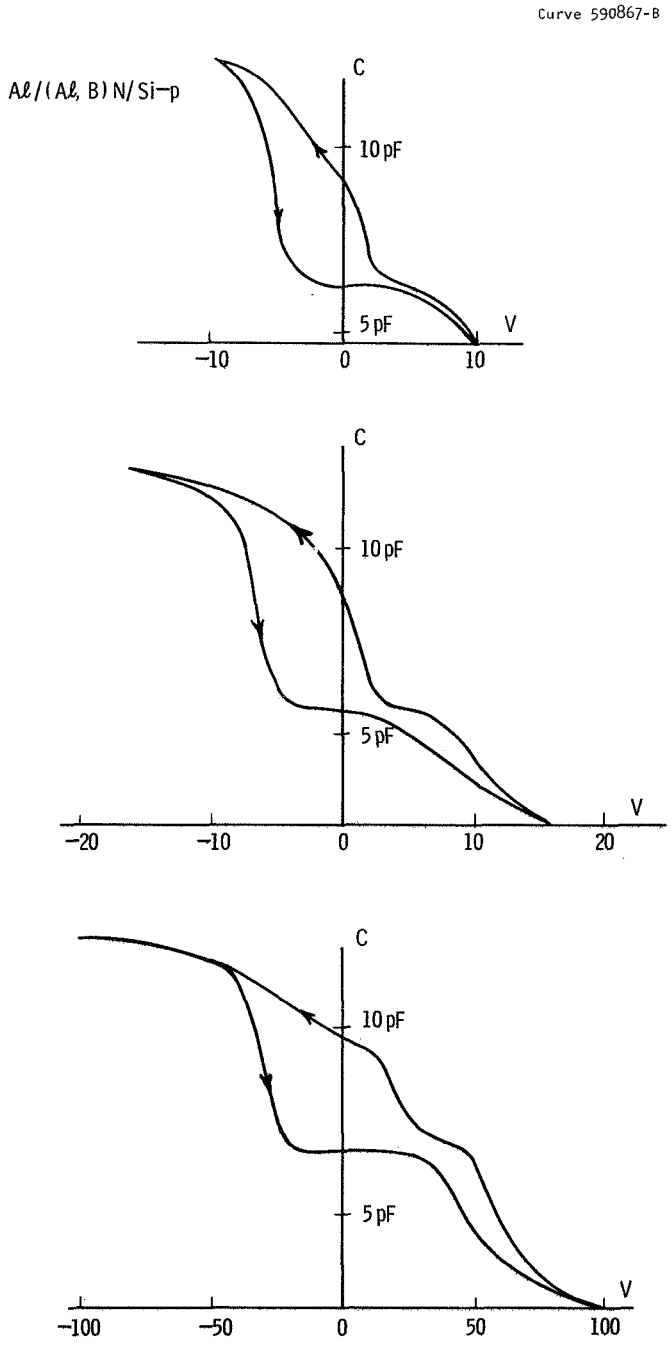

Fig. 64 C-V curves from films with a mixed AlN-BN composition prepared by reactive sputtering. Film thickness = 3600 Å.

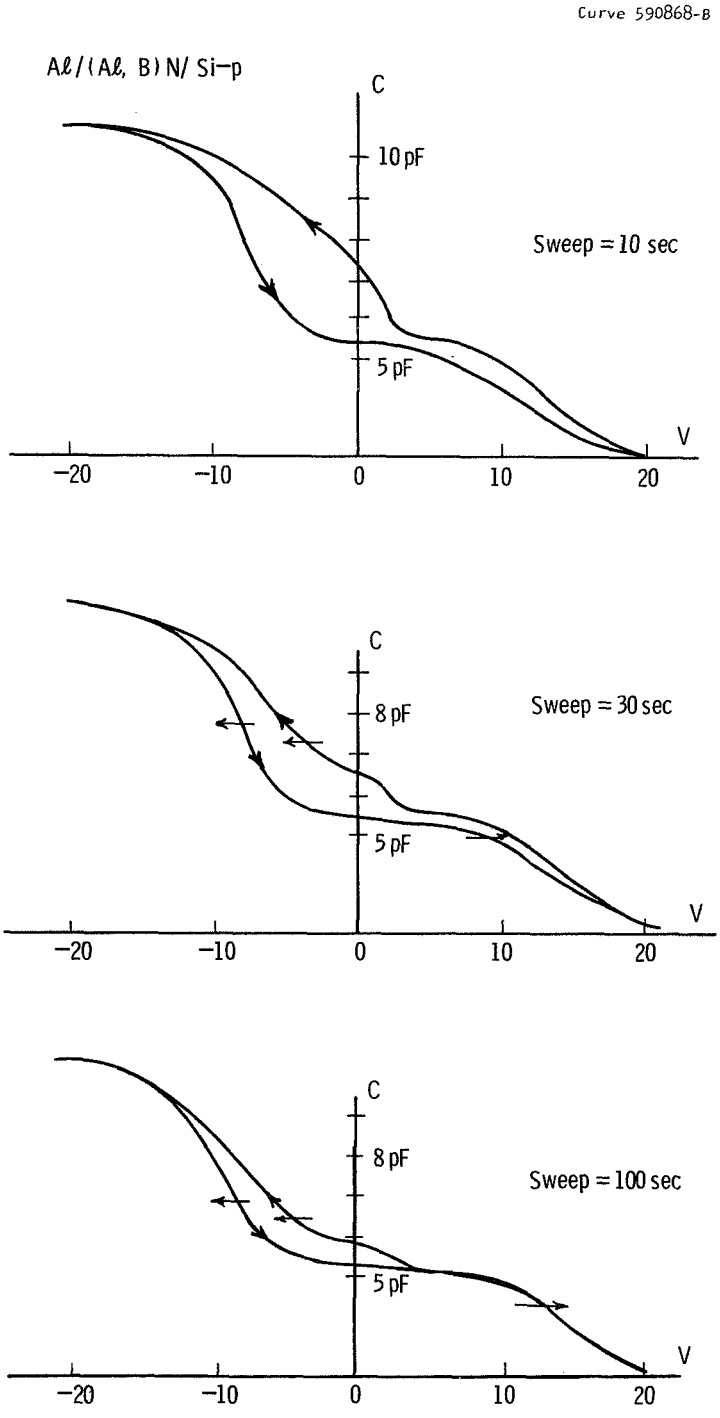

Fig. 65 C-V curves from films with a mixed AlN-BN composition. Thicknesses = 3600 A. Slowed sweep rate permits more extensive interaction of stress generated charge with surface states.

a greater number of surface states are filled when a given voltage is applied more slowly. A voltage sweep in a negative direction is equally more effective in emptying "negative charge" surface states (and filling "positive" charge ones) when applied at slower rates.

The mixed nitride films did show excellent voltage stability, there being no evidence of breakdown at 180 V (the limit of the measuring apparatus). Thus, the breakdown field exceeds 5×10^6 V/cm. The "dual-segment" loop does not lend itself readily to calculation of surface charge. These data were therefore not pursued. Estimates of the dielectric constant, ε, of this mixture were made from difference capacitance measurements made in the accumulation and depletion modes, respectively of the semiconductor. The data indicate a value of 6.9 ± 0.3, a figure between the reported values for AlN, 8.5 (Ref. 5) and BN, 3.8 ± 0.2 (Ref. 30) and 5.12 (Ref. 76).

3.5 Reactively Sputtered BN Films

Since the mixed AlN-BN films had not adopted a completely amorphous structure even when the Al/B ratio was approaching unity, it was decided to investigate the BN component alone for possible use as the insulating film in an MIS device.

3.5.1 Preparation - The uhv, diode sputtering apparatus used for the preparation of AlN was modified only slightly. A cathode was fabricated by imbedding slices of bulk boron (99.9999) into a, "research grade", BN block, Fig. 66. The combined surface area of the imbedded boron slices was approximately 5 cm^2. It was noted that with an applied

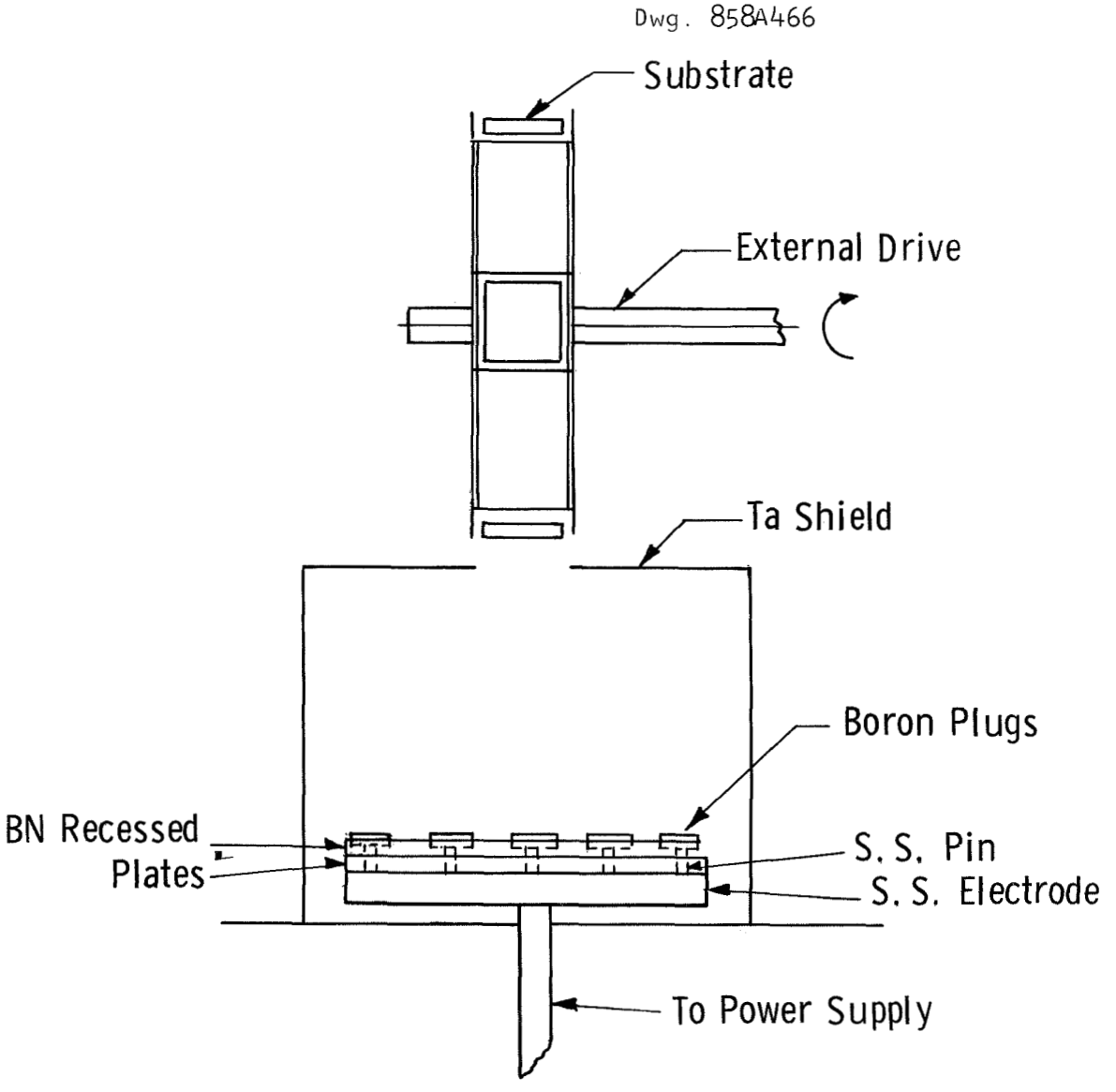

Fig. 66 Schematic of arrangement used to reactively sputter BN films. Plugs of B are imbedded in BN plates. Electrical contact to the B is made via hidden stainless steel pins.

voltage of -2800 Vdc, a current density of 4 ma/cm^2, a target-substrate spacing of 5 cm, and a substrate temperature of 1000°C, films could be formed at growth rates of 10 Å/min.

3.5.2 Structural Studies on BN Films - A study was made to investigate the structural effects produced by variation of substrate temperature during deposition. Several films were deposited onto resistively heated Si(111) substrates. Three substrates were held at 1150°C, 950°C and 600°C, respectively. A fourth substrate was not heated intentionally. Electron diffraction showed that the film deposited at 1150°C possessed a (0001)-fiber orientation, Fig. 67, while the lower temperature deposits possessed no preferred orientation and showed rather diffuse ring patterns no differences due to temperature are evident. Using the diffraction spots (included with the diffraction rings for the unheated films and due to scattering from surrounding areas of the single crystal Si(100) substrate) for calibration, the transmission data can be indexed on a hexagonal cell with the following parameters.

$$a = 2.45 \text{ Å} \quad , \quad c = 6.88 \text{ Å}$$

When compared to the bulk values (Ref. 44) for the hexagonal form, viz.,

$$a = 2.51 \text{ Å} \quad , \quad c = 6.66 \text{ Å}$$

we note the difference to be of the order of 2-4%. The source of this deviation in the thin film lattice parameters is not known, but it appears possible that it may be associated with structural disorder, non-stoichiometry or the occlusion of trapped argon. A list of d-values

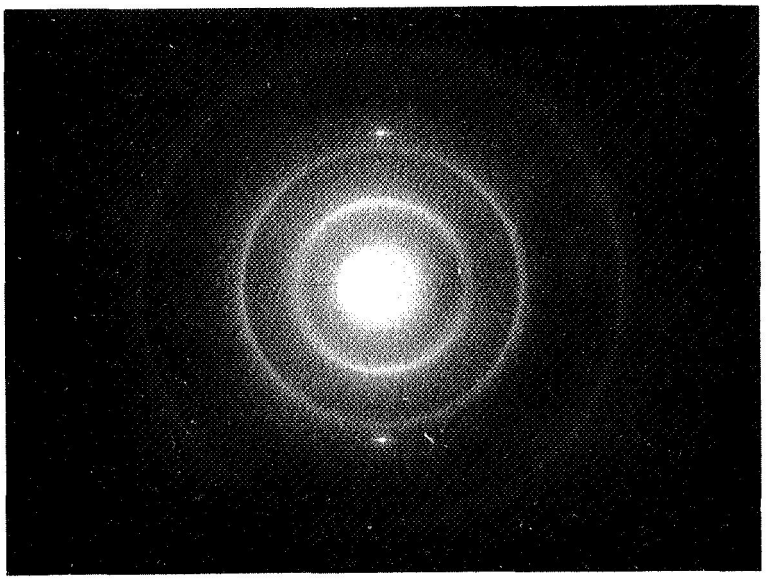

Fig. 67 Electron diffraction pattern of reactively sputtered BN film deposited on Si at 1150°C; (00.1) fibre texture denoted by arced diffraction rings.

and relative intensities are given for the bulk and thin film forms in Table VIII.

Table VIII Diffraction Data for BN

BN (bulk)			BN (film)		
d(Å)	I	(hk.l)	d(Å)	I	(hk.l)
3.33	vs	00.2	3.48	vs	00.2
2.17	m	10.0	2.12	m	10.0
2.06	w	10.1			
1.82	m	10.2			
1.67	w	00.4	1.72	w	00.4
1.55	vs	10.3			
1.32	vw	10.4			
1.25	w	11.0	1.23	mw	11.0
1.17	w	11.2			
1.14	vvw	10.5			
1.11	vw	00.6	1.16		00.6
1.08	vw	20.0	1.06	vw	20.0
a = 2.51 c = 6.66			a = 2.45 c = 6.88		

A transmission electron microscopy investigation of these films revealed some additional features. The lower temperature (unheated, 600°C) deposits showed little contrast being uniformly microcrystalline. The 1150° and 950°C deposits comprised the microcrystalline component interspersed with larger isolated shapes, Fig. 68; the lateral dimensions of these regions varied, being 700 Å for the 1150°C film and approximately 300 Å for the 950°C one. Identification of the larger areas as a separate phase could not be made from x-ray or electron diffraction examinations of these films; (Rand and Roberts (Ref. 30) report the presence of

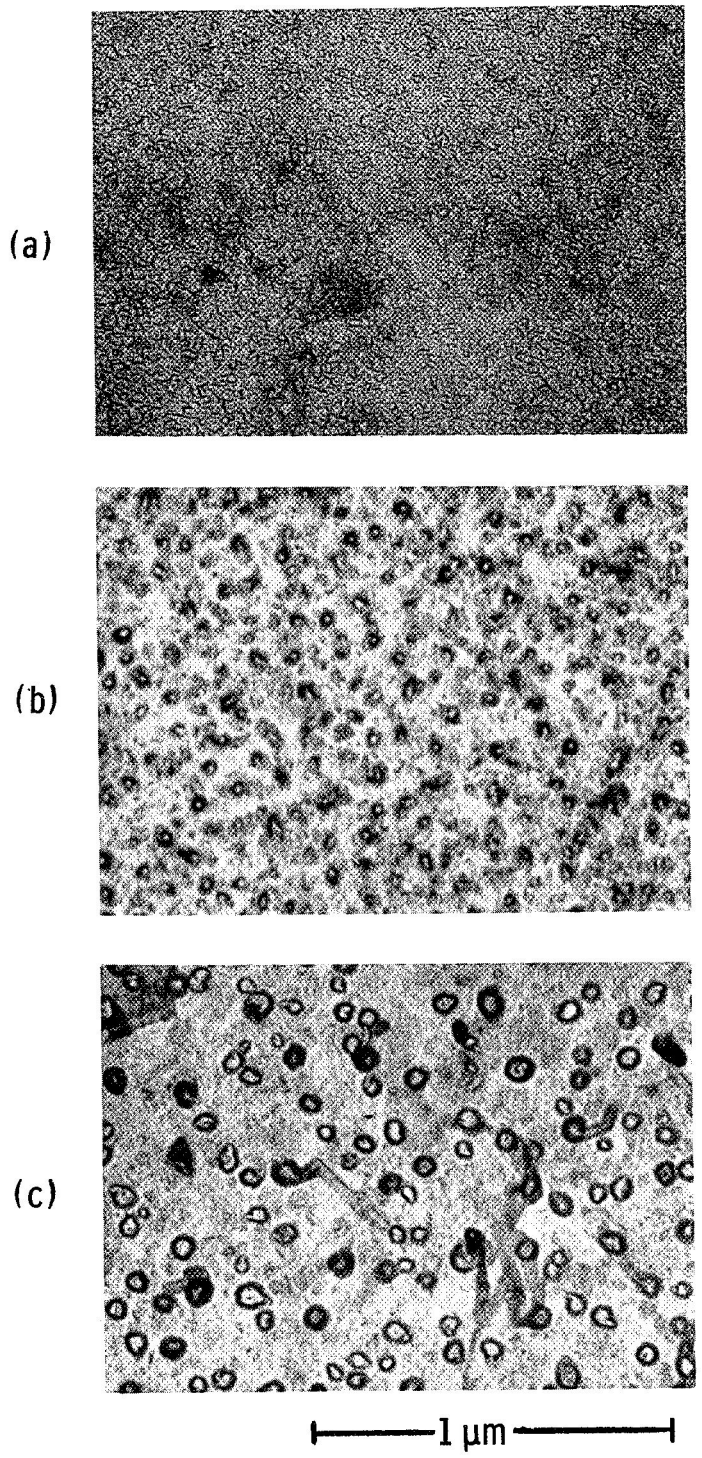

Fig. 68 Electron micrographs from reactively sputtered films of BN on resistively heated Si substrates, (a) T_S = 600°C; (b) T_S = 950°C, (c) T_S = 1150°C. Average film thicknesses = 1000 Å.

large crystals of boric acid in pyrolytic BN as a result of prolonged exposure to the atmosphere.)

3.5.3 Optical Measurements I-Infrared - Infrared absorption measurements, Fig. 69, were conducted on the film described in Sec. 4.2. The prominent feature in each case was a strong absorption band centered near 1380 cm^{-1} (7.25 μm) which is characteristic of BN (presumably due to a B-N band stretch) in both bulk (Ref. 77) and pyrolytic forms (Ref. 78). An additional band is observed near 810 cm^{-1} (12.3 μm), again in agreement with the bulk value.

An infrared investigation of some mixed AlN-BN films was also carried out at this time, and the strong 1380 cm^{-1} band was again clearly noticeable, Fig. 70. These results confirm electron diffraction data which indicate that free BN is present together with an AlN rich, AlN-BN solid solution phase in the mixed composition films.

3.5.4 Optical Measurements II-Visible and Ultraviolet - Optical absorption measurements were also performed in the visible and ultraviolet on four pairs of BN films deposited on silica substrates. In these films the substrates were either unheated during deposition or heated to 600°, 900° or 1100°C, respectively. One member of each pair was subsequently annealed near its deposition temperature in nitrogen (an excpetion to the annealing schedule involved a deposit on an unheated substrate, annealing being performed at 600°C). The experimentally observed short wavelength limits of observed absorption edges from this series are shown in Table IX.

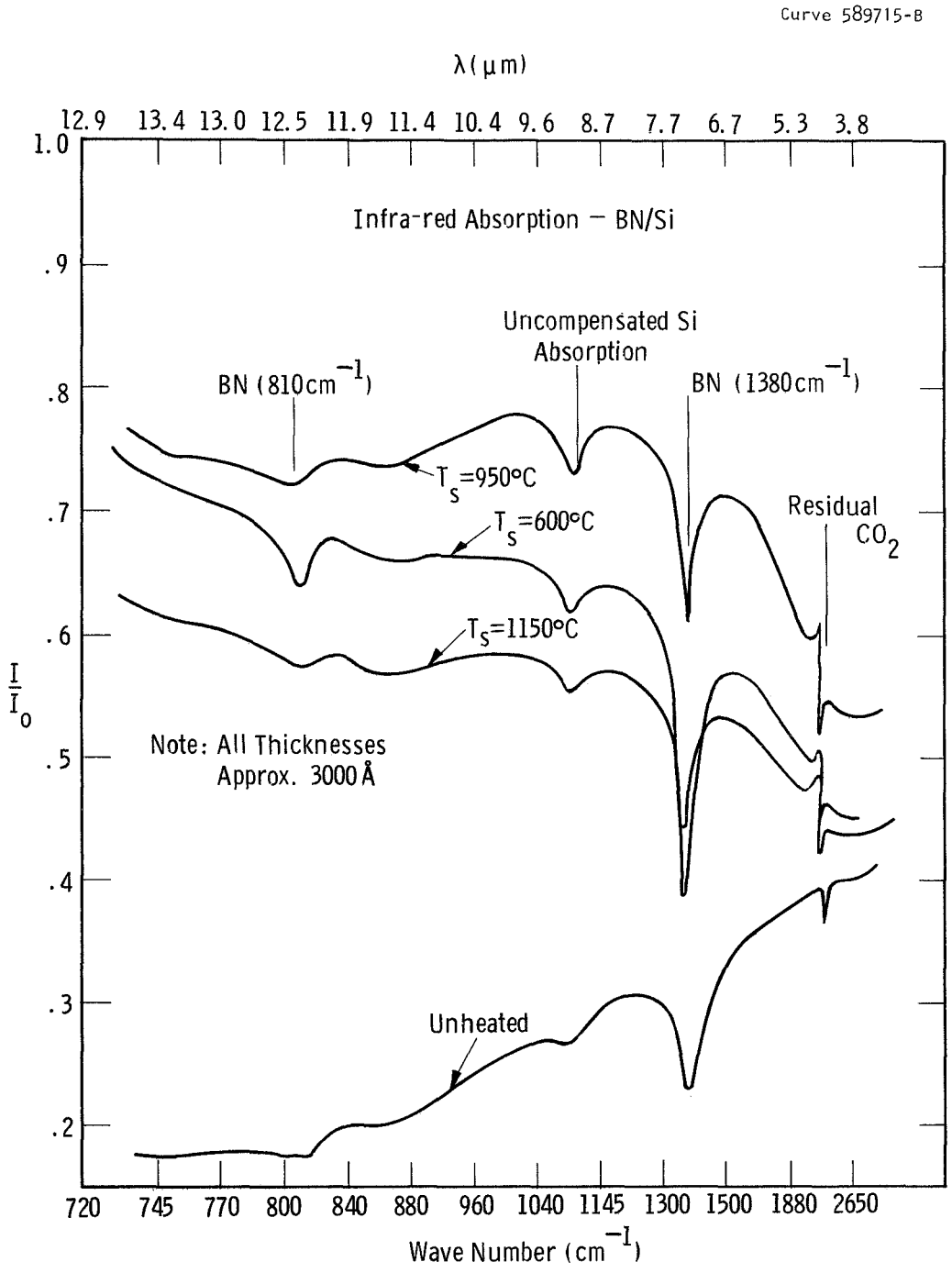

Fig. 69 Infrared absorption spectra for reactively sputtered BN films on Si substrates. Strong absorption at 1380 cm^{-1} and 810 cm^{-1} are likely due to BN bond stretching (observed also in bulk BN).

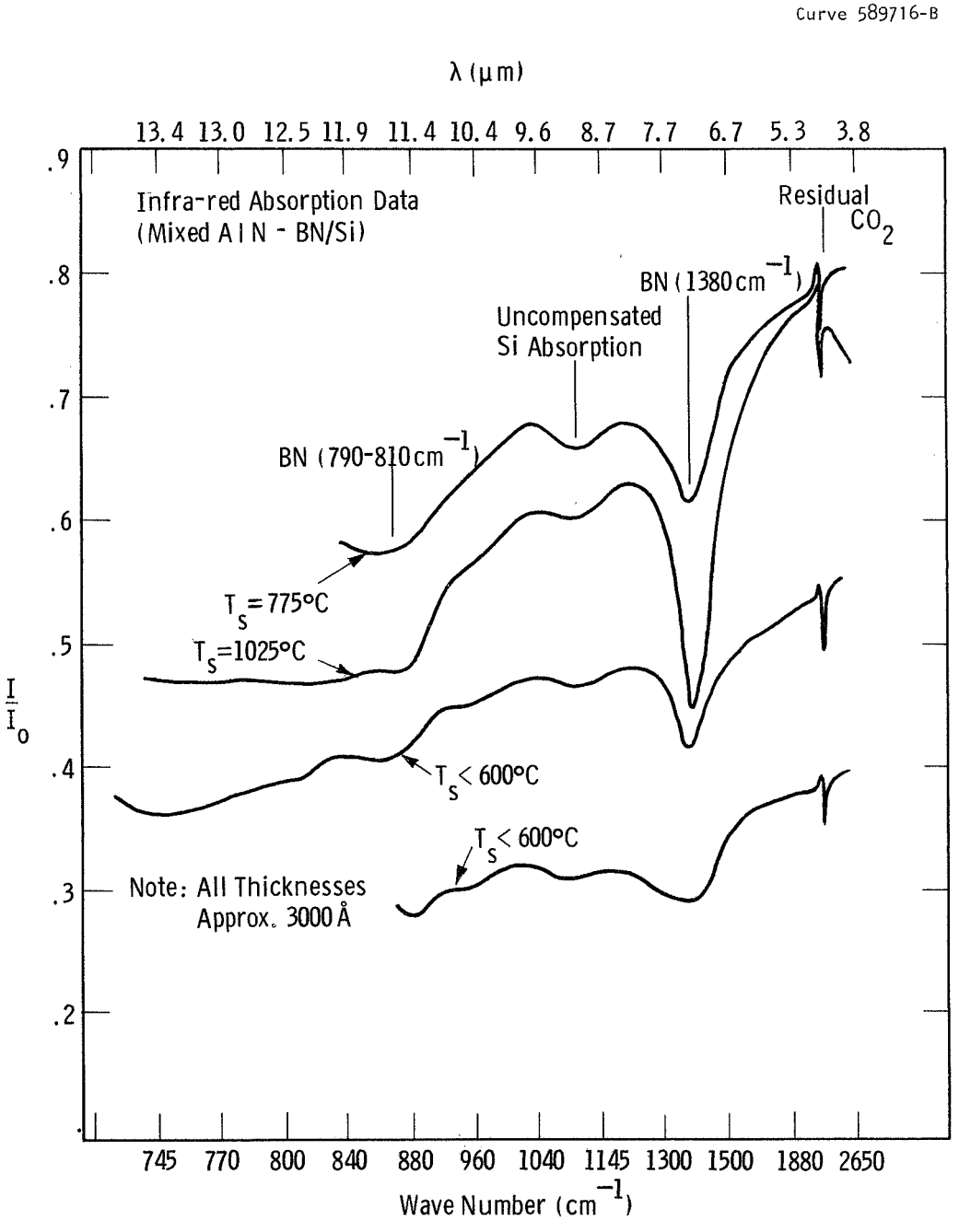

Fig. 70 Infrared absorption spectra for reactively sputtered films of a mixed (Al,B)N-BN composition. The strong absorption at 1380 cm^{-1} is related to the pure BN component.

TABLE IX

Relative Displacement of Absorption Edge in BN Films

T_s	Absorption Edge (eV) 4.0 — 5.0 — 6.0
unheated	4.21 |←——————→| 5.8 annealed at 600°C
600°C	5.1→||←5.2 annealed at 600°C
900°C	5.7→||←5.7 + annealed at 900°C
1100°C	5.8||←5.9 annealed at 1100°C

We note a progressive shift of the absorption edge to higher energies with increasing deposition temperature. A further shift is observed for films which are subsequently annealed in nitrogen. The latter effect is most pronounced when the annealing temperature is significantly greater than the deposition substrate temperature (T_s).

Several deposits were prepared at 1000°C on "Suprasil" and examined in the ultraviolet spectrum by means of the precision spectrophotometers described in Sec. 2.2.4. The results, Fig. 71, indicate that the observed absorption edge occurs at 5.72 ± 0.05 eV. Reported values for CVD deposits are 3.8 (Ref. 30), 5.0 (Ref. 31) and 7.8 (Ref. 79). The calculated value for bulk hexagonal boron nitride is 7.533 (Ref. 80). The present data seem to be most consistent with the value ($\sim$5.0), given for an isotropic form of BN deposited at temperatures between 1065° and 1355°C (Ref. 31).

3.5.5 Dielectric Measurements - Partly metallized silica slices served as substrates for the BN films which were used in evaluating dielectric properties. Initially, sputtered tantalum was used as the base

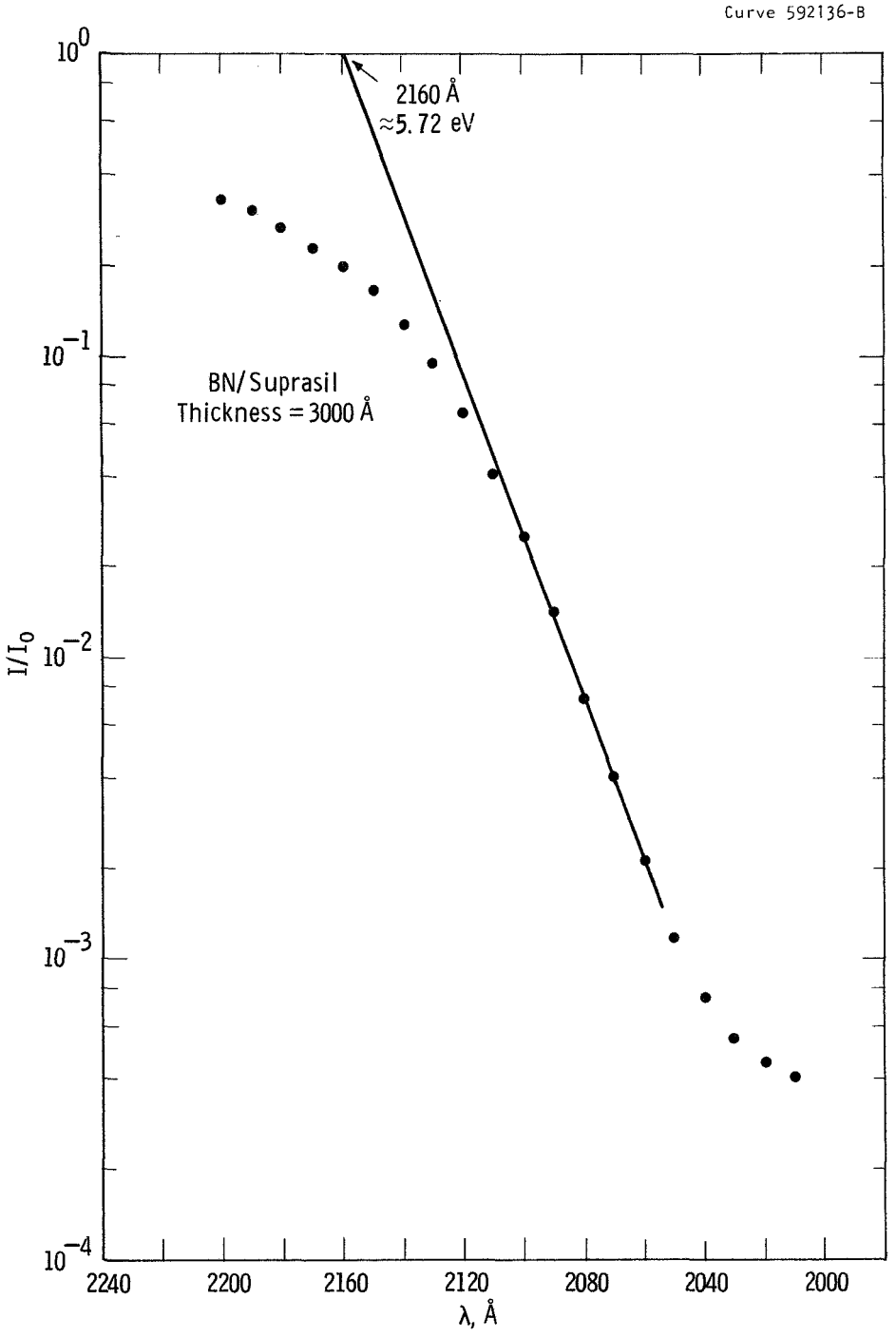

Fig. 71 Transmittance data (uv) for reactively sputtered BN film; thickness = 3000 Å. Data normalized so that $I/I_o = 1$ at $\lambda = 3000$ Å.

electrode material with evaporated aluminum or gold as the counterelectrode. Some data from these deposits prepared over a range of temperatures (voltage and current density held constant) are presented in Table X.

We note that the room temperature dielectric constant for the low temperature deposits falls in the range reported for bulk BN, viz., 3.5 (E $\|$ c-axis) and 5.1 (E $\perp$ c-axis) (Ref. 81). The deposits on substrates held at 900°C and 1100°C give values which differ from those measured for the lower temperature deposits. The value observed

TABLE X

Dependence of ε on Growth Temperature for BN Films

	ε (dielectric constant)			
f(kHz)	unheated	600°C	900°C	1100°C
500	4.9	5.05	2.3	4.1
100	4.9	5.05	2.35	4.1
50	5.0	5.1	2.4	4.16
20	5.2	5.2	2.4	4.2
10	5.35	5.25	2.4	4.2
5	5.4	5.35	2.45	4.24

in the 1100°C films possibly may occur as a result of the onset of some preferred orientation (the observed (0001)-fiber orientation, Fig. 67; the applied field would thus be oriented parallel to a relatively strong c-axis component. The results for 900°C deposits at first seemed anomalous. When a high temperature evaluation of BN film capacitors was begun, aluminum counterelectrodes were replaced

by sputtered platinum. Initially, there were no irreversible changes in film properties due to electrode diffusion and platinum electroding was extended to include the base electrode. Deposits prepared on platinum base electrodes at 900°-1000°C, however, did show some marked differences from those grown on tantalum electrodes. Measured values of dielectric constant, ε, were less than unity. Evaluation of these results indicated formation of a platinum-boron layer between the original platinum base electrode and the BN film. Initially, incomplete reaction of boron with nitrogen and later reaction with platinum (a platinum-boron eutectic is formed at 830°C (Ref. 82) are likely processes involved in the formation of this conductive layer. Platinum was abandoned in favor of tantalum and the temperature dependence of ε for films prepared at 1000°C is shown in Fig. 72. At room temperature, values of ε are approximately 4.3. This value is also less than the 5.1 reported for bulk BN. Since there also appears to be appreciable solid solubility of boron in tantalum at temperatures above 950°C (Ref. 83), the possibility of a tantalum-boron layer formed from unreacted boron cannot be excluded as a cause for the lower dielectric constant in these films. The ε vs T data do, however, show exceptionally stable properties between room temperature and 500°C in a range of frequencies between 5×10^3 to 5×10^5 kHz.

Measurements of dissipation factor were made using a Boonton 75C Direct Capacitance bridge. Values of D were calculated using the measured conductivity, G, of the films according to the formula

$$D = \frac{G}{2\pi fC}$$

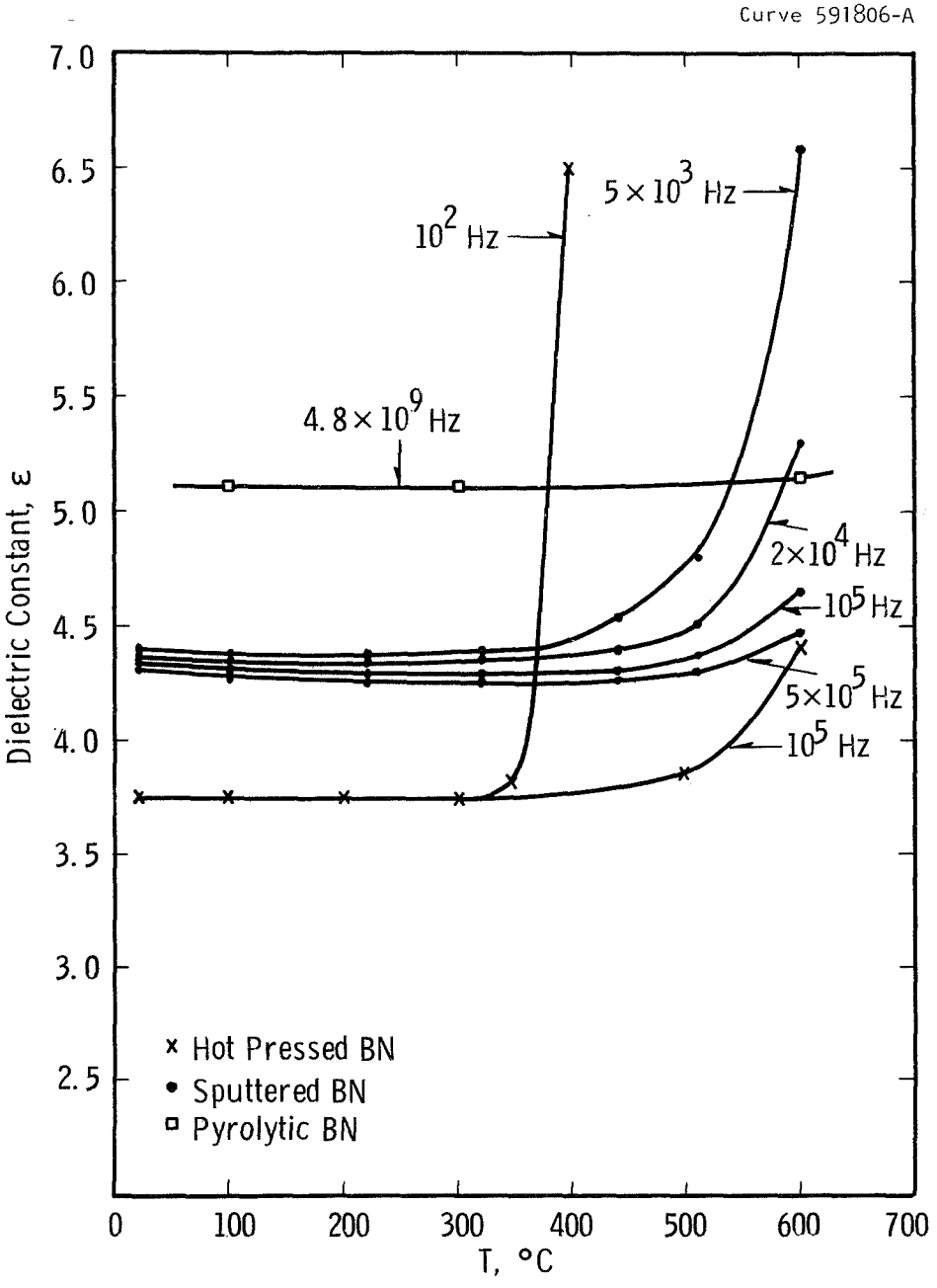

Fig. 72 Temperature dependence of dielectric constant of reactively sputtered BN.

where G is given in μ-ohms, C in pF, and f (frequency) in MHz. Room temperature values ranged consistently between 0.02 and 0.07 (film thicknesses being between 1000 and 5000 Å. These values are considerably greater than those reported for thick CVD deposits, e.g., in 75-100 μm films, $D \simeq 1.4 \times 10^{-4}$ (Ref. 32) but compare more favorably with thin pyrolytic deposits (5000 Å) on Cu and Mo (Ref. 84) viz., $.003 < D < .01$. In thicker sputtered BN deposits (1-3 μm) values of D decreased, $D < .0055$.

3.5.6 Structural Studies on Boron Films - In view of the implied reluctance of boron to react completely with nitrogen, a layer of boron was sputtered (voltage-current density parameters consistent with those used for sputtering of BN) in argon onto a silicon surface. Electron diffraction patterns and transmission electron micrographs are shown in Figs. 73 and 74. The diffuse diffraction rings, Fig. 73, are a match to those previously identified as BN (Ref. 74). The topography, however, is somewhat different to that for sputtered films of BN, Fig. 74. The available data do not, therefore, exclude the presence of unreacted boron in BN films.

3.5.7 C-V Measurements - The C-V characteristics of some reactively sputtered BN films on unheated n-type silicon substrates are shown in Fig. 75. Thicknesses are approximately 3000 Å. A small hysteretic effect is observed as the bias voltage is swept through a cycle and the sense in which the hysteresis loop is traversed indicates some ion motion. On application of a $\pm$ 10 volt bias, the flat band voltage (V_{FB}) is typically -8 V and the associated induced charge in the semiconductor is

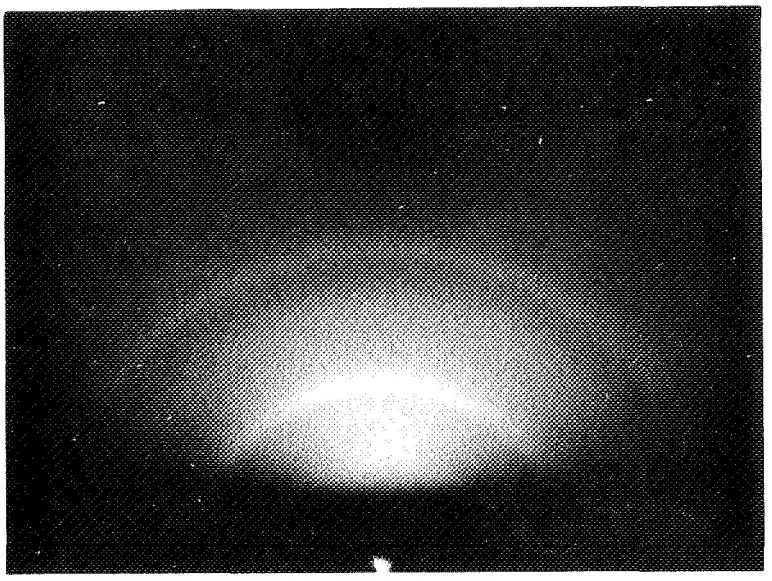

a

b

Fig. 73 Electron diffraction patterns of reactively sputtered films which condense in an amorphous state; (a) boron; (b) boron nitride.

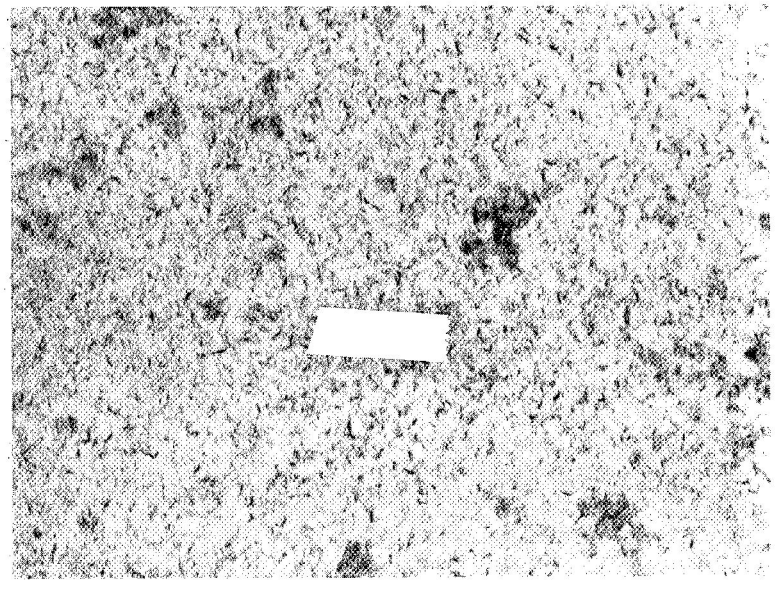

Fig. 74 Electron micrographs of reactively sputtered films which condense in an amorphous state; (a) boron; (b) boron nitride.

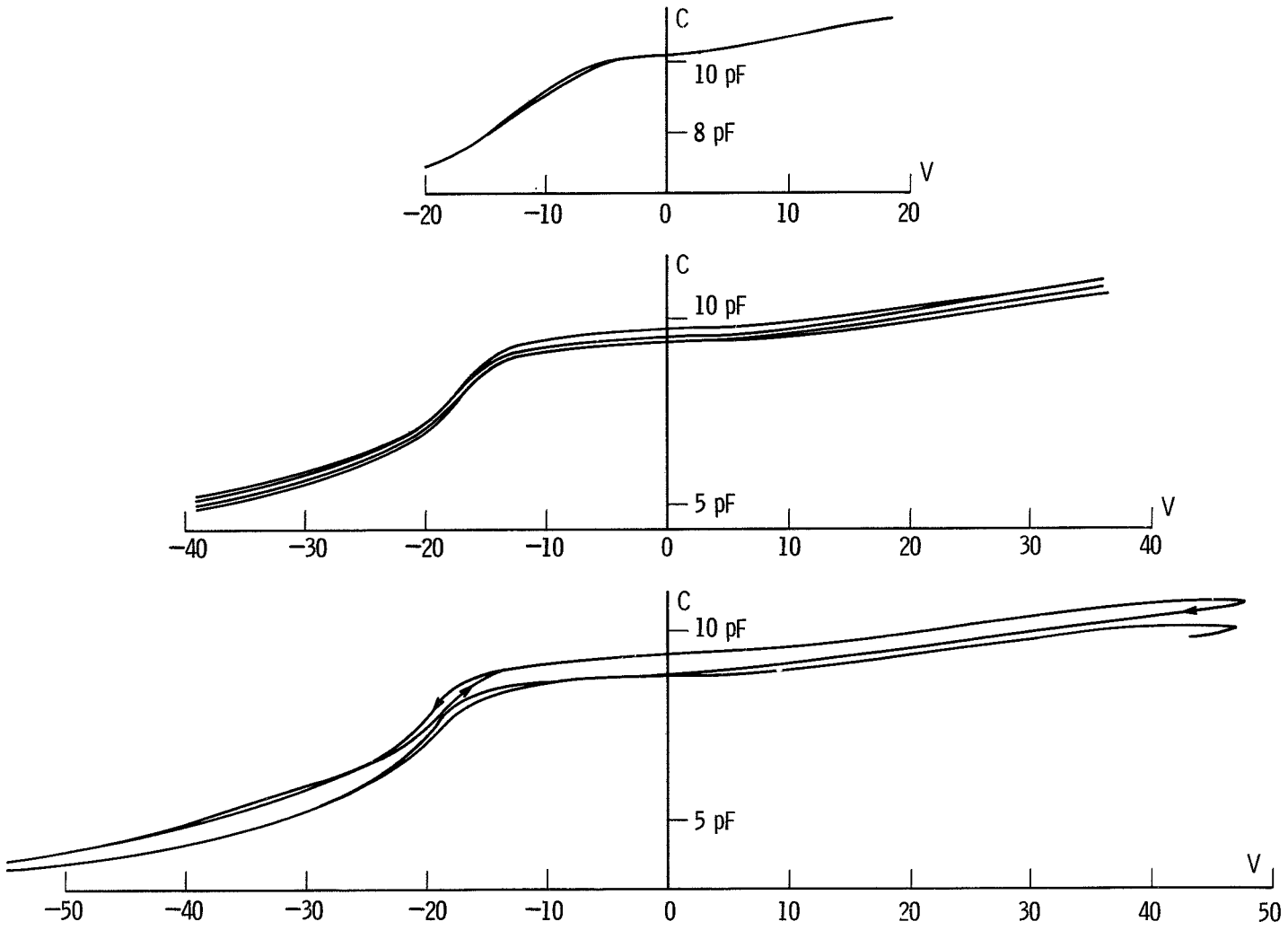

Fig. 75 C-V traces of 3000 Å film of reactively sputtered BN on n-type Si. The small hysteresis loop is traversed in a sense denoting ion motion. The inability of the trace to repeat itself is associated with a gradual erosion of the counter-electrodes under applied electric field. The film was deposited on a unheated substrate.

approximately -7 x 10^{12} charges/cm^2 (Ref. 62). As the voltage is increased we note a progressive and irreversible shift of the flat band voltage to more negative values, at 40 V bias V_{FB} = -17 V, at 70 V bias V_{FB} = -30 V. A decrease in the value of capacitance (maximum in the accumulation mode) is also noted after each sweep, the decrease being greater for higher biases. The ultimate effect, if a sufficient number of sweeps are traversed, is an apparent reduction of the capacitance to zero. An inspection of the capacitor at this point revealed that the counter-electrode (usually a 0.3 mm diameter aluminum pad) had vanished, thus accounting for the gradual decrease of capacitance.

A voltage was next applied to an adjacent MIS structure so that the effect on the counterelectrode might be followed. On application of a small bias, $\pm$ 20 V, a slight discoloring was observed at the edge of the metallic aluminum pad. A larger bias, $\pm$ 40 V, increased the discolored (nonmetallic appearance) region gradually and an even larger, $\pm$ 70 V bias, produced a fairly rapid change culminating in the complete disappearance of the metallic electrode. On the tentative assumption that field-induced aluminum diffusion into a porous film was the cause of the observed effect, a portion of the nitride film was counterelectroded with sputtered tantalum (a more refractory and less mobile metal). There appeared good stability of the C-V loops up to biases of $\pm$ 20 V. When higher biases were applied, however, the capacitance began to decrease once more. Although the BN films deposited on unheated silicon substrates seem apparently porous to metal atom diffusion, they exhibited considerable dielectric strength showing no evidence of spontaneous breakdown even

when biased at $\pm$ 100 V (3×10^6 V/cm). Films prepared at intermediate temperature, ∿500°-600°C, behaved less erratically and data are shown in Fig. 76. Ion motion is again predominant and the associated induced charge is -6.3×10^{11} charges/cm^2. Films deposited at the highest temperatures of preparation, ∿1000°C, frequently suffered breakdown at low applied voltage (∿5 V). Analysis of the C-V trace from such breakdowns indicates that breakdown occurs at a Schottky barrier (metal-semiconductor junction). Contact between the counterelectrode and the semiconductor seems possible if the dielectric contains voids or is porous. Since the intermediate temperature data seem most promising, future studies might well concentrate in this area.

3.6 Discussion

The excellent chemical stability of reactively sputtered AlN films enabled a wide variety of measurements to be made. Included were x-ray and electron diffraction studies, optical absorption measurements, resistivity, capacitance, I-V and C-V measurements and evaluations of piezoelectric properties.

Since the films comprised oriented arrays of small crystals, it is not surprising that many of the observed results bear some resemblance to data from hot pressed ceramic AlN as well as from small bulk single crystals. In general, the resemblance is nearest that of the latter. Dielectric properties are less affected by a temperature excursion than are those of the hot pressed form and suggest the absence of conducting impurities. I-V behavior seems consistent with a space-charge-limited mechanism and C-V data suggest the possibility of "built-in"

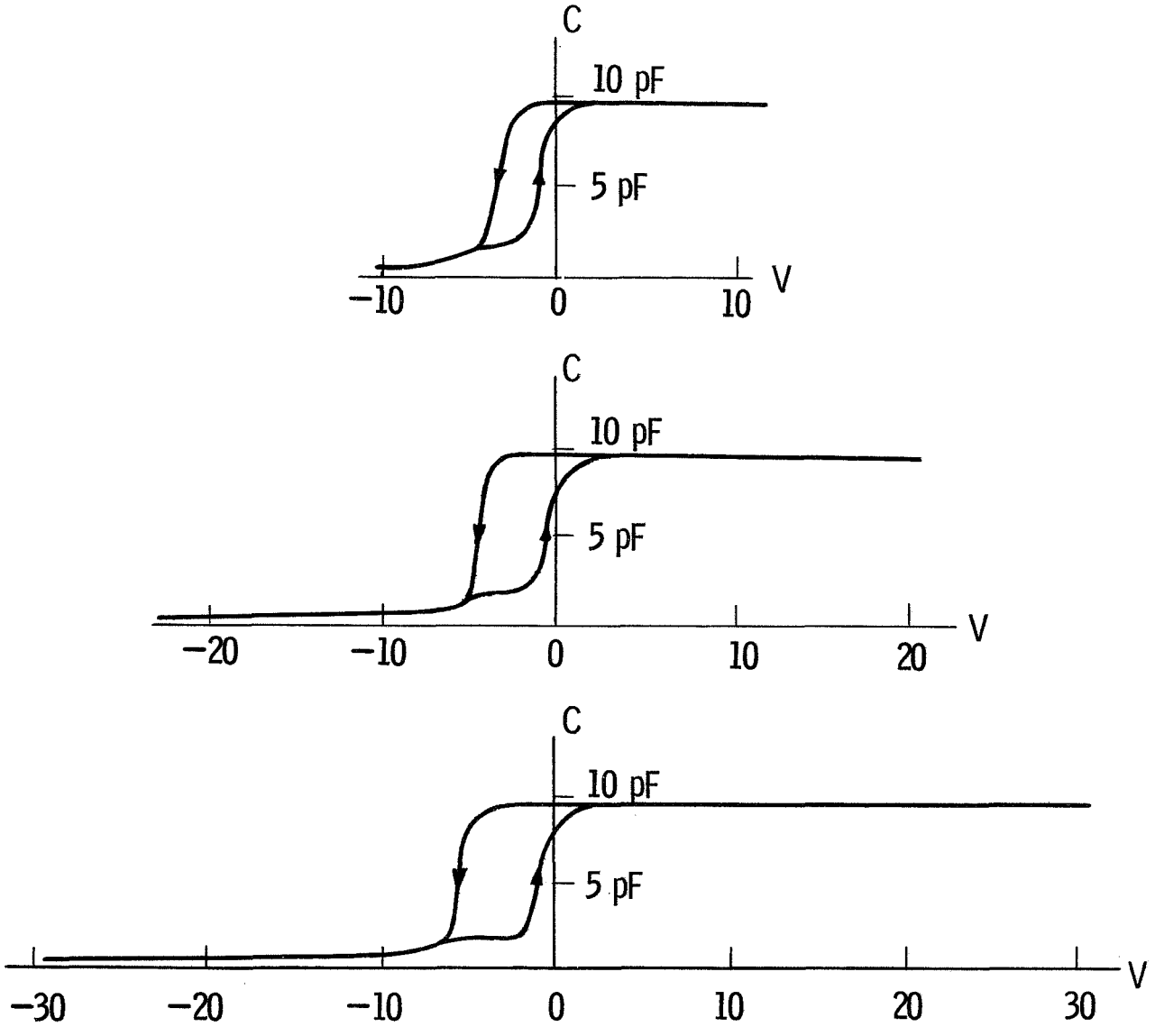

Fig. 76 C-V curves from reactively sputtered BN films prepared on Si at 550°C. Film thickness = 2700 Å.

dipoles which display the motions of both positive and negative ions when subjected to electrical stresses.

The most obvious physical anomaly noted, the shift of the optical absorption edge in as-deposited, diode sputtered films, bears a marked resemblance to the bulk data obtained by Cox, et al. (Ref. 56). Nitrogen deficiency initiated by argon occlusion offers an acceptable cause especially since the bulk parameter can be attained by subsequent annealing in a pure nitrogen ambient.

Although perfect epitaxy is not generally achieved in deposits onto Al_2O_3 surfaces, piezoelectric measurements were made using films which showed strong fiber-texture orientations. Some data indicated strong electromechanical response and allowed comparison with previously examined CdS layers. At best, the AlN films compare favorably.

Mixed films of AlN-BN and AlN-Si_3N_4 were prepared in attempts to disrupt the long-range crystalline order of AlN films. The experiments were only partly successful in that disorder was never complete up to the stage where properties began to deviate from those of AlN.

BN, the boron analogue of AlN, was studied as a separate entity. Prepared by the reactive sputtering of high purity boron, films of BN show bulk values of dielectric constant. Dielectric loss while appearing high in very thin films, $t < 500$ Å, is similar, for films of greater thickness, to values observed for pyrolytic deposits. The BN films are structurally less crystalline than AlN films. Some measured or deduced parameters differ from those reported for bulk samples; bulk material appears to be highly anisotropic. The position of the optical

absorption edge, for example, approximates a value more consistent with a theoretically isotropic sample. Deduced lattice parameters differ somewhat from reported bulk values and are thought due to structural disorder, non-stoichiometry or possible disruption of short range order by argon occlusion.

Although some ion motion is associated with C-V behavior of BN/Si, the amorphous character of the films coupled with high resistivities suggests a further look at this material for use in MIS-device application.

4. CONCLUSIONS

4.1 Evaporated films of AlAs and AlP have been prepared for the first time and the conditions of deposition leading to stoichiometric compositions have been defined. These conditions differ from those used for other III-V compound films due to the high decomposition temperatures of the Al-compounds.

4.2 The structural and optical properties of the vacuum deposited AlSb, AlAs and AlP films agree with the corresponding bulk properties. These properties degrade, however, when the films are exposed to moist air environments.

4.3 Resistivities measured in the antimonide, arsenide and phosphide, before deterioration were comparable to bulk values. Mobilities, however, were very low and were attributed to the grain boundaries inherent in films made up of small crystallites. This fact, together with the difficulties encountered in developing epitaxy, indicate that Al-V films grown by vacuum deposition are not attractive for the manufacture of the junctions.

4.4 Films of AlN have been sputtered for the first time in residual ultra-high vacuum environments. A full range of preferred orientations, none to epitaxial, were observed on a variety of substrates.

4.5 The structural, electrical and dielectric properties of AlN films compared favorably to those of bulk polycrystalline and single crystal materials. The dielectric properties appeared to surpass those of sintered, polycrystalline AlN at high temperature.

4.6 Optical properties showed that the absorption edge in sputtered AlN is a function of substrate temperature and the composition and pressure of the sputtering atmosphere. Films deposited in an argon-nitrogen mixture unbalanced heavily in favor of argon showed strong absorption characteristics as low as 3.4 eV. Annealing at high temperatures restored the absorption edge to a bulk value of 5.9 eV. As-deposited films were thus believed to contain occluded argon which gave rise to a nitrogen deficiency condition.

4.7 Although the reproducibility of microwave acoustic measurements for a series of reactively sputtered AlN films was rather poor, the overall data from such measurements indicated that the best films display piezoelectric properties which rival those of highly ordered CdS films. Causes of the inconsistencies appear associated with either poor substrate interfaces or possible substrate contamination.

4.8 Efforts to determine the optical absorption coefficient, α, of AlN using oriented films were unsuccessful due to an inherent property, viz., the mosaic structure of such films. Light scattering at grain boundaries increases α by at least an order of magnitude.

4.9 Mixed films of AlN-BN were prepared and analyzed for percentage of boron content. In films prepared at 900°C, lattice parameter data suggest that not more than 6 - 7-1/2% boron is taken into the AlN lattice. The solid solution still retains a wurtzite structure but with cell dimensions smaller than that for AlN. BN as a separate excess phase is observed in deposits where the Al/B ratio is 2.4/1.

4.10 Mixed films of AlN-Si_3N_4 retained properties similar to those observed for pure AlN. Deposits in which the Al/Si ratio was 1/1 were almost amorphous and showed I-V characteristics which indicated space-charge limited behavior.

4.11 BN films, prepared by reactive sputtering from high purity boron targets, displayed dielectric properties which equalled or excelled those of bulk or pyrolytically prepared BN. Unlike bulk material, the sputtered films were predominately isotropic (electron diffraction and u.v. absorption data). The absorption edge of sputtered BN is associated with a band gap of 5.72 eV.

5. REFERENCES

1. Grimmeiss, H. G., Kischio, W. and Rabenau, A., J. Phys. Chem. Solids, 16, 1960, p. 302.

2. Moss, T. S., Photoconduction in III-V Compounds, Semiconductors and Semimetals, Vol. 2 of Physics of III-V Compounds, Chap. 9, Sec. 11, Willardson, R. R. and Beer, A. C., ed., Acad. Press (New York), 1966, p. 235.

3. Braunstein, R. and Kane, E. O., J. Phys. Chem. Solids, 23, 1962 p. 1423.

4. Long, G. and Foster, L. M., J. Am. Ceram. Soc. 42, 1959, p. 53.

5. Taylor, K. M., and Lenie, C., J. Electrochem. Soc., 107, 1960, p. 308.

6. Pastrnak, J. and Roskovcova, L., Phys. Stat. Sol., 26, 1968, p. 591.

7. Collins, A. T., Lightowlers, E. C., and Dean, P. J., Phys. Rev., 158, 1967, p. 833.

8. Delavignette, P., Kirkpatrick, H. B., and Amelinckx, S., J. Appl. Phys., 32, 1961, p. 1098.

9. Drum, C. M., J. Appl. Phys., 36, 1965, p. 816.

10. Chu, T. L., Ing, D. W., and Noreika, A. J., Solid-State Electron., 10, 1967, p. 1023.

11. Pastrnak, J. and Souckova, L., Phys. Stat. Sol., 3, 1963, p. k71.

12. Chu, T. L., Ing, D. W., and Noreika, A. J., Electrochem. Technol., 6, 1968, p. 56.

13. Wauk, M. T., and Winslow, D. K., Appl. Phys. Lett., 13, 1968, p. 286.

14. Rairden, J. R., Abstract 468, Extended Abstracts-134th Natl. Meet. Electrochem. Soc., Montreal, Oct. 1968, p. 357.

15. Noreika, A. J., Francombe, M. H. and Zeitman, S. A., J. Vac. Sci. Technol. 6, 1969, p. 194.

16. Lewis, D. W., Properties of Aluminum Nitride Derived From $AlCl_3 \cdot NH_3$, Westinghouse Research Report 69-9B5-INORM-P1, Pittsburgh, 1969, p. 8.

17. Allred, W. P., Paris, B. and Genser, M., J. Electrochem. Soc., 105, 1958, p. 93.

18. Schell, H. A., Z. Metallk., 49, 1958, p. 140.

19. Schell, H. A., Z. Metallk., 46, 1955, p. 58.

20. Johnson, J. E., J. Appl. Phys. 36, 1965, p. 3193.

21. David, J. P., Capella, L., Laude, L., and Martinuzzi, S., Rev. de Phys. Appl., 1, 1966, p. 172.

22. Reid, F. J., Miller, S. E., and Goering, H. L., J. Electrochem. Soc., 113, 1966, p. 467.

23. Bailar, J. C., Jr., Inorganic Syntheses, Vol. 4, McGraw-Hill Publ. Co., (New York), 1953, p. 23.

24. Addamiano, A., J. Am. Chem. Soc., 82, 1960, p. 1537.

25. Wolff, G., Keck, P. H., Broder, J. D., Phys. Rev., 94, 1954, p. 753.

26. Stambaugh, E. P., Preparation of Aluminum Arsenide, Chap. 21, Compound Semiconductors Vol. I - Prepration of III-V Compounds., Willardson, R. K., and Goering, H. L., ed., Reinhold Publ. Corp. (New York), 1962, p. 184.

27. Mansuri, Q. A., J. Chem. Soc., 121 , 1922, p. 2272.

28. Vertoprakh, V. N., and Grigor'eva, A. G., Izv. Vyssh. Ucheb. Zavedenii, Fiz., 1958, p. 133.

29. Basche, M. and Schiff, D., Mat. in Design Eng., 59, 1964, p. 78.

30. Rand, M. J., and Roberts, J. F., J. Electrochem. Soc., 115, 1968, p. 423.

31. Steele, S. R., Chemical Vapor Deposited Materials for Electron Tubes, Ratheon Tech. Rpt., ECOM-01343-2, Waltham, Mass. Jan. 1966 (AD-477-126).

32. Stapleton, R. W., High Temperature Capacitor Topical Rpt, Westinghouse Tech. Rpt. -- Lima, Ohio, WAED 67.24E prep. under NASA-Lewis Contract NAS3-6465, May 1967.

33. Gunther, K. G., Vaporization and Reaction of the Elements, Chap. 35, Compound Semiconductors Vol. I - Preparation of III-V Compounds, Willardson, R. K. and Goering, H. L., ed., Reinhold Publ. Corp. (New York), p. 313.

34. Davey, J. E., J. Appl. Phys. 32, 1960, p. 877.

35. Molnar, B., Flood, J. J., and Francombe, M. H., J. Appl. Phys., 35, 1965, p. 3554.

36. Davey, J. E., and Pankey, T., J. Appl. Phys. 35, 1964, p. 2203.

37. Cardona, M., Semiconductors and Semimetals, Vol. 3, Willardson, R.K., and Beer, A. C., ed., Acad. Press. (New York) 1967.

38. Sorokin, G. P., Izv. Vyssh. Ucheb. Zavedenii, Khem. tekhnol, 5, 1962, p. 407.

39. Abraham, A., Czech. J. Phys., 6, 1956, p. 624.

40. Mead, C. A. and Spitzer, W. G., Phys. Rev. Letters 11, 1963, p. 358.

41. Fomenko, V. S., Handbook of Thermionic Properties, Plenum Press (New York), 1966.

42. Kover, F., Solid State Phys. Electron. Telecommun. 2, 1960, p. 768.

43. Shaw, D. and McKell, H. D., Brit. J. Appl. Phys. 14, 1963, p. 295.

44. Minden, H. T., Sylvania Tech. 11, 1958, p. 13.

45. Gunther, K. G., The Use of Thin Films in Physical Investigations, Anderson, J. C., ed., Academic Press (London), 1966, p. 213.

46. Agrain, P. and Balkanski, M., Selected Constants Relative to Semiconductors, Pergamon Press, 1961.

47. Weisberg, L., Contract SD-182, AD-432-272, March 1964.

48. Wieder, H. H., Solid-State Electron. 9, 1966, p. 373.

49. Bube, R. H., Photoconductivity of Solids, John Wiley and Sons, 1960.

50. Madelung, O. (Meyerhofer, D., Trans.) Physics of III-V Compounds John Wiley and Sons, 1964.

51. Rhodin, T. N., Disc. Fraday Soc., 5, 1949, p. 215.

52. Noreika, A. J. and Ing, D. W., J. Appl. Phys., 39, 1968, p. 5578.

53. Lewis, B. and Campbell, D. S., J. Vac. Sci. Technol., 4, 1967, p. 209.

54. Walton, D., J. Chem. Phys., 37, 1962, p. 2182.

55. Jeffrey, G. A. and Parry, G. S., J. Chem. Phys., 23, 1955, p. 406.

56. Cox, G. A., Cummins, D. O., Kawabe, K. and Tredgold, R. H., J. Phys. Chem. Solids, 28, 1967, p. 543.

57. Moss, T. S., Absorption Processes in Semiconductors, Optical Properties of Semiconductors, Chap. 3, Butterworths (London), 1961, p. 36.

58. Wheeler, B. E., Solid-State Comm., 4, 1966, p. 173.

59. von Hippel, A. R., Dielectrics and Waves, John Wiley and Sons (New York), 1954, p. 5.

60. Kawabe, K. Tredgold, R. H., and Inuishi, Y., Elec. Engr. in Japan, 87, 1967, p. 62.

61. Lampert, M. A., Phys. Rev., 103, 1956, p. 1648.

62. Grove, A. S., Deal, B. E. Snow, E. H., and Sah, C. T., Solid State Electron., 8, 1965, p. 145.

63. Krikorian, E. and Sneed, R. J., Technical Report AFAL-TR-67-139, August 1967, p. 112.

64. deKlerk, J., Ultrasonics, 2, 1964, p. 137.

65. deKlerk, J., J. Appl. Phys., 37, 1967, p. 4522.

66. Hu, S. M., J. Electrochem. Soc., 113, 1966, p. 693.

67. Murray, L. A., and Scott, J. H., Paper 152, Proc. Electrochem Soc., Philadelphia, Oct. 1966.

68. Doo, V. Y., Nichols, D. R., and Silvey, G. A., J. Electrochem. Soc., 113, 1966, p. 1279.

69. Deal, B. E., Fleming, P. J., and Castro, P. L., J. Electrochem. Soc. 115, 1968, p. 300.

70. Barnes, C. R. and Geesner, C. R., J. Electrochem. Soc., 107, 1960, p. 98.

71. Gregor, L. V., Study of Silicon Nitride as a Dielectric Material for Microelectronic Applications, Tech. Rpt. AFAL-TR-67-248, Sept. 1967.

72. Elliott, R. P., Constitution of Binary Alloys, 1st. Suppl., McGraw-Hill Publ. Co., (New York) 1965, p. 26.

73. Pauling, L. C., The Nature of the Chemical Bond, 3rd. ed., Cornell Univ. Press (Ithaca, N. Y.), 1960, p. 246.

74. Noreika, A. J., Francombe, M. H., and Zeitman, S. A., Research and Development Study on Wide Band-Gap Semiconductor Films, Interim Rpt., NASA-ERC Contract NAS12-568, December 1968.

75. Zaininger, K. H., SCP and Solid-State Technol., 10, 1967, p. 17.

76. Li, P. C., Chemically Vapor Deposited Boron Nitride, Tech. Rpt., NASA, N65-11827, June 1964.

77. Brame, E. G., Jr., Margrove, J. L., and Meloche, V. W., J. Inorg. Nucl. Chem., 5, 1957, p. 48.

78. Neuberger, M., Boron Nitride, Tech. Data Sheet DS-158 EPIC-Culver City, Calif., Contract AF33-615-2460, November 1967.

79. Schaffer, P. S., High Temperature Electrical Conductivity Device for Use with Thermal Image Heating, Tech. Rpt., Lexington Labs, Cambridge, Mass., Contract AF 19 628-1616, December 1964, AD-610 496.

80. Bassani, F. and Yoshimine, M., Phys. Rev., 130, 1963, p. 20.

81. von Hippel, A., Studies on the Formation and Properties of High Temperature Dielectrics, Tech. Report, MIT Lab for Insulation Research, Contract No. AF 33 616-8353, July 1964, DDC AD-459 511.

82. Elliott, R. P., Constitution of Binary Alloys, 1st Suppl., McGraw-Hill, (New York), 1965, p. 130.

83. Hansen, M., Constitution of Binary Alloys, 2nd ed., in cooperation with Andirko, K., McGraw-Hill (New York), 1958, p. 258.

84. Habrecht, R. R., Patterson, R. J. and Humphries, R. D., Insulation 10, 1964, p. 33.

6. APPENDIX (NEW TECHNOLOGY)

Preparation of Stoichiometric Al-V Films by Three Temperature Evaporation

The following conditions were used to ensure the preparation of stoichiometric evaporated films of the compounds AlSb, AlAs and AlP. Al source temperatures should be in the range 1000-1200°C to provide incidence rates up to 100 monolayers per minute. The Group V element should be screened from the Al source to prevent formation of the compound at the surface of the melt. Adjustment of the source temperatures should be such that the Group V element flux is 1 to 1.5 times that for Al. Substrate temperatures must be greater than 700°C, high enough to prevent or reduce significantly the deposition of Al alone. The upper limit for the substrate temperature is set only by the decomposition temperature of the respective compound.

More detailed data are given for the individual compounds in Sec. 2.1.1 (AlSb), Sec. 2.3.1 (AlAs) and Sec. 2.4.1 (AlP).

Report Distribution List for Contract NAS 12-568

National Aeronautics & Space Administration
Attn: US/Winnie M. Morgan
Sci. and Tech. Info. Division
Washington, D. C. 20546
2 copies

National Aeronautics & Space Administration
Attn: REE/Mr. C. E. Pontious
Washington, D. C. 20546

National Aeronautics & Space Administration
Attn: Office of Technology Utilization
Washington, D. C. 20546

National Aeronautics & Space Administration
Attn: Mr. S. Gaudiano, Code EE-2
Manned Spacecraft Center
Houston, Texas 77058

National Aeronautics & Space Administration
Attn: Dr. Alvis M. Holladay, R-ASTR-R
Geo. C. Marshall Space Flight Center
Huntsville, Alabama 35812

National Aeronautics & Space Administration
Attn: Mr. C. A. Hermach, Code SVM
Ames Research Center
Moffett Field, California 94035

National Aeronautics & Space Administration
Attn: Mr. C. Husson, Mail Stop 470
Langley Research Center
Hampton, Virginia 23365

National Aeronautics & Space Administration
Attn: Mr. R. Van Allen, Code 711
Goddard Space Flight Center
Greenbelt, Maryland 20771

Jet Propulsion Laboratory
Attn: Mr. R. Powell
Research Programs Office
4800 Oakgrove Drive
Pasadena, California 91103

Department of the Army

Commanding General
U.S. Army Electronics Command
Attn: AMSEL-KL-S, Dr. H. Jacobs
Fort Monmouth, New Jersey 07703

Commanding General
U.S. Army Electronics Command
Attn: AMSEL-KL-I, Mr. R. A. Gerhold
Fort Monmouth, New Jersey 07703

US Army Electronics Command
Attn: Mr. H. Mette
Code AMSEL-KL-ID
Fort Monmouth, New Jersey 07703

Army Research Office Durham
Attn: Dr. R. Mace
Director, Physics Division
Box CM
Duke Station, North Carolina 27706

Commanding Officer
Harry Diamond Laboratories
Attn: Mr. N. Doctor
Washington, D. C. 20438

Commanding Officer
USAMERDC
Attn: SMEFB-IR (Mr. K. Steinbach)
Fort Belvoir, Virginia 22060

Commanding Officer
Picatinny Arsenal
Attn: Mr. A. Hendrickson, SMUPA-T
Dover, New Jersey 07801

Department of the Navy

Naval Weapons Center
Attn: Dr. H. H. Weider, Code C 6134
Corona Laboratories
Corona, California 90720

Department of the Navy Cont.

Department of the Navy
Naval Electronic Systems Command
Attn: Mr. A. H. Young, ELEX-05143A
Washington, D. C. 20360

Director, Naval Research Laboratory
Attn: Mr. G. Abraham, Code 2027
Washington, D. C. 20390

Res. Coordinator Materials
Office of Naval Research
Attn: Mr. Ancel E. Cook, Code 403C
Department of the Navy
Washington, D. C. 20360

U.S. Naval Ordnance Laboratory
Attn: Mr. Albert D. Krall
White Oak
Silver Spring, Maryland 20910

Department of the Air Force

Air Force Avionics Laboratory
Attn: J. Blasingame
Chief, Electronic Res. Branch
Wright Patterson AFB, Ohio 45433

Air Force Avionics Laboratory (AVTA)
Attn: Mr. H. H. Steenbergen
Wright Patterson AFB, Ohio 45433

Air Force Office of Scientific Res.
Attn: Dr. T. Ratchford
Office of Aerospace Research
Washington, D. C. 20333

Commander, RADC
Attn: Mr. J. Brauer, EMERM
Griffiss Air Force Base
New York 13440

Air Force Materials Laboratory
Attn: Mr. L. F. Salzberg
Wright Patterson AFB, Ohio 45433

Other Government Agencies

Director, National Security Agency
Attn: Mr. Oliver H. Bartlett Jr., R-42
Fort George G. Meade,
Maryland 20755

Private Organizations

Dr. R. D. Baxter
Battelle Memorial Institute
505 King Avenue
Columbus, Ohio 43201

Dr. H. Manasevit
North American-Rockwell Corp.
Antonetics Division
Muraloma Avenue
Anaheim, California

Dr. G. S. Kamath
Xerox Corporation
Research Laboratory
Webster, New York

Dr. T. B. Light
IBM Corporation
Thomas Watson Research Center
Yorktown Heights, New York

Applied Physics Laboratory
The John Hopkins University
Attn: Dr. Charles Feldman
Silver Spring, Maryland 20910

Lincoln Laboratory, MIT
Attn: Mr. Donald J. Eckl
P.O. Box 73
Lexington, Massachusetts 02173

J. L. Moll
Stanford University
Stanford, California 94304

P. L. Hower
Research and Development Laboratory
Fairchild Semiconductor
Palo Alto, California

L. Cohen
General Telephone & Electronics
Laboratories, Incorporated
Bayside, New York

H. C. Casey
Bell Telephone Laboratories, Inc.
Murray Hill, New Jersey

Private Organizations Cont.

W. W. Hooper
Research and Development Laboratory
Fairchild Semiconductor
Palo Alto, California

A. M. Barnet
General Electric Company
Electronics Laboratory
Syracuse, New York

Dr. J. J. Tietjen
David Sarnoff Research Center
Princeton, New Jersey

G. E. Renner
General Electric Research and
Development Center
Schenectady, New York

H. Rupprecht
T. J. Watson Research Laboratory
IBM Corporation
Yorktown Heights, New York

W. G. Spitzer
Department of Materials Science
and Electrical Engineering
University of Southern California
Los Angeles, California

F. J. Reid
General Telephone & Electronics
Laboratories, Incorporated
Bayside, New York

C. M. Wolfe
Lincoln Laboratories
Mass. Institute of Technology
Lexington, Massachusetts 02173

J. Kinoshita
Central Research Laboratories
Varian Associates
Palo Alto, California

C. S. Kang
Hewlett-Packard Laboratories
Palo Alto, California

Private Organizations Cont.

M. Ilegems
Stanford Electronics Laboratory
Stanford University
Stanford, California 94304

R. Solomon
Fairchild Semiconductor Research &
Development Laboratory
Palo Alto, California

K. L. Ashley
Southern Methodist University
Dallas, Texas 75222

G. L. Pearson
Stanford Electronics Laboratory
Stanford University
Stanford, California 94304

M. T. Wauk
Microwave Laboratory
Stanford University
Stanford, California 94305

D. K. Winslow
Microwave Laboratory
Stanford University
Stanford, California 94305

J. DeKlerk
Westinghouse Research Center
Pittsburgh, Pa. 15235

R. E. Stapleton
Westinghouse Electric Corp.
Aerospace Elec. Div.
Lima, Ohio

R. A. Lindberg
NASA/Lewis Research Center
Space Power Systems Div.

S. E. Miller
Columbus Laboratories
Battelle Memorial Inst.
Columbus, Ohio

H. L. Goering
Columbus Laboratories
Battelle Memorial Inst.
Columbus, Ohio

S. M. Hu
IBM Components Div.
E. Fishkill Facility
Hopewell Junct., New York 12533

L. V. Gregor
IBM Components Div.
E. Fishkill Facility
Hopewell Junct., New York 12533

A. R. Janus
Research & Development Labs.
Sprague Elect. Co.
North Adams, Mass.

G. A. Shirn
Research & Development Labs.
Sprague Elect. Co.
North Adams, Mass.

L. A. Murray
Radio Corp. of America
Electronic Components & Devices
Somerville, New Jersey

J. H. Scott
Radio Corp. of America
Electronic Components & Devices
Somerville, New Jersey

J. R. Rairden
General Electric Corp.
Research and Development Center
Schenctady, New York

M. J. Rand
Bell Telephone Labs, Inc.
Allentown, Pa.

J. F. Roberts
Bell Telephone Labs, Inc.
Allentown, Pa.

D. Richman
RCA Laboratories
Princeton, New Jersey

Contracting Center Distribution List

NASA Electronics Research Center
575 Technology Square
Cambridge, Massachusetts 02139

AT/Technical Information Branch
(20 + 1 reproducible) copies
Technical Monitor - 5 copies
T/Technology Utilization
M/Patent Counsel